Review Article

Yunyi Dai, Chunli Liu, Yang Bai, Qingquan Kong, and Huan Pang*

Framework materials for supercapacitors

https://doi.org/10.1515/ntrev-2022-0042
received October 6, 2021; accepted January 4, 2022

Abstract: Framework materials, including metal–organic framework materials (MOFs), Prussian blue/Prussian blue analogs (PB/PBAs), and covalent framework materials (COFs), are promising candidates for fabricating electrodes for use in electrochemical devices, especially supercapacitors. Supercapacitors have been widely investigated over the past decade. Active materials as electrode materials are vital to the development of the next generation of supercapacitors. Therefore, designing and fabricating novel electrode materials endowed with superior specific capacitance, perfect cycling stabilities, and distinguished power/energy density are crucial. In this review, we focus on framework materials – MOFs, PB/PBAs, and COFs – and report electrode materials based on their pristine forms, derivatives, and composites for supercapacitors. Recent advances and potential applications of framework materials in supercapacitors are also discussed. Furthermore, we discuss the opportunities and challenges for the future direction of supercapacitors based on framework materials.

Keywords: supercapacitors, frameworks materials, metal–organic framework materials

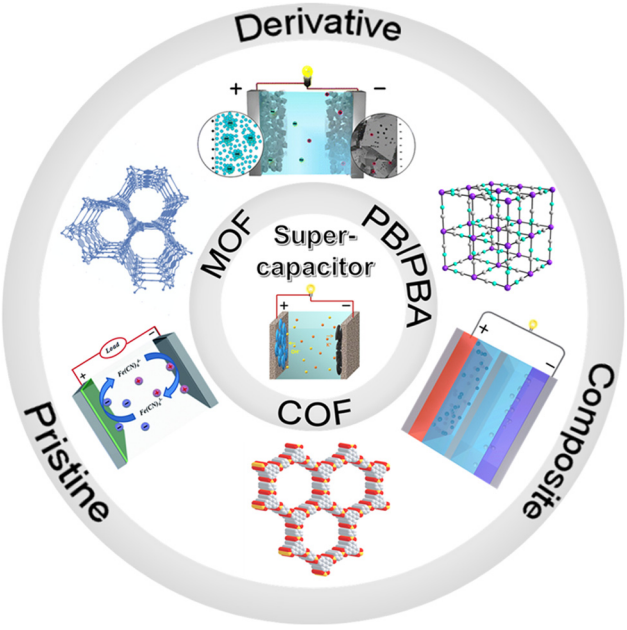

Graphical abstract: Framework materials for supercapacitors: Supercapacitors are perfect energy storage devices with superior cycling life, remarkable power/energy density, fast charge–discharge rates, and environmental friendliness. Frameworks materials, including metal organic frameworks (MOFs), Prussian blue/Prussian blue analogs (PB/PBAs), and covalent organic frameworks (COFs), are outstanding candidates in supercapacitors. In this review, we mainly report typical research progress on framework materials, their derivatives, and composites in a supercapacitor.

1 Introduction

Severe environmental pollution, increasing fossil fuel consumption, and global warming have become critical societal issues [1,2]. To overcome these issues, the exploration and development of renewable and environmentally friendly energy sources, including wind, solar, biomass, hydraulic, ocean energy, are necessary [3]. Effectively utilizing these new sustainable energy sources, thus driving the development of effective energy storage and conversion technologies, is also required [4,5]. Among these, chargeable batteries and supercapacitors are recognized as some of the most efficient and reliable technologies. Chargeable batteries such as Li-ion, Li-sulfur, Na-ion, *etc.* are popular owing to their excellent energy density and promising cycling life [6–8]. However, their high internal resistance considerably curtails their power delivery capability and cyclic life [9]. Moreover, the battery could not be discharged fast enough in the sudden power consumption in the application of electrical vehicles [10].

Supercapacitors are electrochemical energy storage devices that connect batteries and capacitors to produce a rapid charging energy storage device for intermediate specific energy [11,12]. Supercapacitors deliver superior power

* **Corresponding author: Huan Pang,** School of Chemistry and Chemical Engineering, Yangzhou University, Yangzhou, China, e-mail: huanpangchem@hotmail.com
Yunyi Dai, Chunli Liu, Yang Bai: School of Chemistry and Chemical Engineering, Yangzhou University, Yangzhou, China
Qingquan Kong: Institute for Advanced Study, Chengdu University, Chengdu, 610106, SiChuan, China

density, remarkable cycling life, fast charge/discharge rate, and environmental friendliness, making them attractive for various applications. [13–15]. Nowadays, supercapacitors are widely applied in the regenerative braking system in electronic vehicles. Due to their fast energy recovery, they can compensate the charge at the time when battery power is not sufficient, which improved the lifetime of the braking system and overall efficiency [16,17].

The energy storage mechanisms of supercapacitors can be divided into electric double-layer capacitance (EDLC) and pseudocapacitance [18–20]. EDLC is based on charge storage between the electrolyte and electrode interface without any electron transfer, and it mainly occurs in carbon-based materials. Pseudocapacitance involves the storage of charges *via* reversible redox reactions between the electrode and the electrolyte [21,22]. Several studies have shown that supercapacitor electrode materials with pseudocapacitance mechanisms are usually composed of metal oxides, metal sulfides, and conductive polymers, delivering an ultrahigh specific capacitance.

To develop high-performance supercapacitors, fabricating and developing active electrode materials is important. In particular, framework materials play a vital role in this field. Framework materials including covalent framework materials (COFs), Prussian blue and its analogs (PB and PBAs), and metal–organic frameworks (MOFs), all exhibit promising characteristics in supercapacitor applications. COFs are typical crystalline porous polymers that allow for the precise integration of redox-active organic building blocks into an ordered nanostructure atomically, thus creating predesigned skeletons and nanopores [23]. Owing to their promising structural characteristics, COFs have been burgeoned as new candidates for developing promising electrochemical devices, such as gas storage, catalysis, and electrochemical devices, especially for supercapacitors [24]. PB and PBAs are also crystalline porous materials; their typical formula is $M_3^{II}[M^{III}(CN)_6]_2{\cdot}nH_2O$ (M = Fe, Co, Ni, Mn, Cu, Zn, among others). They have received considerable attention in electrochemical devices owing to their diverse morphologies and easily controllable size [25]. MOFs are well-known crystalline porous materials that have been extensively investigated owing to their excellent structural characteristics [26,27]. MOFs are nanoporous materials comprising metal ions and organic ligands, which have been explored widely in a broad range of fields, such as water desalination, imaging, gas storage and separation, catalysis, drug delivery, capacitive sensor, and so on [28–32]. Their high porosity and a large surface area provide numerous Faradaic redox centers [33]. They are also perfect precursors and sacrificial templates for fabricating various derivatives such as nanoporous carbon, metal oxides, metal hydroxides, and mixed metal oxides [34,35]. With the addition of specific materials to MOFs, MOF composites have been developed for application in supercapacitors.

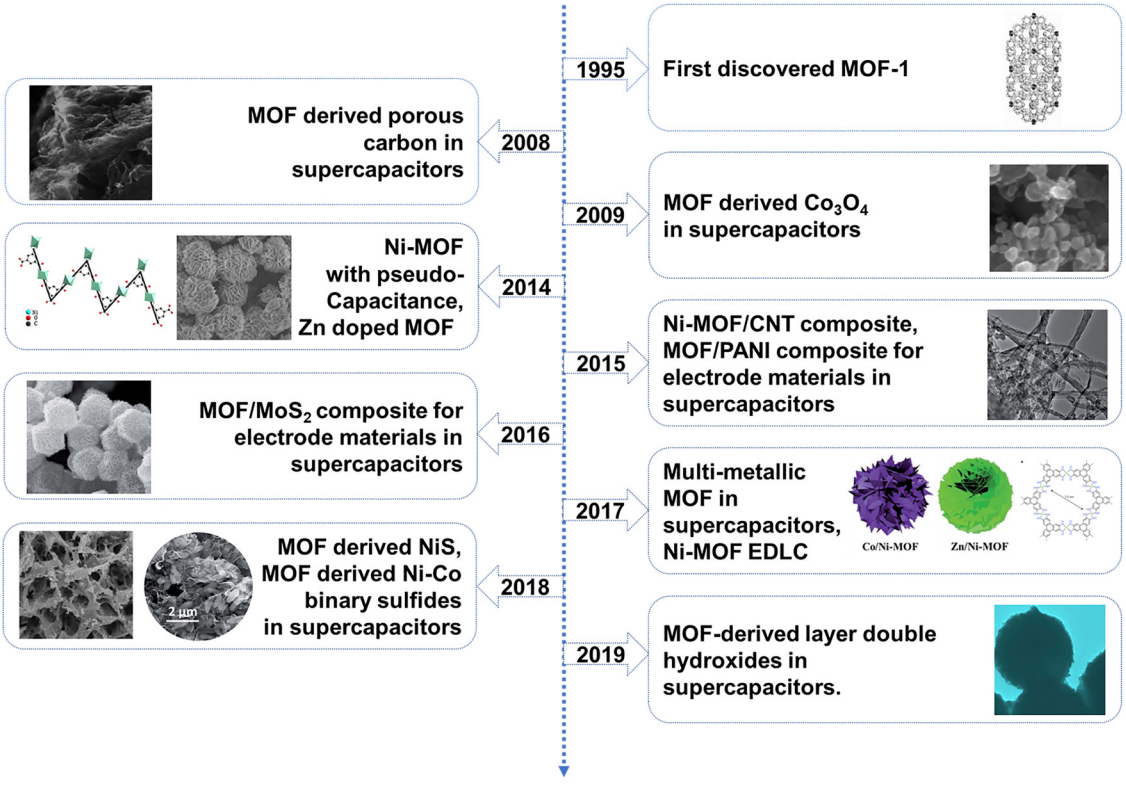

Scheme 1: The timeline of key research about MOFs in supercapacitors.

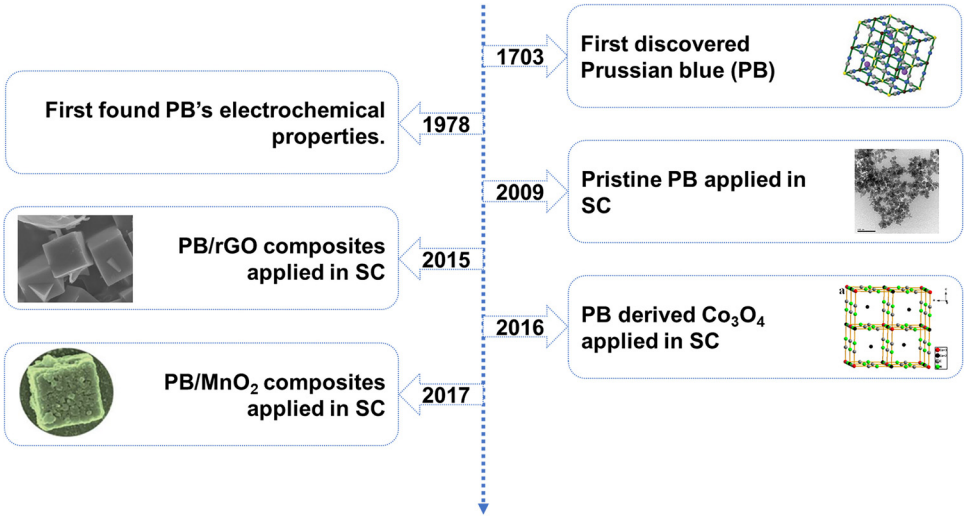

Scheme 2: The timeline of key research about PB/PBA in supercapacitors.

In this review, we mainly report typical research progress on framework materials in supercapacitor applications. The timeline of breakthrough for framework materials in supercapacitors is illustrated in Schemes 1–3 [36–61]. The current issues of frameworks materials, their derivatives, and their composites in the field of supercapacitors, as well as possible future development directions, are also summarized.

2 MOFs

Metal–organic frameworks (MOFs) are important crystalline and porous, organic–inorganic hybridized materials with a periodic network structure [62]. Most of them comprise metal ions or metal ion clusters and organic ligands that are usually connected through coordination bonds, metallic bonding, auxiliary hydrogen bonds, or van der Waals force interaction [13,34,63]. This perfect framework was first observed and constructed by Yaghi *et al.* in 1995 [36,64]. Based on their previous work, more functional and porous MOFs were synthesized. Owing to their controllable pore sizes, tunable chemical compositions, lower steric hindrance, remarkable electrolyte penetrability, and metal ions with redox activities, MOFs have become promising electrode materials for supercapacitors [3,65]. Compared with traditional porous materials, MOFs possess the advantages of a large specific surface area (SSA), various scaffold structures, and abundant active sites [13,66]. However, the electrical conductivity of MOFs is inferior to that of carbonaceous materials owing to their ordered network constructed *via* coordination bonds, which

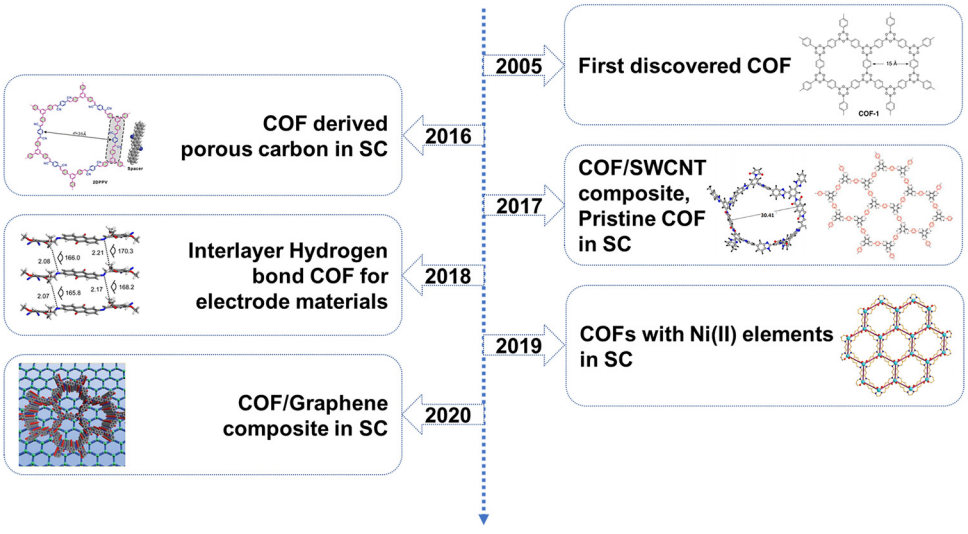

Scheme 3: The timeline of key research about COFs in supercapacitors.

hinders their application in supercapacitors. Therefore, the application of MOFs in supercapacitors can be classified into three categories. (i) pristine MOFs can be utilized as new electrode materials by adjusting their morphologies, nanometer sizes, and areas of the active material [67,68]. (ii) MOFs can be utilized as templates to prepare nanoporous carbons, metal oxides, metal hydroxides, metal sulfides, among others [69,70]. (iii) Some functional materials, carbon materials, metal or metal compounds, conductive polymers, and other unique metal compounds are widely used to compound with MOF to prepare composites with excellent electrochemical performance and cycling stability [71].

2.1 Pristine MOFs

2.1.1 Monometallic MOF

The limited electrical conductivity of pristine MOFs considerably hinders their application in supercapacitors [72,73]. High-performance electrode materials, especially conductive nickel-based MOFs, are outstanding candidates for design and synthesis to obtain unique pristine MOFs that can deliver great conductivity and cycling stability [74,75]. Sheberla *et al.* prepared conductive Ni-MOF $Ni_3(HITP)_2$ (HITP = 2,3,6,7,10,11-hexaiminotriphenylene) as electrode materials through the coordination interaction between Ni ions and HITP ligands without any conductive additives or other binders. This research demonstrated the special performance of conductive Ni-MOF with a favorable areal capacitance value of 18 μF cm^{-2} at 0.05 A g^{-1} and outstanding electrochemical stability, retaining 90% of the initial values after 10,000 cycles [61]. Novel one-dimensional (1D) Ni-MOF nanorods ($[Ni(HOC_6H_4COO)_{1.48}(OH)_{0.52}{\cdot}1.1H_2O]$) with uniform morphology were successfully fabricated by Xu *et al.* under mild conditions [76]. In 6 M KOH, the Ni-MOF presented 1,698 F g^{-1} at 1 A g^{-1}. Meanwhile, a promising cyclic retention of 94.8% was achieved over 1,000 cycles. Furthermore, in an assembled hybrid supercapacitor (HSC)—Ni-MOF//graphene, the HSC showed 166 F g^{-1} at 1 A g^{-1}, exhibiting a promising capacitive property. Jiao *et al.* designed a special HSC that assembles Ni-MOF with CNTs-COOH in a solution with 3 M KOH and 0.1 M $K_4[Fe(CN)_6]$, delivering 55.8 W h kg^{-1} and a power density of 7,000 W kg^{-1} [77]. These favorable performances can be ascribed to Ni-MOF that utilizes the redox reaction to store energy, exhibiting a large surface area, high porosity, and owe a unique 1D chain structure.

A hexagonal Ni-MOF (denoted as [Ni(HBTC)(4,4′-bipy)]) (HBTC = 1,3,5-benzenetricarboxylic acid, 4,4′-bipy = 4,4′-bipyridine) material was fabricated by Li *et al.* through a one-pot hydrothermal method [78]. They observed that the (001) crystal plane displays an outstanding structure for electron transport and electrolyte ion diffusion. In addition, the cross-inked mesh and porous nanostructure coating on the crystal plane (001) also facilitated the diffusion and storage of electrolyte ions compared with the crystal plane (100), indicating ideal electrochemical performance for supercapacitors (Figure 1a). From the scanning electron microscope (SEM) images, the Y3 sample displayed a clear mesh structure (Figure 1b). Hence, the electrode fabricated with Ni-MOF in the Y3 sample exhibited 977.04 F g^{-1} at a current density of 0.5 A g^{-1} as well as 92.34% capacitance retention over 5,000 cycles (Figure 1c). Galvanostatic charge/discharge (GCD) curves of Y1-5 samples at 0.5 A g^{-1} indicated that the Y3 sample was superior to the other four, demonstrating perfect cycling stability. Moreover, the constructed asymmetric supercapacitor (ASC) manifested an outstanding energy density value of 55.26 W h kg^{-1} with 362.50 W kg^{-1} power density, while maintaining 33.98 W h kg^{-1} with 3624.87 W kg^{-1}. Its excellent performances were ascribed to its layered framework structure, the (001) crystal plane, and cross-linked nanoporous nanostructure coating on the (001) crystal plane.

Apart from Ni-MOF, Co-MOF is also of great interest owing to its conjugate π bonds, excellent electrolyte penetrability, controllable functionality, and lower steric hindrance, which makes it a good solution to conductivity and stability problems [79]. Sanati *et al.* fabricated a new Co-MOF (Co (II)-TMU-63, $\{[Co_3(\mu4\text{-tpa})_3(\mu\text{dapz})(DMF)_2]{\cdot}2DMF\}_n$, H_2tpa = terephthalic acid, dapz = pyrazine-2,5-diamine), and an assembled Co(II)-TMU-63//AC device was successfully built. It was tested in a 2 M KOH electrolyte; the specific capacitance of this electrode material was up to 384 F g^{-1} at 6 A g^{-1}, while maintaining approximately 90% of the original values over 6,000 charge–discharge cycles [80]. Liu *et al.* obtained a layered Co-LMOF that exhibited a specific capacitance of 2,474 F g^{-1} at 1 A g^{-1} and 94.3% retention over 2,000 cycles [81]. These reports demonstrate that a high-performance specific capacitance may have a trade-off with high stability and *vice versa*. Typically, EDLC materials have long cyclic lives, high power, and low capacitance performances. Some frameworks with pseudocapacitive properties usually deliver higher capacitance values but a slightly shorter cycling life than their EDLC counterparts [82]. To obtain MOFs with both high-performance capacitance and high cycling stability, Zheng *et al.* prepared an ultrathin two-dimensional (2D) Co-MOF nanosheet ($Co_2(OH)_2BDC$, BDC = 1,4-benzenedicarboxylate) by controllable one-pot facile hydrothermal preparation methods (Figure 1d) [83].

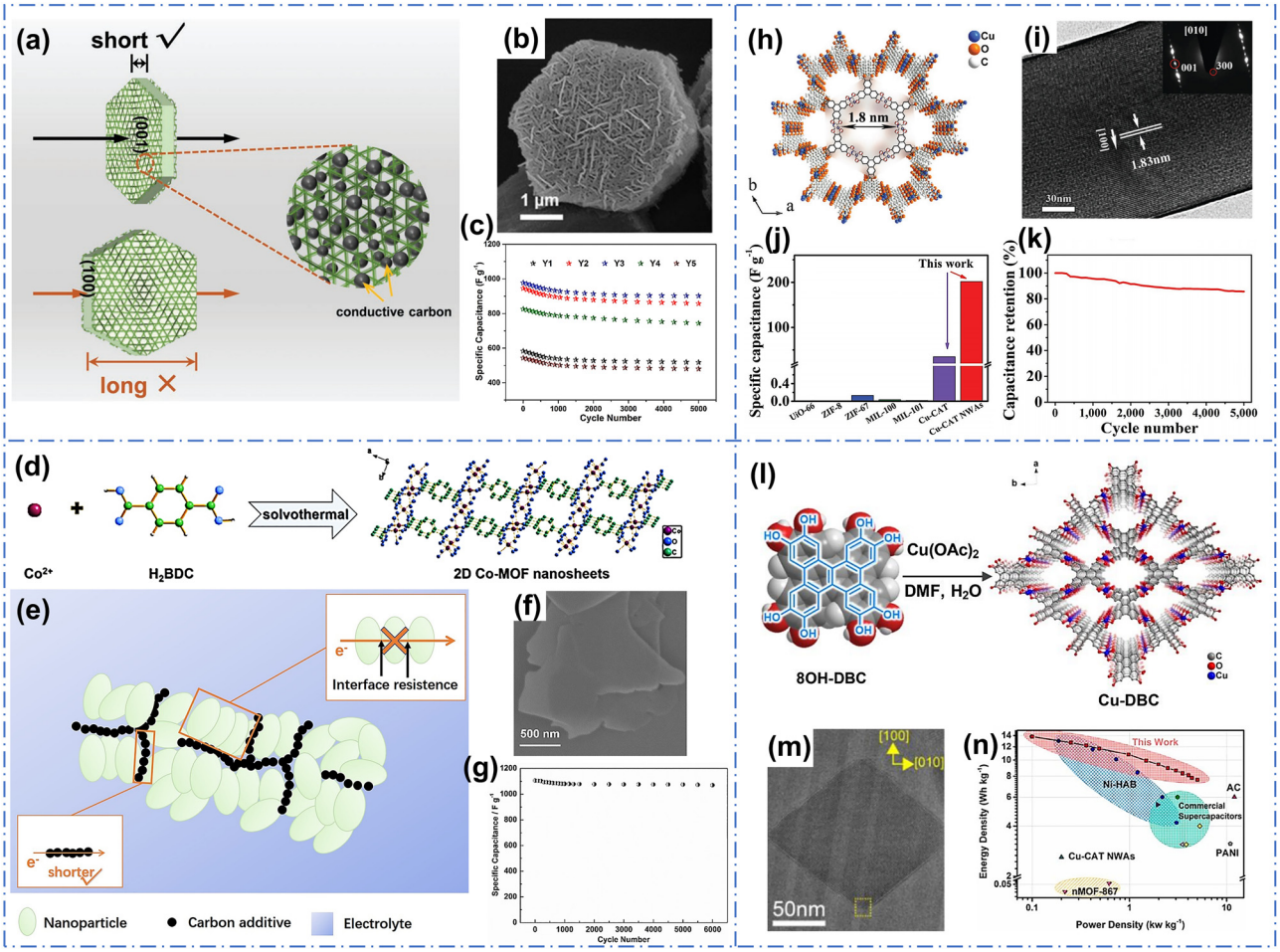

Figure 1: (a) Schematic illustration of charge transfer process on (001) and rectangular crystal planes, respectively. (b) SEM image of hexagonal Ni-MOF Y3 sample. (c) Cyclic performance of hexagonal Ni-MOF Y1-5 samples at 0.5 A g^{-1}. Reproduced with permission from [78]; Copyright 2019, Wiley. (d) The preparation of ultrathin 2D Co-MOF nanosheets. (e) Schematic illustration of the length of electron transportation in nanoparticle-based electrode. (f) SEM image of ultrathin 2D Co-MOF nanosheets. (g) Cycling performance of ultrathin 2D Co-MOF nanosheets at a current density of 2.0 A g^{-1}. Reproduced with permission from [83]; Copyright 2019, Elsevier. (h) Crystal structure of Cu–CAT viewed along the *c*-axis. (i) TEM image of Cu–CAT nanowire (insets: SAED pattern). (j) Comparison of the specific capacitances of the electrodes. (k) Cycling performance of Cu–CAT NWA-based supercapacitor. Reproduced with permission from [85]; Copyright 2017, Wiley. (l) Schematic illustration of the synthesis process of Cu-DBC. (m) HRTEM image taken along *c*-axis. (n) Energy density and power density of comparison with other reported materials. Reproduced with permission from [86]; Copyright 2019, Wiley.

The SEM image showed that the ultrathin Co-MOF had a more regular and larger layered structure than the bulk and micro–nano samples (Figure 1f), which could offer numerous redox-active sites for the rapid surface redox reaction and display desirable pseudocapacitive behaviors. Owing to the ultrathin structure of the 2D Co-MOF, its conductivity could be enhanced when mixed with carbon additives (Figure 1e). When fabricated with ultrathin 2D Co-MOF and tested in 3 M KOH, this electrode showed 1,159 F g^{-1} at 0.5 A g^{-1} and maintained at 96.7% during 6,000 cycles, where the electrode capacity changed from 1,106 to 1,070 F g^{-1} at 2.0 A g^{-1} (Figure 1g). These behaviors could be ascribed to the ion-exchange mechanism. Furthermore, an aqueous device with three different morphologies (ultrathin, micro–nano, and bulk) of Co-MOFs (positive) and active carbon (AC) (negative) was constructed. The ultrathin morphology delivered the best electrical performance in the ultrathin sample compared with the other two samples. Their research also proved that ultrathin 2D nanomaterials are promising novel nanomaterials owing to their excellent electrochemical properties [84]. The research in MOFs with unique ultrathin morphologies is reasonable.

Designing and synthesizing unique MOFs with other metal ions may also improve the conductivity of pristine MOFs. Conductive MOF Cu-CAT nanowire arrays (NWAs) were fabricated by Li *et al.* for the first time [85]. These

NWAs were constructed *via* the coordination between Cu ions and ligands HHTP (HHTP = 2, 3, 6, 7, 10, 11-hexahydroxytriphenylene), forming honeycomb-like porous structures (Figure 1h). Numerous oriented and high-density nanowires homogeneously wholly covered the fibers and formed a uniform hexagonal top facet and hexagonal-prism shape. This could facilitate the transportation of electrolyte solutions to realize high-rate behaviors. HRTEM image and SAED revealed the single-crystal features of NWAs (Figure 1i). In the 3 M KCl solution, the electrode fabricated using Cu-CAT NWAs could exhibit 202 F g^{-1} at 0.5 A g^{-1} compared with other well-known low-conductivity MOF materials (Figure 1j). It also maintained 80% of the initial values after 5,000 cycles. Moreover, a solid-state supercapacitor based on Cu-CAT NWAs shows perfect stability, retaining more than 85% of its initial value after 5,000 cycles (Figure 1k). Liu *et al.* prepared a new conductive Cu-MOF (Cu-DBC) based on linker 8OH-DBC (8OH-DBC = dibenzo[*g*,*p*]chrysene-2,3,6,7,10,11,14,15-octaol) (Figure 1l) [86]. High-resolution transmission electron microscopy (HRTEM) image displayed a uniform microcrystalline structure, indicating its high crystallinity and perfect orbital interaction (Figure 1m). Owing to the perfect orbital interaction between Cu ions and 8OH-DBC, these Cu-MOFs could possess excellent chemical stability. Hence, Cu-DBC could be used in nonflammable and low-cost aqueous electrolytes compared with other traditional MOFs. In 1 M NaCl solution, its gravimetric capacitance calculated from the discharge curve was 479 F g^{-1} at 0.2 A g^{-1}. The electrode materials also maintained 72% of their initial capacity during 2,000 cycles, even at 5 A g^{-1}. Moreover, the assembled symmetric solid-state supercapacitor based on Cu-DBC electrodes exhibited 13.8 W h kg^{-1} energy density with 0.1 kW kg^{-1} power density and maintained 7.6 W h kg^{-1} under 5.0 kW kg^{-1} (Figure 1n). This indicated that supercapacitors based on Cu-DBC frameworks possess promising energy density and power density as well as better electrochemical performance than other reported conductive MOFs.

2.1.2 Multimetallic MOF

The design and construction of monometallic MOFs with unique structures have received significant attention [87]. However, monometallic MOFs still have shortcomings, such as low specific capacitance values and unsatisfactory stability. Hence, the design and fabrication of multimetallic MOFs as electrode materials is an effective and outstanding strategy for addressing these problems [88]. Multimetallic MOFs, also denoted as mixed metal–organic frameworks, embedded various central metal ions into the same framework structure. This not only enhances the stability of the pristine MOF structure but also improves the framework stability and the tuning of breathing behavior, thereby delivering better performance compared to that of monometallic MOFs [89,90]. To develop multimetallic

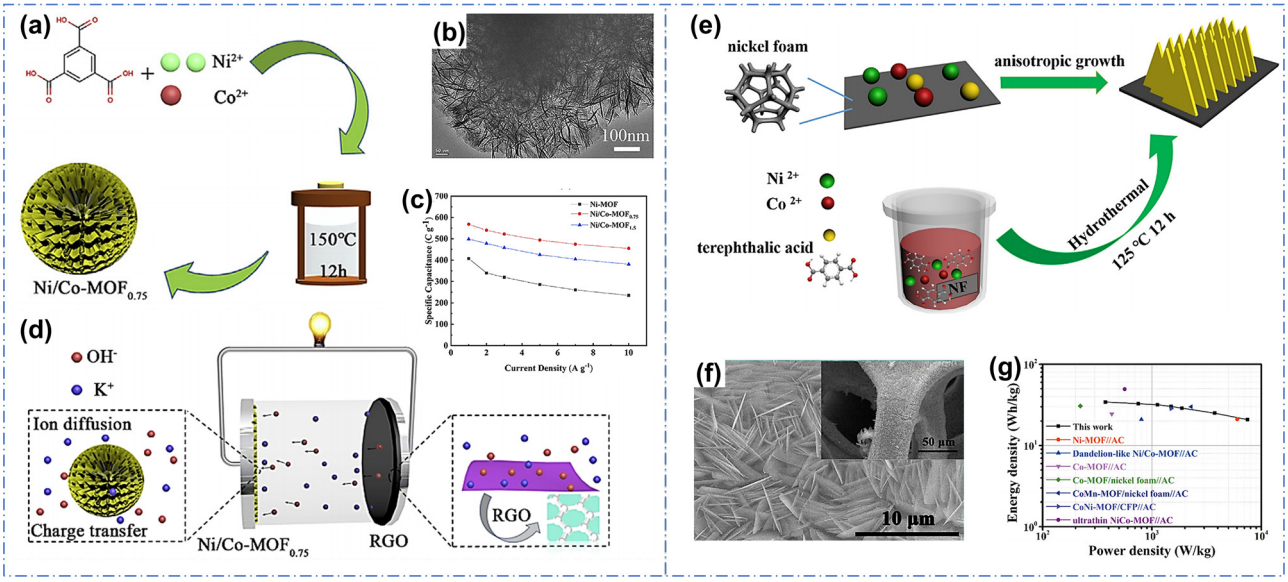

Figure 2: (a) Schematic illustration of the synthetic process of the Ni/Co-MOFs. (b) SEM image of Ni/Co-$MOF_{0.75}$ sample. (c) Comparison of specific capacitances of MOFs. (d) Electrode design of the present ASC. Reproduced with permission from [91]; Copyright 2020, Elsevier. (e) Schematic illustration of the formation of 3-2 NiCo-MOF nanosheets arrays on nickel foam. (f) SEM image of 3-2 NiCo-MOF/NF. (g) Ragone graphs of the 3-2 NiCo-MOF/NF//AC device. Reproduced with permission from [92]; Copyright 2019, Elsevier.

MOFs, two or more different metal ions can be incorporated into the same frame structure. This would provide MOFs with additional degrees of structural stability and endow them with new behaviors [60]. However, research on multimetallic MOFs in the field of supercapacitors remains largely unexplored, which may become one of the breakthroughs in improving the electrochemical performance of supercapacitors.

In the recent research, Ni/Co-MOFs have exhibited uniform size, oriented morphology, and ordered distribution, which could enhance their electrochemical performance [93]. To explore their applications, Zhang *et al.* synthesized a lamellae-like Ni/Co-MOF through a facile hydrothermal route (Figure 2a) [91]. With the combination of multimetallic components and special lamellae-like nanostructures, the fabricated Ni/Co-$MOF_{0.75}$ displayed a significant improvement in capacitance values and cycling stability. The morphology analysis indicates the ultrathin nanosheets, which are conducive to its electrochemical properties (Figure 2b). The specific capacitance of this electrode was 568.0 C g^{-1} at 1.0 A g^{-1} (Figure 2c), along with the 75.5% initial values remaining after 3,000 cycles. In an assembled ASC based on this electrode material with the reduced graphene oxide (rGO) (Figure 2d), this device delivered excellent cycling performance, with 82.6% capacitance retained during the 10,000 cycling tests. It also delivered 42.24 W h kg^{-1} along with a power density of 800 W kg^{-1}. Bu and coworkers also prepared Ni/Co-MOF (Ni/Co-terephthalic acid/NF) nanosheet arrays on conductive substrates *via* a facile one-step synthesis method (Figure 2e) [92]. According to the SEM image, the 3-2 NiCo-MOF (Ni:Co = 3:2) displayed a triangle-like nanosheet morphology and completely covered the nickel foam surface (Figure 2f). This could produce a three-dimensional (3D) shape network with numerous open spaces, making more efficient and faster ion charge transfer and electron transport possible. When tested in 6 M KOH solution, the 3-2 NiCo-MOF sample preserves 1003.5 C g^{-1} (2,230 F g^{-1}) at 1 A g^{-1}. In a hybrid supercapacitor (assembling Ni/Co MOF with AC), this device exhibited 34.3 W h kg^{-1} energy density under 375 W kg^{-1} power density and 20.83 W h kg^{-1} energy density with 7.50 kW kg^{-1} power density values (Figure 2g). Remarkably, this HSC maintained approximately 75.2% of the initial capacitance values during 6,000 cycles.

Remarkable works on pristine MOF as electrode materials for supercapacitors are listed in Table 1.

2.2 MOF derivatives

The relatively poor conductivity and chemical stability of pristine MOFs still hinder the further application of MOFs in supercapacitors. To address these issues, using MOFs as precursors to derive carbon materials or metal compounds, such as metal oxides, hydroxides, sulfides, among others, is a favorable strategy. These MOF derivatives display satisfactory porous properties, unique morphologies, and tunable and controllable chemical compositions [17,59]. These outstanding behaviors could further enhance the capacitance values, couductivity, and stability of MOF derivatives. For example, the MOF-derived metal oxides, hydroxides, or sulfides exhibited superior capacitance values, along with promising capacitance retentions.

Table 1: Selected pristine MOFs for supercapacitors

Samples	Electrolyte	SC	CR (%/cycles)	ED/PD	Ref.
$Ni_3(HITP)_2$	1 M $TEABF_4$/ACN	18 μF cm^{-2} (0.05 A g^{-1})	90/10,000 (2 A g^{-1})	—	[61]
$[Ni(HOC_6H_4COO)_{1.48}(OH)_{0.52}{\cdot}1.1H_2O]$	6 M KOH	1,698 F g^{-1} (1 A g^{-1})	94.8/1,000 (1 A g^{-1})	—	[76]
$[Ni_3(OH)_2(C_8H_4O_4)_2{\cdot}(H_2O)_4]{\cdot}2H_2O$	3 M KOH/0.1 M $K_4[Fe(CN)_6]$	175.3 mA h g^{-1} (1 A g^{-1})	93/3,000 (10 A g^{-1})	55.8/7,000	[77]
Ni(HBTC)(4,4′-bipy)	3 M KOH	977.04 F g^{-1} (0.5 A g^{-1})	92.34/5,000 (0.5 A g^{-1})	33.98/ 3264.87	[78]
$\{[Co_3(\mu4\text{-tpa})_3(\mu dapz)(DMF)_2]{\cdot}2DMF\}_n$	2 M KOH	384 F g^{-1} (6 A g^{-1})	90/6,000 (12 A g^{-1})	24.13/4,420	[80]
$(\{[Co(Hmt)(tfbdc)(H_2O)_2]{\cdot}(H_2O)_2\}_n$	1 M KOH	2,474 F g^{-1} (1 A g^{-1})	94.3/2,000 (2 A g^{-1})	—	[81]
$[Co_2(OH)_2BDC]$	3 M KOH	1,159 F g^{-1} (0.5 A g^{-1})	96.7/6,000 (2 A g^{-1})	—	[83]
Cu-CAT	3 M KCl	202 F g^{-1} (0.5 A g^{-1})	85/5,000 (50 mV s^{-1})	≈2.6/≈200	[85]
Cu-DBC	1 M NaCl	479 F g^{-1} (0.2 A g^{-1})	80/2,000 (5 A g^{-1})	7.6/5,000	[86]
$NiCo\text{-}MOF_{0.75}$	2 M KOH	568 C g^{-1} (2 A g^{-1})	82.6/6,000 (10 A g^{-1})	42.24/800	[91]
3-2 NiCo-MOF/NF	1 M KOH	2,230 F g^{-1} (1 A g^{-1})	75.2/6,000 (1 A g^{-1})	20.83/7,500	[92]

Abbreviations: SC, specific capacitance; CR, capacitance retention; ED, energy density; PD, power density.

Moreover, the addition of some functional materials could compensate their disadvantages and enhance electrochemical performances.

2.2.1 Porous carbon

Nanoporous carbon is an excellent supercapacitor candidate owing to its optimized pore size distributions, perfect thermal and physiochemical stability, high surface area, and low cost for regeneration [94,95]. These advantages offer a shorter pathway for the diffusion of electrolyte solutions, buffering the volume charge during the cycling process and obtaining more electrochemically active sites for the adsorption and desorption of electrolyte ions [96]. Hence, designing and synthesizing nanoporous carbon materials as electrode materials for supercapacitors is necessary. In the previous research, MOFs possessing high SSAs and highly customizable pore structures have been explored as perfect templates for preparing carbon materials to support capacitive active materials [97,98]. MOF-derived carbon materials have attracted significant attention owing to their controllable morphologies and pore structures [99]. The porous carbon derived from MOFs can possess abundant nanoscale cavities and provide larger surfaces for electron desorption–adsorption as electrode materials for supercapacitors [100].

To further study MOF-derived porous carbon materials, Qian *et al.* chose a zinc-organic framework as a precursor to prepare robust cage-based mesoporous carbon materials (BMM-9) through carbonization at high temperatures [101]. BMM-9-900 (calcinated at 900°C) exhibited 182.8 F g^{-1} at 1.0 A g^{-1}, and the stability texts showed that BMM-9-900 retained 98.5% initial values at 10 A g^{-1} during 1,000 cycles. Khan *et al.* utilized MOF-5/AC as a soft template to derive carbon nanospheres *via* carbonization at 850°C, exhibiting 300 F g^{-1} at 1.5 A g^{-1} along with 91.5% capacitance values retained during 3,000 charge–discharge cycles [102]. Recently, some researchers observed that nitrogen doping in carbon materials can improve the surface polarity and humidity, ultimately optimizing the electrical conductivity, which could also improve specific capacitance [103–105]. Tang *et al.* prepared flexible 3D N-doped porous carbon bubbles (CTAs@NCBs) connected *via* carbon tube arrays derived from a ZnO@ZIF-8 nanoarray template [106]. This material-assembled supercapacitor yielded an areal capacitance of 580 mF cm^{-2} in 1 mA cm^{-2}, and 98.5% of its initial capacitance remained over 10,000 cycles. This could be ascribed to its structural characteristics because it possessed excellent ionic conductivity and a high surface area.

Although porous carbon derived from MOFs has attracted increasing attention, partial breakdown in the initial MOF structure during the carbonization and annealing processes cannot be completely avoided. This results in a decrease in the surface area and redox-active sites, limiting the conductivity of the as-prepared nanoporous carbonaceous materials and their rate performance [108]. To solve the problems, Wang *et al.* fabricated a unique porous carbon possessing a "brick-and-mortar" sandwiched structure by using MOF-5-derived nanoporous carbon film as "mortar" and the graphene nanosheets as "brick" (Figure 3a) [107]. This porous carbon material (denoted as C-GMOF) remained a layered structure, and TEM analysis confirmed the formation of this morphology (Figure 3b). A sandwich-shaped structure with a superior surface area was conducive for convenient electron transportation with less transport length and charge storage. In an electrochemical test, the GCD curve was almost linear and symmetrical, indicating its excellent reversibility (Figure 3c). This C-GMOF-based electrode material exhibited 345 F g^{-1} at 2 mV s^{-1}, along with 201 F g^{-1} at 2 V s^{-1}, which was relatively higher than other materials (Figure 3d). Furthermore, the specific capacitance remained at 99% of its initial values after 10,000 cycles (Figure 3e), suggesting its outstanding cycling stability.

2.2.2 Metal oxides

Metal oxides, especially transition metal oxides (TMOs), have attracted considerable attention in the scientific community as electrode materials in supercapacitors owing to their high electrochemical response, perfect electrical conductivity, low manufacturing costs, large SSA, and easy processability [109,110]. TMOs such as Co_3O_4, NiO, RuO_2, Mn_2O_3, Fe_2O_3, and some binary transition metal oxides have already been extensively researched for application in supercapacitors [111]. Among these TMOs, Co_3O_4, whose theoretical specific capacitance can reach up to 3,560 F g^{-1}, is one of the most widely utilized oxides in electrode materials for supercapacitors [112,113]. Previous research has demonstrated that Co_3O_4 can be obtained *via* the calcination of ZIF-67 precursors [114]. However, approaching the theoretical capacitance of Co_3O_4 is still difficult, which limits its application in supercapacitors considerably [115]. To improve their capacity and cycling performance, Li *et al.* prepared nanoporous Co_3O_4 nanotubes by calcining nanoscale Co-MOF-74 crystals at 350°C [116]. A hexagonal cuboid morphology was achieved during the annealing process. In the electrochemical tests with 2 M KOH electrolyte, Co_3O_4-350 presented 647 F g^{-1} at 1 A g^{-1}, and there was no obvious decrease

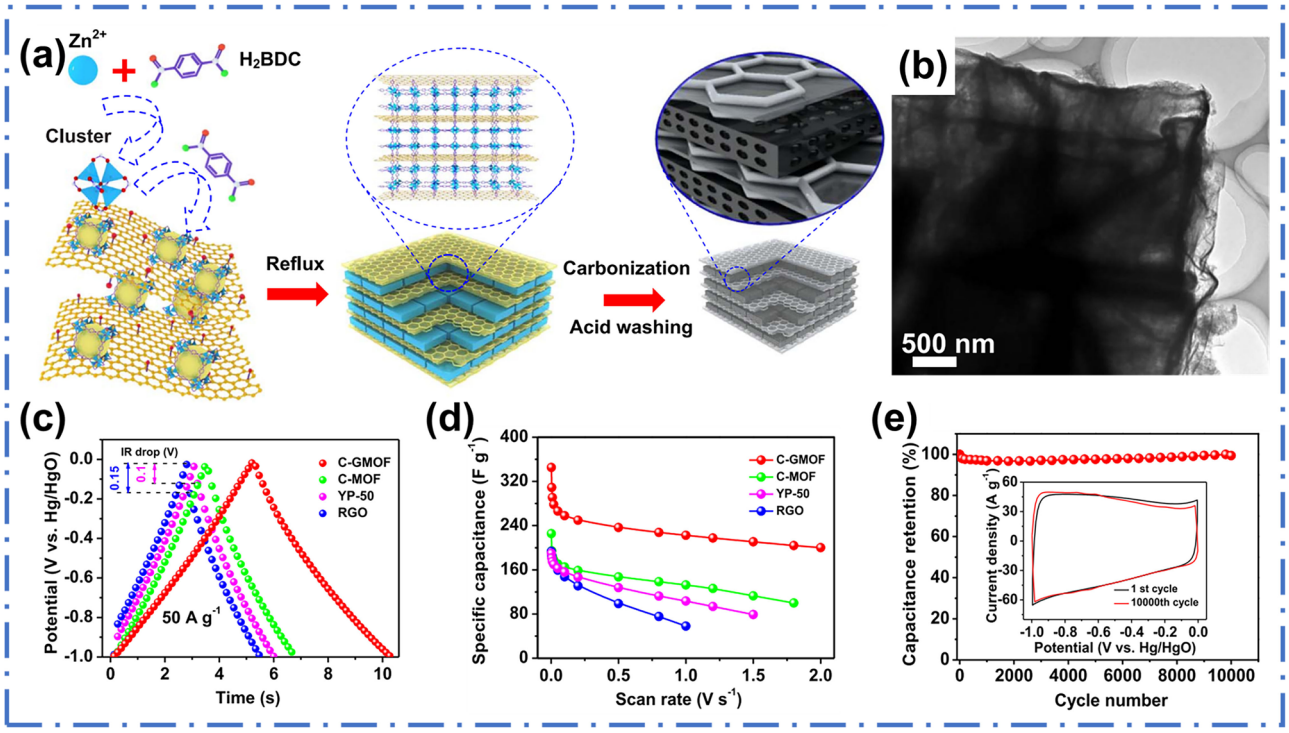

Figure 3: (a) Schematic illustration of the fabrication process for porous carbon building using MOFs and GO as precursors. (b) TEM image of the C-GMOF. (c) GCD curves of the C-GMOF, C-MOF, YP-50, and RGO at 50 A g^{-1}. (d) Specific capacitances of the C-GMOF, C-MOF, YP-50, and RGO at various scan rates. (e) Cycling performance of the C-GMOF at 200 mV s^{-1}, and the inset shows CV curves before and after 10,000 cycles. Reproduced with permission from [107]; Copyright 2016, Elsevier.

during the 1,500 cycles tests in 2 A g^{-1}. Liu *et al.* fabricated dodecahedral $NaBH_4$-reduced Co_3O_4 (R-Co_3O_4) through a conformal transformation route [117]. In their work, $NaBH_4$ was used to modify the surface state of Co_3O_4 that displayed a dodecahedral morphology, uniform dimensions, and rhombic dodecahedron morphology. This resulted in a capacitance of 329 F g^{-1} at 1 A g^{-1}, and 92% of the original values were retained during 1,000 cycles.

Although Co_3O_4 has emerged as an excellent electrode material, researchers still observed that it has limitations such as low ionic diffusivity, lack of outstanding electron conductive routes, and drastic volume expansion [75]. The incorporation of conductive substrates such as graphene or carbon cloth is a promising solution to these problems [118]. Vilian *et al.* incorporated rGO onto MOF-derived Co_3O_4 *via* a hydrothermal route [119]. In this work, Co_3O_4 has a hexagonal sheet-like structure, which assists in the electron accessibility of the electrode materials. The rGO-Co_3O_4 delivered 1,300 F g^{-1} and 80.5% of its original capacitance over 5,000 cycles in 4 M KOH at 4 A g^{-1}. Furthermore, the assembled ASC exhibited 65.8 W h kg^{-1} energy density values under a 2.05 kW kg^{-1} power density. Yin *et al.* prepared Co-MOF-derived Co_3O_4 coated with the NiCo layer double hydroxide (NiCo-LDH) nanosheets on a carbon cloth [120]. They first annealed Co-MOF on a carbon cloth to fabricate derived cobalt oxides and then combined them with NiCo-LDHs to construct hybrid Co_3O_4@NiCoLDH. As calculated from the electrochemical tests, this hybrid showed 1,708 F g^{-1} at 1.0 A g^{-1}, representing 89% of the original capacitance values retained during 4,000 cycles at 10 A g^{-1}. Furthermore, the constructed ASC (assembled with AC) delivered 44.44 W h kg^{-1} energy density under 0.80 kW kg^{-1} power density.

Apart from Co_3O_4, NiO is also a competitive candidate for electrode materials in supercapacitors owing to its rich oxidation states, abundant SSA, low cost, thermal stability, and pronounced electrical properties [121]. NiO delivers perfect capacitive properties, expressing 2,584 F g^{-1} theoretical specific capacitance values [122,123]. Wu *et al.* fabricated Ni-MOF-derived NiO nanospheres *via* a simple solvothermal method [124]. After calcination at 400°C, NiO hollow nanospheres with highly uniform shapes were successfully obtained (denoted as N400) with a core-in-double-shell structure. This N400 sample exhibited promising electrochemical performance with 473 F g^{-1} at 0.5 A g^{-1}, and 94% original values were retained during 3,000 cycles. In an asymmetric supercapacitor based on

N400 and AC (N400//AC), this device exhibited 12.5 W h kg^{-1} energy density along with a power density of 7.5 kW kg^{-1}. Fabricating a hybrid nanocomposite is an effective strategy to further improve their electrical conductivity and obtain the theoretical specific capacitance. Li *et al.* prepared nanorod-composed yolk-shell microspheres derived from Ni/Zn-MOF *via* a simple solvothermal method [125]. In this study, the specific capacitances of the material calculated were 497 F g^{-1} at 1.3 A g^{-1}, along with almost 100% of the original values retained during 2,000 cycles, indicating its excellent cycling performance.

Other monometallic oxides have also been developed for use in electrode materials. Yuan *et al.* fabricated layered δ-MnO_2 nanostructure materials using $[Mn(C_8H_4O_4)\cdot(H_2O)_2]_n$ as a precursor to react with $KMnO_4$ *via* a hydrothermal method [126]. Its specific capacitance can deliver 416 F g^{-1} at 0.5 A g^{-1}. The assembled ASC (MnO_2//AC) exhibited 23.2 W h kg^{-1} with a power density of 425 W kg^{-1}. Owing to its layered nanostructure, access to cations from the electrolyte could be accelerated, thus facilitating promising electrochemical performance. Wang *et al.* synthesized ZnO/C materials by directly transforming MOFs into hollow carbonaceous materials and then reacting them with glucose-derived polymers to form hollow Zn-coated carbonaceous composites [127]. ZnO/C-based electrode materials can deliver 394 F g^{-1} at 1 A g^{-1}, indicating its promising electrochemical performance.

Recently, some binary or mixed metal oxides derived from multimetallic MOFs have been widely investigated owing to their high SSA, unique nanostructure, and richer active sites [128]. In addition, their uniform metal distribution is beneficial for reducing lattice distortion and further enhancing the capacity and cycling stability [129]. MOF-derived mixed metal oxides display noticeable strengths compared with their single pure metal oxide counterparts [130]. Zhang *et al.* utilized an Fe-MOF gel (MIL-100-Fe) as a template to fabricate mesoporous $LaFeO_3$ perovskite nanoparticles [131]. Owing to its mesoporous structure and 2 nm concentrated pore size, this synthesized $LaFeO_3$ showed 241.3 F g^{-1} at 1 A g^{-1}. Furthermore, the all-solid-state symmetric supercapacitor based on $LaFeO_3$ delivered 34 W h kg^{-1} energy density values with 900 W kg^{-1} power density, along with the 92.2% initial values remaining after 5,000 cycles. Functional additives can be incorporated into these binary or mixed metal oxides to further improve their electrochemical performance. Xie *et al.* introduced MXene nanosheets into derived $CoFe_2O_4$ nanorods [132]. This could facilitate charge transfer, maintain its excellent flexibility, and enhance its ion transmission path. In the 1 M LiCl electrolyte, the $CoFe_2O_4$/MXene composite exhibited an excellent volumetric capacity of 2467.6 F cm^{-3}. Moreover, a flexible symmetrical supercapacitor retained 88.2% original values over 10,000 cycles. This indicated its promising application potential in supercapacitors. Yin *et al.* synthesized hollow $NiCo_2O_4$ nanocages grown on a SiC nanowire network/carbon cloth [133]. With unique structural advantages such as a hierarchical porous structure and interwoven conductive networks, this material exhibited a specific capacitance of 1,377 F g^{-1} at 1 A g^{-1} and 88.3% capacitance retention over 6,000 cycles. When assembled with AC as a supercapacitor, this supercapacitor delivered 46.58 W h kg^{-1} energy density with 0.80 kW kg^{-1} power density.

Among the diverse binary metal oxides derived from bimetallic MOFs, nickel–cobalt binary oxides have attracted considerable interest from the scientific community because of their high-power supercapacitor applications. Yu *et al.* prepared a NiO/$NiCo_2O_4$ (1:1) derived from MOF-74-Ni/Co MOF (1:1) (Figure 4a) [134]. The morphology analysis showed that the mixed metal oxide samples all inherited the morphology of their precursors with nanowire shapes (Figure 4b). At different Ni/Co ratios, they observed that the NiO/$NiCo_2O_4$ (1:1) sample displayed a hollow nanowire structure, indicating its porous nature. In this study, the calculated 732.0 C g^{-1} derived from NiO/$NiCo_2O_4$ (1:1) was much higher than of the other samples and monometallic oxides at 1 A g^{-1} (Figure 4c). It also retained 92.5% initial capacitance values at 10 A g^{-1} over 3,000 cycles, proving its excellent stability (Figure 4c). In an asymmetric supercapacitor (NiO/$NiCo_2O_4$ (1:1)//AC), the specific energy density reached 36.6 W h kg^{-1} along with a 6791.8 W kg^{-1} power density, which was much better than the reported values (Figure 6c). Jayakumar *et al.* fabricated $Ni_xCo_{3-x}O_4$ derived from ZIF-67 and then synthesized graphene/NiCo oxide hybrids (GNi:Co) [135]. During the hydrothermal treatment, the GNi:Co (Ni:Co = 1:1) composite hydrogel displayed a highly microporous network with interlinked graphene layers on nanosized Ni/Co particles (Ni:Co ratio of 1:1). The morphology analysis showed that these samples possessed a hollow structure, thus helping to connect the graphene layers (Figure 4d). Owing to the conducive porous network from the surrounding graphene, this material showed better electrochemical performance than other compared counterparts. This GNi:Co 1:1 hydrogel displayed the highest specific capacitances of 2,870 F g^{-1} at 1 A g^{-1} compared with other samples (Figure 4e). Moreover, this material presented a significant enhancement in cycle life, maintaining 81% capacitance retention after 5,000 long cycles (Figure 4f). In an ASC assembled with pure graphene hydrogel, the ASC could provide a higher specific energy density of 50.2 W h kg^{-1} along with 750 kW kg^{-1} power

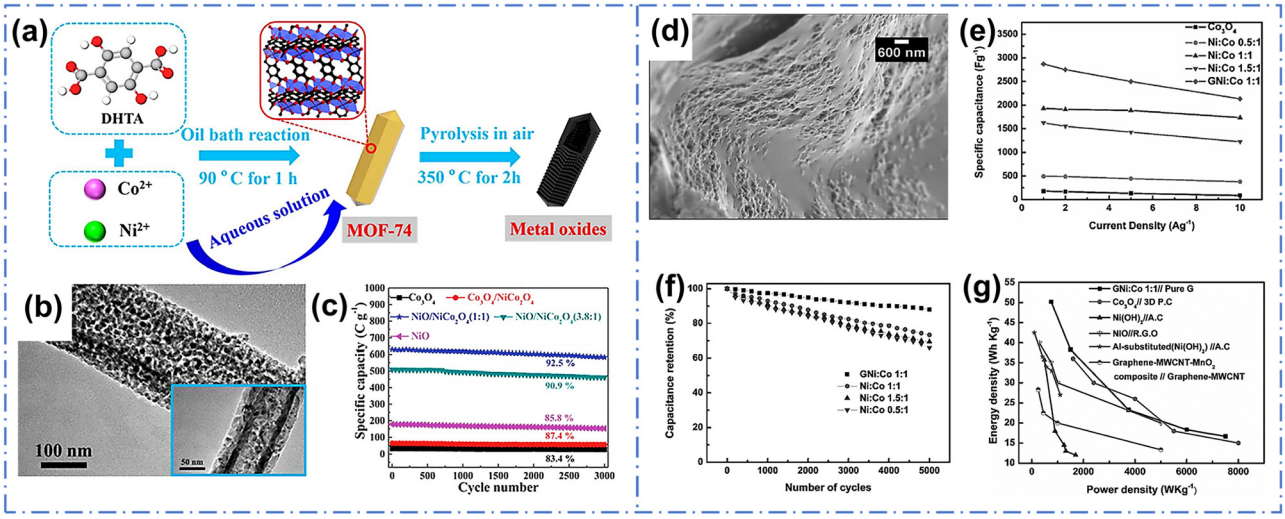

Figure 4: (a) The synthesis process of metal oxides with hollow nanowires. (b) TEM image of an individual NiO/NiCo2O4(1:1) hollow nanowire. (c) Cycling stability at 10 A g^{-1} for 3,000 cycles. Reproduced with permission [134]; Copyright 2018, The Royal Society of Chemistry. (d) SEM image of GNi:Co 1:1. (e) Specific capacitances of samples. (f) Cyclic performances of samples. (g) Ragone Plot of GNi:Co 1:1//Pure graphene with other reported works. Reproduced with permission from [135]; Copyright 2017, Wiley.

density (Figure 4g). These comparisons could be useful in identifying this material for appropriate real-life applications.

2.2.3 Metal hydroxides

In recent years, transition metal hydroxides have been considered as perfect electrode materials owing to their high surface area and ultrahigh theoretical capacitance (3,500–4,600 F g^{-1}) [136]. MOF-derived metal hydroxides are pseudocapacitive materials that can store numerous energies depending on the fast redox reactions that drastically improve energy storage and exhibit much higher discharge capacities than EDLC materials [137,138]. Wu *et al.* synthesized Co/Ni-double hydroxides with a novel wisteria flower-like microstructure on carbon cloth in the $NiSO_4$ solution [139]. This hybrid delivers 929.4 C g^{-1} at 2 mA cm^{-2}. The assembled ASC exhibits 42.5 W h kg^{-1} with 81.5% capacity remaining after 7,500 cycles. Qu *et al.* utilized a classic nickel–cobalt MOF-74 as a precursor to fabricate highly porous double hydroxide (MOF-74-derived double hydroxide, denoted as MDH) *via* a facile alkaline treatment (Figure 5a) [140]. The SEM image showed the formation of nanoscale 65Ni-MDH after KOH treatment of the as-synthesized MOF-74 templates under controlled hydrothermal conditions (Figure 5b). The SSA of MDH reached 299 m^2 g^{-1}. Its superior surface area could be ascribed to its inheritance from the porous nature of pristine MOFs, and the 65Ni-MDH displays promising porous properties. In the electrochemical test, this electrode material displayed 875 C g^{-1} at 1 A g^{-1}, which was better than that of other samples (Figure 5c). The assembled HSC using 65Ni-MDH and N-C as electrodes could retain 91.3% after 10,000 cycles at 13.5 A g^{-1}, and the Faradaic efficiency was close to 100% during the cycling process (Figure 5d). It also showed 81 W h kg^{-1} energy density along with 1.9 kW kg^{-1} power density and maintained 42 W h kg^{-1} under 11.5 kW kg^{-1}.

Many researchers have recently explored MOF-derived LDH. These derivatives exhibit multimetallic hollow structures, enhancing the flow efficiency of ions and reducing the resistance of ion diffusion [142]. Among various LDH materials, Ni/Co LDH exhibits attractive performance, including high theoretical capacitance, rich redox reaction sites, and excellent electronic conductivity [143,144]. However, its easily agglomerated structure greatly hinders its further applications [145,146]. A promising strategy for overcoming this problem involves adjusting the morphology by fabricating a hierarchical structure for instance [147]. Xiao *et al.* utilized a Ni/Co-MOF (with Ni:Co = 7:3) to synthesize LDH with hierarchical microspheres (Figure 5e) [141]. In their work, they constructed hierarchical LDH microsphere structures *via* a controllable alkaline hydrolysis strategy. Owing to the high tunability of MOFs, Ni/Co LDH can have a desirable composition and morphology. Hence, the surface area of the Ni/Co LDH was measured to be 201 m^2 g^{-1}, making it applicable for supercapacitors. In the 1 M KOH solution, the Ni/Co LDH-based electrode material showed 1,652 F g^{-1} at 1 A g^{-1}, presenting almost

100% value after 2,000 cycles. Both these properties are much better than those of other samples (Figure 5f and g). Moreover, an ASC composed of this LDH and AC delivered 32.9 W h kg^{-1}/74.3 W kg^{-1} energy density/power density and maintained 26.0 W h kg^{-1} under 1817.3 W kg^{-1}.

2.2.4 Metal sulfides

Transition metal sulfides have also become one of the most promising candidates for electrode materials in supercapacitors owing to their higher specific

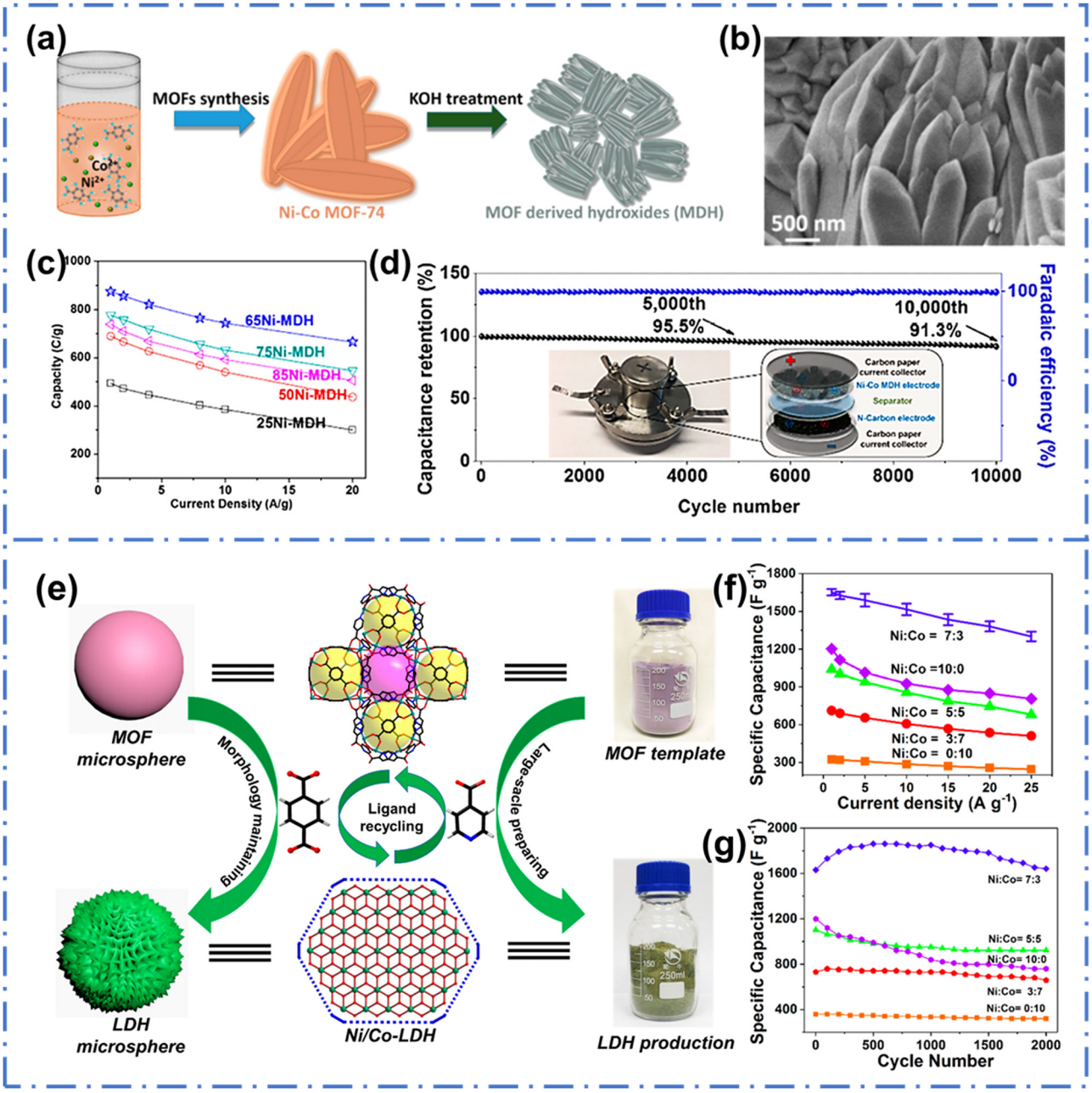

Figure 5: (a) Schematic illustration of MOF-74 converting to Ni–Co MDH. (b) SEM image of 65Ni-MDH. (c) Specific capacity of MDH electrodes with different initial Ni(II)-to-Co(II) ratios. (d) Cycling stability and faradaic efficiency of the 65Ni- MDH//N–C device at 13.5 A g^{-1} for 10,000 cycles. Reproduced with permission from [140]; Copyright 2017, American Chemical Society. (e) Schematic illustration of the synthetic strategy of the Ni/Co-LDH. (f) Specific capacitance of Ni/Co-LDH electrodes at current densities from 1 to 25 A g^{-1}. (g) Cycling performance of the Ni/Co-LDH electrodes at a current density of 5 A g^{-1}. Reproduced with permission from [141]; Copyright 2019, American Chemical Society.

capacitances, higher electrical conductivity, and richer redox reactions than their oxide or hydroxide counterparts [39,148]. Some metal sulfides such as nickel sulfides and cobalt sulfides have attracted considerable attraction as promising candidates of high-performance supercapacitors [149]. However, it is difficult to deliver ideal capacity and cycling stability *via* using single-component forms of those sulfides [150]. To deal with these problems, strategies such as combining carbon-based materials (graphene, carbon nanotubes (CNTs), *etc.*) and other pseudocapacitive materials can improve their conductivity and enhance their cycling stabilities [151,152].

Qu *et al.* reported NiS nanorods combined with rGO derived from a Ni-MOF-74/rGO hybrid (Figure 6a) [38]. In this study, R-NiS/rGO exhibited a remarkable integral area and enriched active sites, implying a significantly improved specific capacitance. The NiS nanorod surfaces in this nanohybrid are very active for rapid redox reactions, indicating their promising pseudocapacitive properties. Moreover, the presence of rGO greatly enhanced its electronic conductivity, providing more efficient current collection for rapid energy storage. In the electrochemical test with 2 M KOH electrolyte, it demonstrated 744 C g^{-1} in 1 A g^{-1} and an impressive capacity retention of 89% over 20,000 cycles (Figure 6b and c). In HSC assembled with R-NiS/rGO and ZIF-8-modified nitrogen-doped graphene aerogel, 54 W h kg^{-1}/46,034 W kg^{-1} energy density/power density was achieved.

Apart from monometallic sulfides, some bimetallic transition metal sulfides also possess better electrochemical activity, more varied stoichiometric chemistry, and richer redox reactions than single-component metal sulfides [154,155]. It was observed that bimetallic metal sulfides express lower kinetic energy barriers, which makes

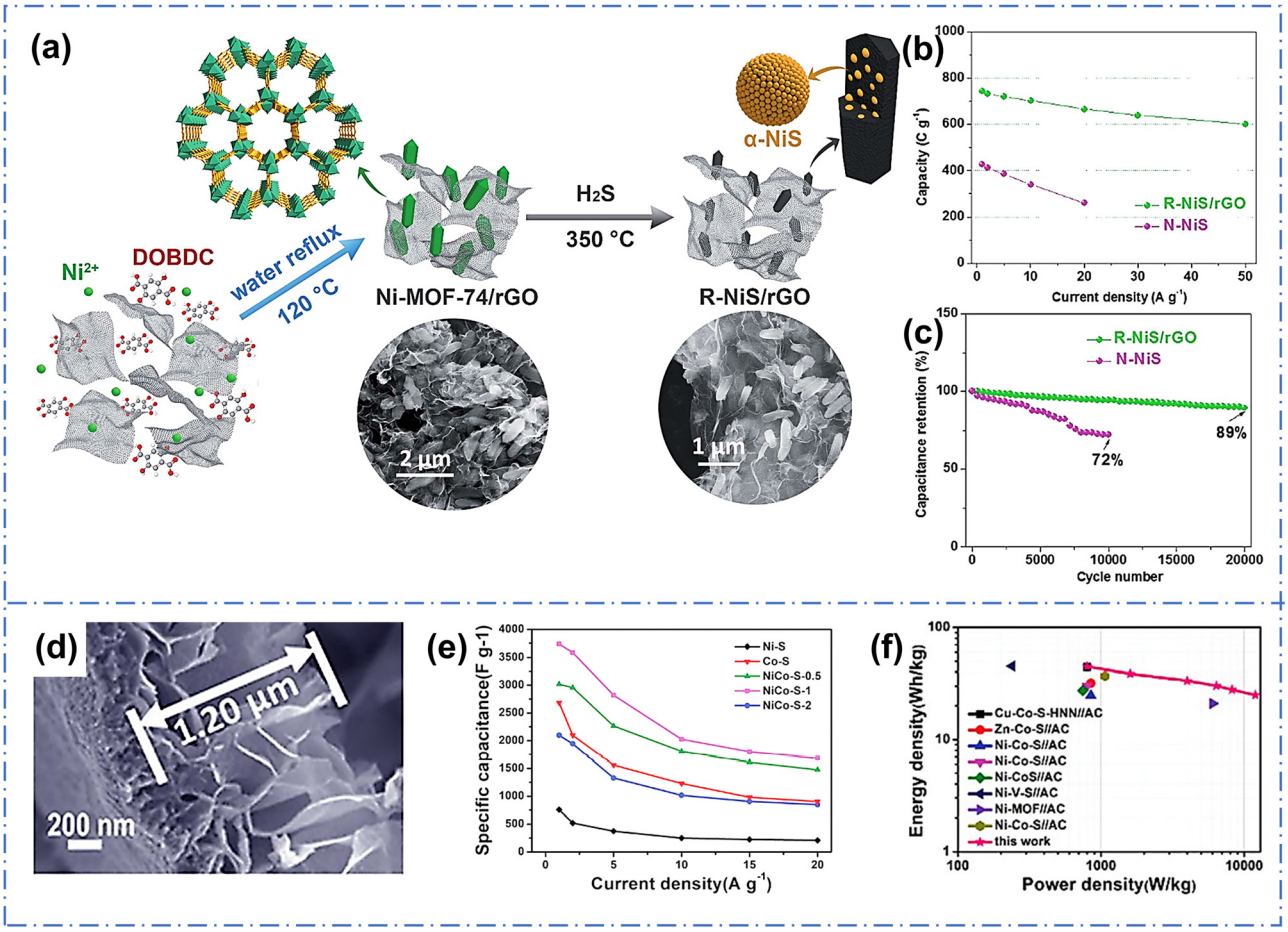

Figure 6: (a) Schematic illustration of the synthesis procedure of the R-NiS/rGO from MOF precursors. (b) Specific capacities of R-NiS/rGO based on different current densities. (c) Cycling performances of R-NiS/rGO and N-NiS. Reproduced with permission from [38]; Copyright 2018, The Royal Society of Chemistry. (d) SEM image of NiCo-S-1 samples. (e) Cycling performance of the NiCo-S-1//AC at 2 A g^{-1}. (f) Ragone plots of the current work and the other related devices. Reproduced with permission from [153]; Copyright 2020, The Royal Society of Chemistry.

their charge transportation more effective than that in monometallic metal sulfides [156]. Zhao *et al.* fabricated porous $NiCo_2S_4$ nanosheet arrays with enriched edge sites on electrochemically activated flexible carbon cloth derived from Co-MOF for the first time [157]. The morphology analysis showed a dense and uniform coverage of the Ni–Co–S nanosheets on the carbon fiber surface. This leads to the formation of the desired hollow and porous structure, thus facilitating the diffusion of electrolyte ions and the insertion and disembedding process in the cycling stability test. This material-based electrode delivered 2,392 F g^{-1} at 1 A g^{-1} and a desirable stability routine with 85.1% capacity retention over 10,000 cycles at 30 A g^{-1}. Furthermore, in an assembled ASC, it exhibited 30.1 W h kg^{-1}/800.2 W kg^{-1} energy density/power density. Zheng *et al.* developed ultrathin NiCo sulfide nanosheet arrays on Ni foam with robust adhesion [153]. Owing to the presence of Ni_3S_2 and $Co(OH)_2$ in the synthesis process, these materials could deliver ultrahigh capacity. The morphology analysis of NiCo-S-1 indicated that its unique structure offers abundant SSA and open channels for electrolyte transportation and penetration (Figure 6d). These properties can reduce the diffusion distance and enhance the electrochemical performance. With its superior structure, this material demonstrated the highest electrochemical performance, delivering an ultrahigh value of 3,724 F g^{-1} at 1 A g^{-1} (Figure 6e). In an assembled NiCo–S//AC supercapacitor, the capacitance retention was stable with 90% retention after 3,000 cycles. The ASC device also showed 44.76 W h kg^{-1}/0.80 kW kg^{-1} energy density/power density and maintained 24.99 W h kg^{-1} at 12.00 kW kg^{-1} (Figure 6f). These results indicate that NiCo–S has excellent potential for application in high-performance supercapacitors.

2.2.5 Other metal compounds

Some metal compounds such as metal selenides, metal phosphides, and nitrile have attracted considerable attention. Transition metal selenides with promising electrochemical activity, promising electronic conductivity, and stability have been investigated for supercapacitor applications [158,159]. Chen *et al.* synthesized porous $CoSe_2$ nanosheets derived from MOFs [160]. Owing to the porous nanostructure of $CoSe_2$, it could express abundant contact interfaces between the electrode and electrolyte, reducing the diffusion path of ions for this fast electrochemical kinetic process. This device showed 713.9 F g^{-1} in 1 mA cm^{-2} accompanying the impressive cycling property that maintained 92.4% initial values in 5 mA cm^{-2} after 5,000 cycles.

Sun *et al.* fabricated bimetallic copper cobalt selenide nanoparticles embedded in N-doped carbon layers (denoted as (CuCo)Se/NC) *via* using CuCo-ZIF as a precursor [161]. Their route involved the fabrication of CuCo-ZIF and the selenization of the as-prepared bimetallic MOF. In the electrochemical tests with 2 M KOH, this hybrid exhibited 121.4 C g^{-1} at 1 A g^{-1}. This is ascribed to the incorporation of Cu elements in CoSe matrix and the combination of N-doped carbon layer. Furthermore, the constructed HSC device based on this hybrid delivered an energy density of 16.3 W h kg^{-1} along with a power density of 155.3 W kg^{-1}. It also possessed an excellent cyclic stability, retaining 96% initial capacity over 5,000 cycles.

Transition metal phosphides have also attracted increasing attention owing to their metalloid nature and perfect electrical conductivity [162,163]. Chu *et al.* fabricated ZnCo phosphide ($Zn_{0.33}Co_{0.67}P$) on Ni foam with a special structure of ZnCo phosphide array [164]. This phosphide electrode delivered 2,115 F g^{-1} at 1.0 A g^{-1} with 83.0% initial values over 7,000 cycles, which is caused by the lower electronegativity of phosphorus. Furthermore, they assembled $Zn_{0.33}Co_{0.67}P$ (positive) with Bi_2O_3 (negative) to form an alkaline supercapacitor. This device delivered 83.05 W h kg^{-1} with a power density of 775.02 W kg^{-1} and a superior power density value of 15642.58 W kg^{-1} along with a 26.94 W h kg^{-1} energy density.

Kshetri *et al.* fabricated MOF-derived cobalt telluride-carbon nanoporous structure composite on nickel foam [165]. The morphology analysis indicated a highly porous nature and a uniform distribution of the constituent elements. This could lead to the unique charge storage process and better electrochemical performances. In this work, the hybrid electrodes delivered an areal capacitance of 307.5 mF cm^{-2} at 20 mA cm^{-2}. Moreover, the assembled symmetric supercapacitor delivered an energy density of 43.84 W h kg^{-1} and a power density 738.88 W kg^{-1}. It also retains 21.95 W h kg^{-1} energy density at a high power density of 6173.44 W kg^{-1}.

Liu *et al.* prepared Ni-doped Co–Co_2N with a heterostructure *via* facial thermal annealing of MOF-derived $NiCo_2O_4$ under an ammonia atmosphere [166]. At different nitridation temperatures, they observed that the sample nitridized in ammonia at 350°C exhibited the best morphology. This made its nanoflakes uniform in morphology, and they grew vertically on the carbon fiber surface, which offered large surface areas for electrolyte ion access. Moreover, its thickness (less than 10 nm) also allows for faster electron transport, enhancing its electrical conductivity. In 1 M KOH, the Ni-doped Co–Co_2N (also denoted as Ni/Co–N-350) delivered 361.93 C g^{-1} at

Table 2: Selected MOF derivatives for supercapacitors

MOFs (precursors)	Samples	Electrolyte	SC	CR (%/cycles)	ED/PD	Ref.
Zn-MOF	BMM-9	3 M KOH	182.8 F g^{-1} (1 A g^{-1})	98.5/1,000 (10 A g^{-1})	—	[101]
MOF-5	MOF-5/AC-C NSP 850	6 M KOH	300 F g^{-1} (1.5 A g^{-1})	91.5/3,000 (5 A g^{-1})	—	[102]
ZnO@ZIF-8	CTAs@NCBs	1 M H_2SO_4	580 mF cm^{-2} (1 mA cm^{-2})	98.5/10,000 (20 mA cm^{-2})	—	[106]
MOF-5	C-GMOF	6 M KOH	345 F g^{-1} (2 mV s^{-1})	99/10,000 (200 mV s^{-1})	10.6/11,900	[107]
Co-MOF-74	Co_3O_4	2 M KOH	647 F g^{-1} (1 A g^{-1})	100/1,500 (2 A g^{-1})	—	[116]
ZIF-67	R-Co_3O_4	1 M KOH	329 F g^{-1} (1 A g^{-1})	92/1,000 (1 A g^{-1})	—	[117]
ZIF-67	RGO-Co_3O_4	0.1 M KOH	1,300 F g^{-1} (4 A g^{-1})	80.5/5,000 (4 A g^{-1})	65.8/2,048	[119]
Ni-MOF	NiO	3 M KOH	473 F g^{-1} (0.5 A g^{-1})	94/3,000(5 A g^{-1})	12.5/7,500	[124]
NiZn-MOF	NiO/ZnO	3 M KOH	497 F g^{-1} (1.3 A g^{-1})	100/2,000(5.2 A g^{-1})	—	[125]
Mn-MOF	δ-MnO_2	1 M NaOH	416 F g^{-1} (0.5 A g^{-1})	60.5/5,000 (5 A g^{-1})	23.2/425	[126]
ZIF-8	ZnO/C	1 M Na_2SO_4	394 F g^{-1} (1 A g^{-1})	—	—	[127]
MIL-100-Fe	$LaFeO_3$	1 M Na_2SO_4	241.3 F g^{-1} (1 A g^{-1})	92.2/5,000 (10 A g^{-1})	34/900	[131]
CoFe-MOF	$CoFe_2O_4$/Mxene	1 M LiCl	2467.6 F cm^{-3} (0.2 mA cm^{-2})	88.2/10,000 (1.5 mA cm^{-2})	—	[132]
ZIF-67	$NiCo_2O_4$/SiC/CC	1 M KOH	1377.6 F g^{-1} (1 A g^{-1})	88.3/6,000 (10 A g^{-1})	46.58/800	[133]
NiCo-MOF-74	NiO/$NiCo_2O_4$	6 M KOH	732 C g^{-1} (1 A g^{-1})	92.5/3,000 (10 A g^{-1})	36.6/6791.8	[134]
ZIF-67	$Ni_xCo_{3-x}O_4$	2 M KOH	2,870 F g^{-1} (1 A g^{-1})	81/5,000 (10 A g^{-1})	50.2/750	[135]
Co-MOF	CoNi-DH@CC	1 M KOH	929.4 C g^{-1} (2 mA cm^{-2})	81.5/7,500 (15 mA cm^{-2})	42.5/70.2	[139]
NiCo-MOF-74	Ni-MDH	2 M KOH	875 C g^{-1} (1 A g^{-1})	91.3/10,000(13.5 A g^{-1})	81/1,900	[140]
NiCo-MOF	Ni/Co-LDH	1 M KOH	1,652 F g^{-1} (1 A g^{-1})	100/2,000 (5 A g^{-1})	26/1817.3	[141]
Ni-MOF-74/rGO	R-NiS/rGO	2 M KOH	744 C g^{-1} (1 A g^{-1})	89/20,000 (20 A g^{-1})	54/46,034	[38]
Co-MOF	NiCo2S4/ACC	6 M KOH	2,392 F g^{-1} (1 A g^{-1})	85.1/10,000 (30 A g^{-1})	30.1/800.2	[157]
NiCo-MOF	NiCo-S	3 M KOH	3,724 F g^{-1} (1 A g^{-1})	90/3,000 (2 A g^{-1})	44.76/800	[153]
Co-MOF	$CoSe_2$	3 M KOH	713 F g^{-1} (1 mA cm^{-2})	92.4/5,000 (5 mA cm^{-2})	—	[160]
CuCo-ZIF	(CuCo)Se/NC	2 M KOH	121.4 C g^{-1} (1 A g^{-1})	96/5,000 (0.8 A g^{-1})	16.3/155.3	[161]
ZnCo-MOF	$Zn_{0.33}Co_{0.67}P$/Ni	6 M KOH	2,115 F g^{-1} (1 A g^{-1})	83/7,000 (10 A g^{-1})	83.05/ 775.02	[164]
Co-MOF	CoTe@C	2 M KOH	307.5 mF cm^{-2} (20 mA cm^{-2})	83.33/10,000 (1 A g^{-1})	43.84/ 738.88	[165]
ZIF-L	Co-Co_2N	1 M KOH	361.93 C g^{-1} (2 mA cm^{-2})	82.4/5,000 (2 mA cm^{-2})	20.4/9,850	[166]

2 mA cm^{-2}, which is much higher than that of other oxide counterparts. Remarkably, an ASC with Ni-doped Co–Co_2N// porous carbon was constructed, which maintained 82.4% of its capacity after 5,000 cycles and achieved 20.40 W h kg^{-1} energy density with 9.85 kW kg^{-1} power density. All of its properties indicate that Ni-doped Co–Co_2N is an advanced electrode material.

Remarkable works on MOF derivatives as electrode materials for supercapacitors are listed in Table 2.

2.3 MOF composites with functional materials

To develop high-performance electrode materials for supercapacitors, many researchers have explored additional materials to further enhance the conductivity and the structural stability of MOFs and their derivatives. One promising approach involves the functionalization of MOFs and their derivatives with conductive materials, such as carbon materials (graphene), metals or their compounds, conductive polymers, and other compounds [17,167], which has greatly broadened the research field of MOFs. Moreover, some metal derivatives also combine with other materials such as carbonaceous materials, metal compounds to construct composites. This helps in considerably enhancing their properties compared to their initial derived forms. The construction of MOF composites could integrate their advantages and mitigate the drawbacks of individual components. For example, the additional nanoporous carbon with MOF could facilitate fast ion diffusion and increase charge storage performances [168].

2.3.1 Carbonaceous material

Carbonaceous materials, including graphene and its derivatives, CNTs, AC, and mesoporous carbon, possess a high surface area and provide EDLC [169,170]. An effective strategy to address the poor conductivity of MOFs is

to combine them with these carbon materials [171]. The as-prepared hybrids with carbon-based materials can also facilitate rapid ion diffusion as well as the increased charge storage properties *via* Faradaic reactions, thereby combining physical and chemical charge storage mechanisms in single-electrode materials [168].

Graphene oxide and reduced graphene oxide (GO and rGO) are considered as outstanding electrode materials for supercapacitors [172–174]. Owing to their unique layered structure, their ion diffusion and transportation can be further enhanced. This could ensure excellent performances in charge storage and delivery [175]. Liu *et al.* prepared an Fe-MOF/graphene aerogel composite. It possessed a high charge–discharge rate, promising capacitive volume, and reliable cycling stability, exhibiting 353 F g^{-1} at 20 A g^{-1} while maintaining 74.4% of the original values retained after 10,000 charge–discharge cycles [176]. RGO has emerged as a unique additive that is incorporated into MOFs as electrode materials for SCs [177]. Gupta *et al.* fabricated a Cu-MOF/rGO composite *via* two steps [178]. They first synthesized Cu-MOF $\{[Cu_2(L)(H_2O)_2]\cdot(5DMF)\cdot(4H_2O)\}_n$ (Figure 7a) through a solvothermal method. The Cu-MOF/rGO composites were then constructed *via* a facile ultrasonication approach. Owing to the synergism between Cu-MOF and rGO, this composite delivered high mechanical strength and conductivity (Figure 7b). The morphology analysis showed that its crease-type structures reduce its ion-diffusion path, accelerating the transport and diffusion of ions on the electrode surface (Figure 7c). The wavy nature of the rGO sheets also improved their cycling efficiency. Combining the porous nature of Cu-MOF and conducting nature of rGO, GCD analysis indicated that this composite (1-GCE) delivered a promising discharge time at 0.8 A g^{-1}. In the electrochemical test, the specific capacitance was calculated to be 462 F g^{-1} at 0.8 A g^{-1}, with 93.75% of the original capacitance retained after 1,000 cycles (Figure 7d and e). This highlights that the Cu-MOF/rGO composite is a promising candidate for supercapacitors.

Apart from graphene, other carbon materials such as CNTs, mesoporous carbon, and carbon nanofibers also possess good availability, low weight, high conductivity, and high chemical stability and are used as conductive materials for combining with MOFs. Rui *et al.* fabricated a multiwall CNT and ZIF-67-Co hybrid fiber *via* a wearable and flexible fibrous device [179]. In the electrochemical test, the ZIF-67-Co/CNTs-derived Co_3O_4/CNTs were 110 F cm^{-3}.

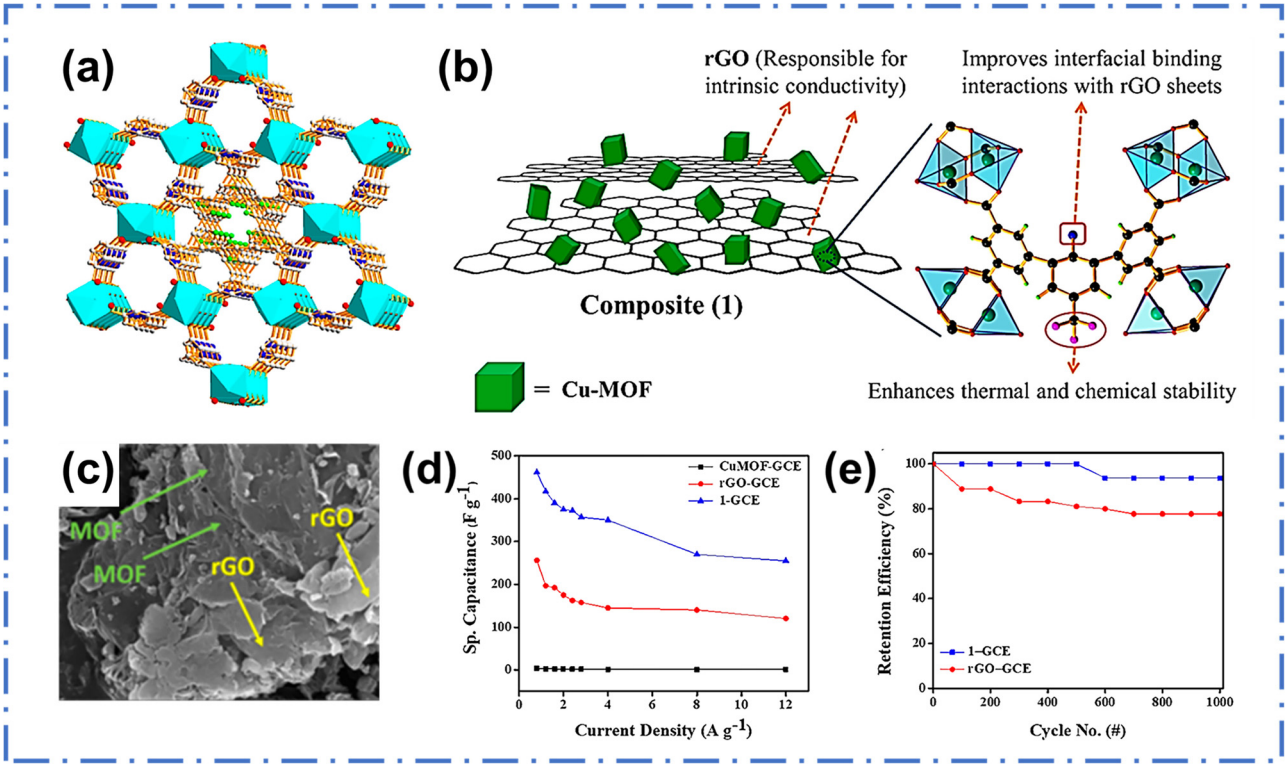

Figure 7: (a) Crystal structure of CuMOF framework. (b) The proposed approach for the construction of composite 1. (c) SEM image of CuMOF/rGO composites. (d) Specific capacitance as a function of current densities for CuMOF–GCE, rGO–GCE, and 1–GCE. (e) Cycling stability of rGO–GCE and 1–GCE over 1,000 cycles. Reproduced with permission from [178]; Copyright 2019, American Chemical Society.

Kim *et al.* synthesized a composite denoted as Ni-MOF@mC (mC: mesoporous carbon) [180]. This composite exhibited 109 F g^{-1} and 91% initial capacitance retention over 5,000 cycles. In a symmetric supercapacitor, the device presented 38.8 W h kg^{-1} energy density and 21,005 W kg^{-1} power density.

2.3.2 Metal and metal compounds

Although some carbonaceous composites can enhance the conductivity and overall electrochemical performance of MOF-based materials to a certain extent, they are usually affected by hidden flaws: (1) the limited contact areas between pristine MOF microparticles and conductive additives, (2) MOFs in impeding their aggregation, (3) blocking of diffusion pores due to the conductive additives on pristine MOF surfaces. This has a negative effect on the diffusion of ions and their accommodation in pristine MOFs, leading to undesirable electrochemical performance [181]. To realize higher specific capacitance values and excellent energy density and power density in supercapacitors, selecting proper electrode materials is essential [182]. Some metal compounds can serve as pseudocapacitive positive electrodes for storing charges through Faradaic redox reactions [183,184]. Designing and fabricating well-aligned transitional metal oxides@MOF composites is a good strategy for dealing with these problems [185].

Accordingly, Zhang *et al.* combined Ni-MOF with NiS_2 to fabricate a Ni-MOF@ NiS_2 nanocomposite [186]. According to the morphology analysis, this composite exhibited nanosheet arrays and possessed a unique heterostructure, which enhanced its conductivity and ability to hold the porous MOF pristine structures. Electrochemical tests revealed 1,128 F g^{-1} at 2 A g^{-1} for this composite-based electrode. Moreover, the assembled ASC delivered 23.5 W h kg^{-1} energy density under 1.4 kW kg^{-1} power density. This ASC also maintained 95.2% of its original capacity retained over 10,000 cycles at 5 A g^{-1}, proving its excellent application in supercapacitors. Yue *et al.* synthesized a hierarchical MoS_2@Ni-MOF composite structure [187]. The morphology of MoS_2@Ni-MOF in the SEM image indicated its perfect crystallinity and noticeable topographic contrast (Figure 8a). In 3 M KOH, the composite delivered 1590.24 F g^{-1} at 1 A g^{-1}, which was much better than that of pristine MOFs and common MoS_2 (Figure 8b). Moreover, the cycling test also demonstrated the excellent stability of the composites, maintaining a retention of 87.97% after 20,000 cycles (Figure 8c). In an ASC assembled with AC, this supercapacitor displayed 72.93 W h kg^{-1} and a power density of 375 W kg^{-1}, which was superior to that of the previously reported supercapacitors.

Other transitional metal compounds, including nickel-based compounds and manganese compounds, possess the high electrochemical activity and good electrical conductivity, which are effective in improving supercapacitors [189,190]. Zhu *et al.* prepared a Co-MOF with a hierarchical structure on nickel foam (Co-MOF/NF) [191]. This composite presented 13.6 F cm^{-2} at 2 mA cm^{-2}. The assembled ASC could achieve 1.7 mW h cm^{-2} energy density with a 4.0 mW cm^{-2} power density. It also maintained 69.7% of the initial values after 2,000 cycles in the cycling stability tests. Li *et al.* combined NiO nanoparticles on a hexagonal Ni-MOF through a simple self-template method [192]. The maximum specific capacitance was calculated to be 1192.7 F g^{-1} at 0.5 A g^{-1} with 93.32% original values retained after 5,000 cycles. In the assembled Ni-MOF@NiO//AC device, a maximum energy density of 62.2 W h kg^{-1} was achieved. Xu *et al.* successfully fabricated ultrathin Cu-MOF@δ-MnO_2 nanosheets in neutral environments *via* a simple reaction (Figure 8d) [188]. Morphology analysis showed a porous and hierarchical structure with micropores and mesopores. Compared with the other samples, this composite delivered 667 F g^{-1} at 1 A g^{-1} (Figure 8e). When assembled with AC to fabricate Cu-MOF@δ-MnO_2//AC ASC, the specific capacitance was 340 F g^{-1} at 1 A g^{-1}. This ASC also exhibited only a 5% drop compared with the initial values after 6,000 cycles (Figure 8f), indicating its excellent cycling performance. These results proved that metal oxides@MOF is a promising material for supercapacitors.

2.3.3 Conductive polymers

Another effective strategy to enhance the conductivity of MOFs is to incorporate pseudocapacitive materials. Conductive polymers (CPs), such as polyaniline (PANI) and polypyrrole (PPy), can serve as a circuit of electron transport in contact with isolated MOF crystals, thus offering extra pseudocapacitance [193,194]. The addition of these polymers helps reduce the number of electroactive sites and increase internal resistance [195]. PANI is an ideal candidate owing to its low cost, simple manufacturing process, superior capacitance performance, excellent conductivity, promising chemical stability, and unique protonic acid doping mechanism [196–199]. Liu *et al.* prepared ZIF-67@PANI composites by coating PANI into the ZIF-67 precursor [200]. From the SEM image, the morphology indicated that ZIF-67 grew *in situ* under the PANI coating (Figure 9a). They also observed that the ZIF-67@PANI-2

sample obtained the best combination of size and dispersion compared with the others. The GCD experiments exhibited the longest discharge times and increased specific capacitance of 224% (Figure 9b), which was 2,497 F g^{-1} at 1 A g^{-1} (Figure 9c). Furthermore, the assembled symmetric supercapacitor constructed by ZIF-67@PANI-2 maintained 92.3% capacitance after 9,000 cycles. The supercapacitor achieved 71.1 W h kg^{-1} energy density with a power density of 504.72 W kg^{-1}.

In addition to PANI, PPy is also an excellent conjugated conductive polymer that acts as a perfect pseudocapacitive additive for electrode materials in supercapacitors owing to its high electrical conductivity, low cost, high biocompatibility, and excellent adhesion to the substrate [202–204]. Jiao *et al.* fabricated a Zn/Ni-MOF/PPy composite by introducing PPy into bimetallic MOFs [205]. In this study, the optimized composite with 0.15 mL PPy added delivered 202 mA h g^{-1} at 1 A g^{-1}. Furthermore, an ASC assembled with carbon nanotubes-COOH was constructed and exhibited 50.9 W h kg^{-1} with a power density of 1,338 W kg^{-1}, retaining 78.8% of its initial value at 10 A g^{-1} over 5,000 cycles. Liu *et al.* prepared NiCo-MOF nanosheet coating on nanotubes PPy *via* a facile ultrasonic method (Figure 9d) [201]. The addition of polypyrrole nanotubes effectively improved the conductivity and prevented aggregation of the NiCo-MOF nanosheets. According to the morphology analysis, NiCo-MOF nanosheets were coated around the polypyrrole nanotubes (PNTs) (Figure 9e). Owing to its unique structure, this composite delivered 1,109 F g^{-1} at 0.5 A g^{-1} (Figure 9f). Furthermore, the fabricated ASC (NiCo-MOF@PNTs//AC)

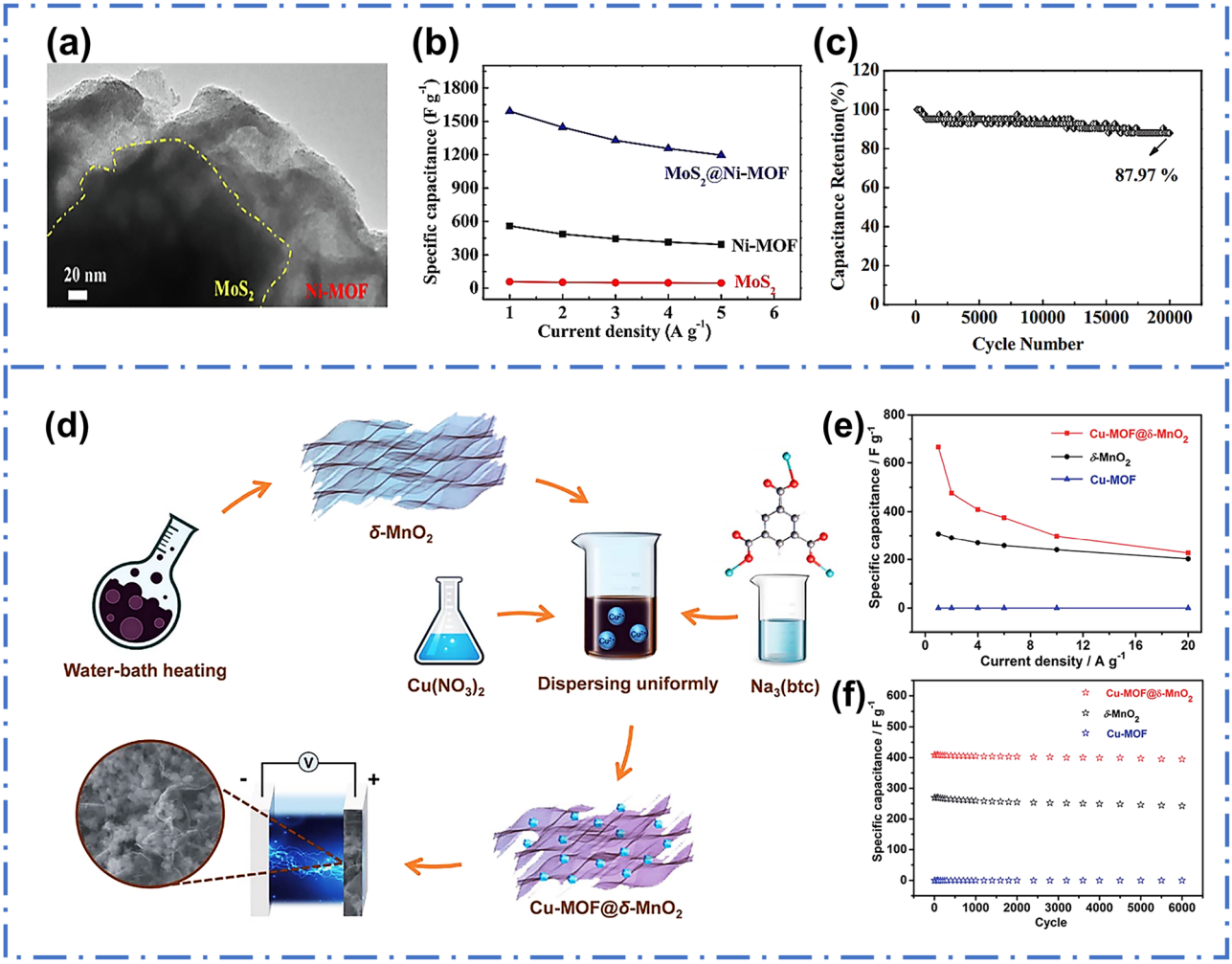

Figure 8: (a) SEM image of MoS_2@Ni-MOF. (b) Specific capacity at various current densities. (c) Cycling stability at a current density of 20 A g^{-1}. Reproduced with permission from [187]; Copyright 2019, Elsevier. (d) The preparation of ultrathin Cu-MOF@δ-MnO_2 nanosheets. (e) The specific capacitance of ultrathin Cu-MOF@δ-MnO_2 nanosheets, ultrathin δ-MnO_2 nanosheets, and Cu-MOF nanoparticles electrodes at different current densities. (f) Cycling stability of ultrathin Cu-MOF@δ-MnO_2 nanosheets, ultrathin δ-MnO_2 nanosheets, and Cu-MOF nanoparticles electrodes at 4 A g^{-1}. Reproduced with permission from [188]; Copyright 2018, The Royal Society of Chemistry.

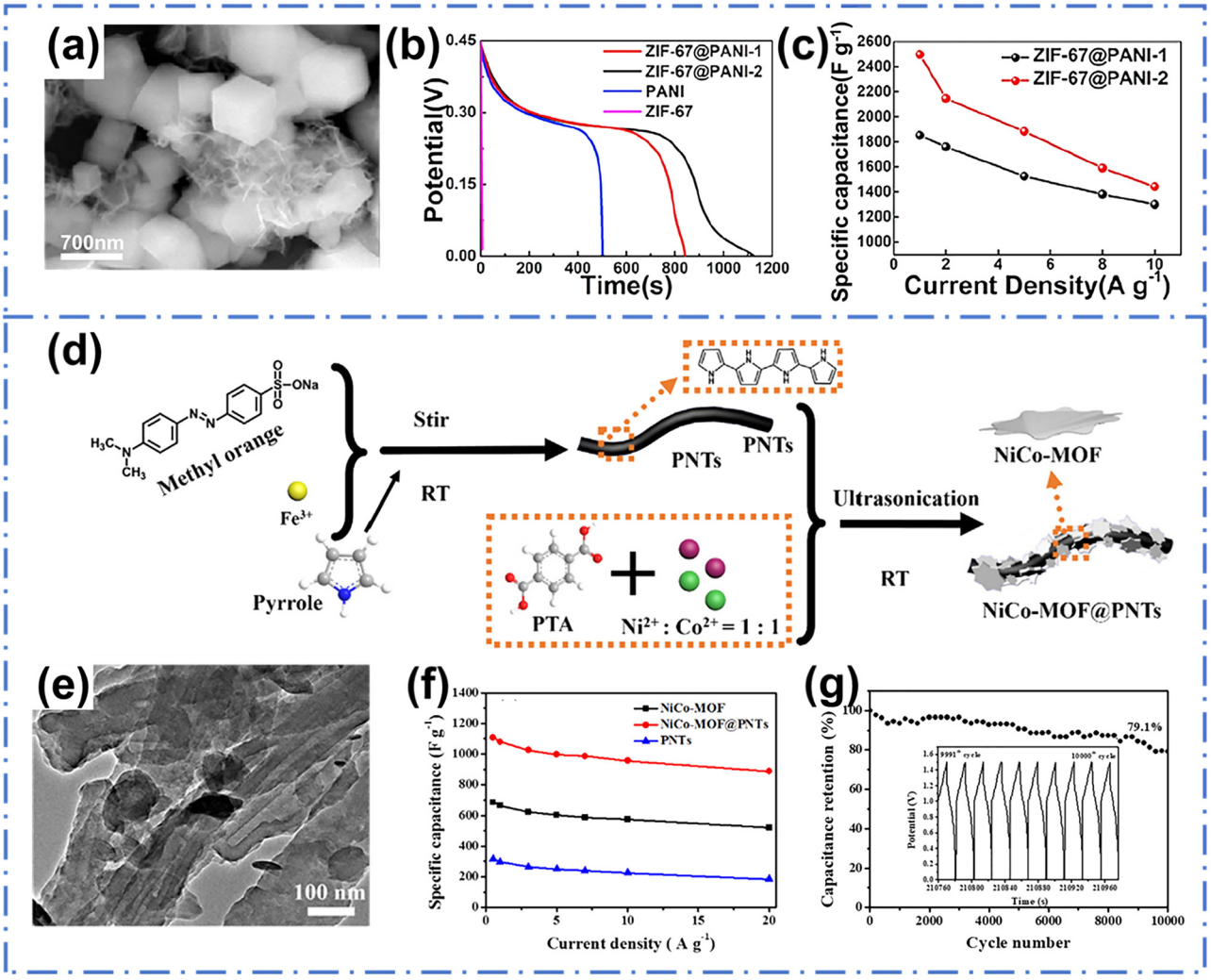

Figure 9: (a) SEM image of ZIF-67@PANI-2 samples. (b) GCD curves of four materials at the scan rate of 1 A g^{-1}. (c) Specific capacity of ZIF-67@PANI-1 and ZIF-67@PANI-2. Reproduced with permission from [200]; Copyright 2020, Elsevier. (d) The synthesis process of NiCo-MOF@PNTs. (e) TEM image of NiCo-MOF@PNTs. (f) The specific capacitances at different current densities. (g) The cycling stability of NiCo-MOF@PNTs (inset: the last ten cycles). Reproduced with permission from [201]; Copyright 2019, Elsevier.

presented 41.2 W h kg^{-1} and a power density of 375 W kg^{-1}. This device also retained 79.1% capacitance after 10,000 cycles (Figure 9g). These results indicated that this nanocomposite is a promising choice for supercapacitors.

2.3.4 Other compounds

Yue *et al.* explore nonmetallic element (N, S, P, Se, *etc.*) modified MOFs in supercapacitors for the first time [206]. There is an increasing amount of research on nonmetallic materials applied to supercapacitors. Transition metal phosphides and other chalcogenides have received significant research interest and are utilized in pseudocapacitor electrodes owing to their superior physical and chemical properties [207–209]. Yu *et al.* prepared hierarchical Ni/P/N/C composites using MOF as a template [210]. In the electrochemical tests, Ni/P/N/C-500 (annealing at 500°C) could reach 2887.87 F g^{-1} at 1 A g^{-1} with a 6 M KOH solution, and the cycling test presented 90% initial values retained after 1,000 cycles at 10 A g^{-1}. Li *et al.* fabricated the N, S co-doped bimetal nanocomposite using a Ni/Co-MOF as the precursor [211]. In this study, the specific capacitance reached 1,529 F g^{-1} at 1 A g^{-1}, while maintaining 89.29% of the original rate after 10,000 cycles. In an ASC assembled with AC, 41.04 W h kg^{-1} with a power density of 750 W kg^{-1} was achieved.

He *et al.* prepared a functional heterostructure NiCoP-MOF nanosheet-stacked lamellar bricks *via* hydrothermal-localized phosphorization method [212]. The composites

combine the intrinsic merits of MOFs and phosphides, enabling higher activity and fast reaction kinetics. Therefore, a high Faradaic capacitance and rate capability could be enhanced. In three-electrode setup with 2 M KOH, this composite exhibited an outstanding capacitance of 728 C g^{-1} at 1 A g^{-1}. Furthermore, the device (AC//NiCoP-MOF) achieved a maximum energy density of 50.3 W kg^{-1} with a power density of 1011.2 W kg^{-1}. It also maintained almost no capacitance loss during 10,000 cycles, proving its excellent cycling stability. Apart from nonmetallic element-related composites, there are other special hybrids that deliver excellent electrochemical performance. Qu *et al.* prepared Ni-MOF/MXene hybrid nanosheets *via* the ultrasonic method [213]. In this study, MXene nanosheets are dispersed on the surface of Ni-MOF uniformly, which is a benefit for enhancing its electronic conductivity and preventing the aggregation of Ni-MOF nanosheets. This hybrid showed 867.3 F g^{-1} specific capacitance at 1 A g^{-1} and 87.1% capacitance retention after 5,000 cycles at 5 A g^{-1}. Ramachandran *et al.* synthesized a Co-MOF/MXene hybrid directly on Ni foam [214]. The morphology analysis indicated that the unique interlayer voids space of MXene and Co-MOF on Ni foam could shorten the diffusion path and promote ion intercalation. In 6 M KOH, this composite could achieve an ultrahigh specific capacitance value of 3,741 F g^{-1} at 3 mA cm^{-2}, and 92.1% capacitance remained after 3,000 cycles. Liu *et al.* reported a facile route for preparing NiCo-MOF/acetylene black composites [215]. In the electrochemical measurements, NiCo-MOF/AB-5 achieved 916.1 F g^{-1} at 1 A g^{-1}. In an assembled ASC, it achieved 33.84 W h kg^{-1} with a power density of 750 W kg^{-1}. It also maintained 85.25% of the original values after 5,000 cycles, proving its outstanding cycling stability.

Remarkable works on MOF composites as electrode materials for supercapacitors are listed in Table 3.

3 PB/PBAs

Prussian blue/Prussian blue analogs (PB/PBAs) are functional coordination polymers with tunable chemical composition, large surface area, fast charge–discharge rate, *etc*. They are the oldest and most invaluable MOFs branches owing to their excellent electrochemical performance [216,217]. The discovery of the first PB can be traced to the 18th century. However, research on their electrochemical properties and applications has been studied until 1978. The typical formula of PB/PBA is $A_xM_y[M'(CN)_6]_z$, where A denotes the alkaline metal ion and M and M′ are transition metal ions such as Mn^{2+}, Fe^{2+}, Co^{2+}, Ni^{2+}, Cu^{2+}, and Zn^{2+} [21,218,219]. $[Fe_4^{III}[Fe^{II}(CN)_6]_3]$ is a typical PB structure [220,221]. In this cubic molecule, the Fe^{III} and Fe^{II} are located on the alternating corners of the cube, and the corner-shared octahedral in the PB is bridged by the linear CN anions [222]. The redox process of Fe ions in PB could also facilitate the electron transfer pathway. Moreover, owing to the crystal structure of PB, the reversible intercalation and extraction of ions in electrolytes are well promoted, demonstrating its excellent electrochemical performances. Some metal hexacyanoferrates (MCHFs, M = Co, Mn, Cu. *etc*.) also have

Table 3: Selected MOF composites for supercapacitors

Sample	Electrolyte	SC	CR (%/cycles)	ED/PD	Ref.
MIL-88-Fe/GA	1 M H_2SO_4	353 F g^{-1} (20 A g^{-1})	74.4/10,000 (1 A g^{-1})	27/4,300	[176]
CuMOF/rGO	1 M Na_2SO_4	462 F g^{-1} (0.8 A g^{-1})	93.75/1,000 (12 A g^{-1})	—	[178]
Co_3O_4/CNTs	—	110 F cm^{-3}	—	—	[179]
Ni-MOF@mC	$TEABF_4$	109 F g^{-1} (0.3 A g^{-1})	91/5,000 (5 A g^{-1})	38.8/21,005	[180]
Ni-MOF@NiS_2	3 M H_2SO_4	1,128 F g^{-1} (2 A g^{-1})	95.2/10,000 (5 A g^{-1})	23.5/1,400	[186]
MoS_2@Ni-MOF	3 M KOH	1590.24 F g^{-1} (1 A g^{-1})	87.97/20,000 (5 A g^{-1})	72.93/375	[187]
Co-MOF/NF	2 M KOH	13.6 F cm^{-2} (2 mA cm^{-2})	79.93/1,000 (50 mA cm^{-2})	1.7 mW h cm^{-2}/4.0 mW cm^{-2}	[191]
NiO@Ni-MOF	3 M KOH	1192.7 F g^{-1} (0.5 A g^{-1})	93.32/5,000 (0.5 A g^{-1})	62.2/352.5	[192]
Cu-MOF@MnO_2	1 M Na_2SO_4	667 F g^{-1} (1 A g^{-1})	95/6,000 (4 A g^{-1})	—	[188]
ZIF-67@PANI	1 M KOH	2,497 F g^{-1} (1 A g^{-1})	92.3/9,000 (5 A g^{-1})	71.1/504.72	[200]
Zn/Ni-MOF/PPy	3 M KOH	202 mA h g^{-1} (1 A g^{-1})	78.8/5,000 (10 A g^{-1})	50.9/1,338	[205]
NiCo-MOF/PPy	2 M KOH	1,109 F g^{-1} (0.5 A g^{-1})	79.1/10,000 (5 A g^{-1})	41.2/375	[201]
Ni/P/N/C	6 M KOH	2887.87 F g^{-1} (1 A g^{-1})	90/1,000 (10 A g^{-1})	—	[210]
NS-BNs	6 M KOH	1,529 F g^{-1} (1 A g^{-1})	89.29/10,000 (1 A g^{-1})	41.04/750	[211]
NiCoP/NiCo-MOF	2 M KOH	728 C g^{-1} (1 A g^{-1})	100/10,000 (2 A g^{-1})	50.3/1011.2	[212]
Ni-MOF/MXene	2 M KOH	867.3 (1 A g^{-1})	87.1/5,000 (5 A g^{-1})	—	[213]
Co-MOF/MXene@Ni	3 M KOH	3,741 F g^{-1} (3 mA cm^{-2})	92.1/3,000 (6 mA cm^{-2})	—	[214]
Ni/Co-MOF/AB-5	2 M KOH	972.2 F g^{-1} (0.5 A g^{-1})	94.1/3,000 (5 A g^{-1})	33.84/750	[215]

typical PBA structures. Metal hexacyanoferrates are of low cost, show fine reversible redox performance, and have unique structure, high capacity, and excellent cyclic stability [223,224]. PBAs are usually utilized as precursors for the fabrication of functional transition metal compounds or other nanoparticles [221]. Owing to its structural advantages, the application of PB/PBA in supercapacitors has attracted considerable attention. To better utilize PB/PBAs in supercapacitors, their applications can be also divided into three categories: (1) Design and synthesize Pristine PB/PBAs with unique morphology and hollow nanostructures; (2) the outstanding precursors of PB/PBAs to fabricate derivatives, including metal oxides, phosphides, and selenides; and (3) functional materials, such as graphene and metal compounds, to further enhance the performances of PB/PBAs.

3.1 Pristine PB/PBAs

PB/PBAs are promising materials for energy storage devices, especially supercapacitors. However, their performances were unsatisfactory. In the previous research, hollow nanostructures with low density, tunable composition and morphology, and large surface areas have garnered considerable research interest, which enhances the electrochemical performance of pristine PB/PBAs [225]. Hence, considering the advantages of PB/PBA morphology with hollow nanostructures, developing a simple, cost-effective, and self-templating method is desirable. To further explore the ideal synthesis method for hollow structures, some effective modifications were made in the preparation of hollow structures.

Yin *et al.* developed an effective self-templating method for the rational fabrication of cobalt hexacyanoferrate (CoHCF) with hollow structures using water-soluble precursors at room temperature [226]. In the electrochemical tests with 0.5 M Na_2SO_4 solution, the CoHCF-based electrode delivered 284 F g^{-1} at 1 A g^{-1}, along with 92% initial values retained for 5,000 cycles. When assembled with AC, this asymmetric hybrid supercapacitor delivered an energy density of 47 W h kg^{-1} with a power density of 1,000 W kg^{-1}. Yin *et al.* fabricated hollow CoHCF microtubes using polyacrylonitrile-$Co(Ac)_2$ composite nanofibers as templates [227]. In the Na_2SO_4 aqueous electrolyte, the capacitance of this hollow CoHCF microtube was 281.8 F g^{-1} at 1 A g^{-1}. Meanwhile, 93% of the initial values remained over 5,000 charge–discharge cycles. When assembling with AC, the supercapacitor exhibited 43.89 W h kg^{-1} energy density and 27.78 kW kg^{-1} power density.

Wang *et al.* fabricated hollow structure cobalt hexacyanoferrate submicroboxes through a cation exchange method (Figure 10a) [228]. They selected manganese

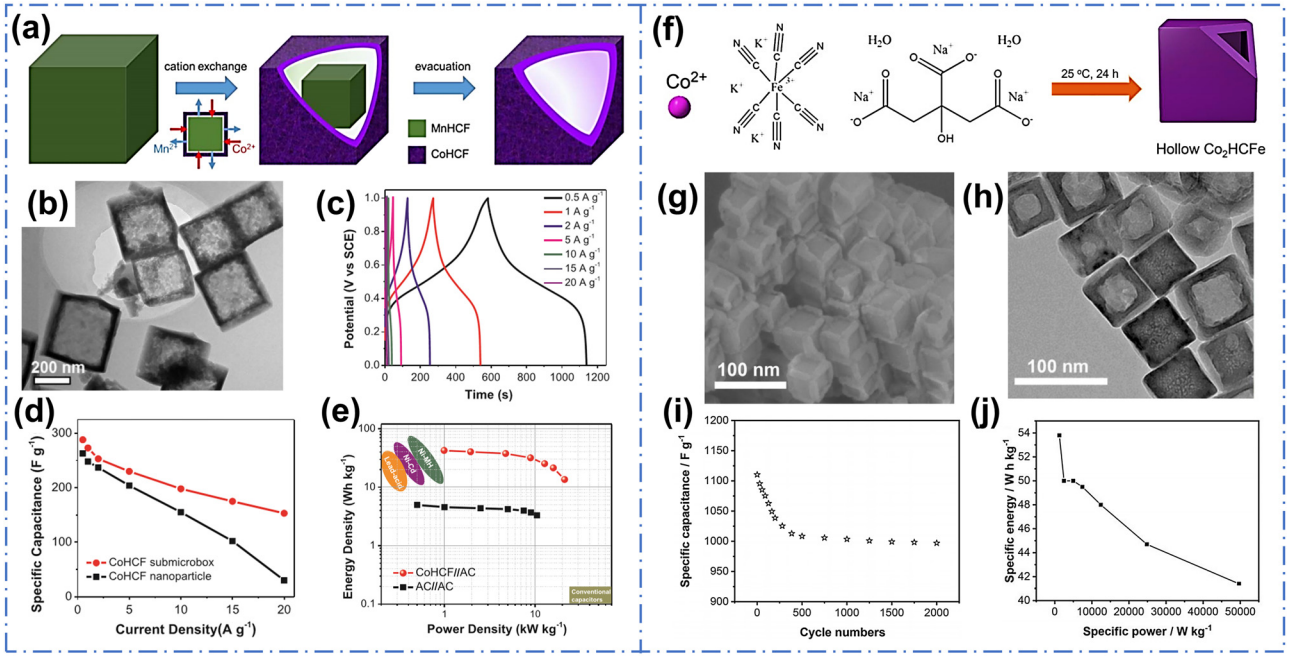

Figure 10: (a) Schematic illustration of the formation mechanism of CoHCF submicrobox. (b) TEM image of CoHCF submicroboxes. (c) GCD curves of the CoHCF at different current densities. (d) Specific capacitance of COHCF. (e) Ragone plots of the CoHCF//AC hybrid cells. Reproduced with permission from [228]; Copyright 2017, Elsevier. (f) Schematic illustration of synthesizing hollow Co_2HCFe nanocubes. (g) SEM image of Co_2HCFe nanocubes. (h) TEM image of Co_2HCFe nanocubes. (i) The cycling stability of Co_2HCFe at current densities of 5 A g^{-1}. (j) The specific energy of Co_2HCFe. Reproduced with permission from [229]; Copyright 2018, Elsevier.

hexacyanoferrate (MnHCF) as a sacrificial template and Co^{2+} was added to the system, making soluble $[Fe(CN)_6]^{2-}$ coordinate with Co^{2+} to easily construct CoHCF. Then, the CoHCF layer was crystallized and deposited onto the MnHCF surface, and a distinct hollow and robust nanoshell was obtained. The TEM image exhibited distinct hollow interiors in the CoHCF structure (Figure 10b). The electrochemical tests indicated that the electrode material delivered 288 F g^{-1} at 0.5 A g^{-1} (Figure 10d), which was better than that of its nanoparticle counterparts. Moreover, the CoHCF submicrobox preserved 93.1% capacitance after 8,000 cycles, indicating outstanding cycling performance. After CoHCF assembly with AC, the ASC delivered 42.5 W h kg^{-1} energy density under 990 W kg^{-1} power density, sustaining 21.1 kW kg^{-1} power density along with 13.5 W h kg^{-1} energy density (Figure 10e).

Zhu *et al.* fabricated hollow cobalt hexacyanoferrate (Co_2HCFe) nanocubes with uniform and dense hollow structures (Figure 10f) [229]. The SEM image showed a uniform size of 50 nm (Figure 10g). The HRTEM image showed the hollow structure of the Co_2HCFe nanocubes (Figure 10h). The GCD analysis at different current densities indicated its excellent redox-activated properties. This also led to a specific capacitance of 2,526 F g^{-1} at 0.5 A g^{-1}, and the value also reached 378 F g^{-1} even at 20 A g^{-1} (Figure 10i). Moreover, Co_2HCFe maintained 90.25% retention after 2,000 cycles (Figure 10i). All of its prominent electrochemical performances are attributed to its unique hollow structure. In an assembled ASC (Co_2HCFe//AC), the maximum value of energy density could reach 53.8 W h kg^{-1} with 1,242 W kg^{-1} power density. The maximum power density was 49,680 W kg^{-1}, whereas the energy density was 41.4 W h kg^{-1} (Figure 10j). These tests indicated that Co_2HCFe nanocubes can become superior electrode materials for future supercapacitors.

3.2 PB/PBA derivatives

Compared to the pristine form of PB/PBAs with porous and hollow morphology, the PB/PBA derivatives possess higher surface areas, conductivity, and more open diffusion channels. These lead to an obvious improvement in electrochemical performances. Hence, PB/PBAs have been widely used as precursors or sacrificial templates to fabricate derivatives, including TMOs or other metal compounds with micro/nanostructured materials [218,230,231]. Xie *et al.* utilized Ce–Fe PBAs as precursors to synthesize Fe–Ce oxides [232]. They first prepared pristine $Ce[Fe(CN)_6]$ and then annealed it at different temperatures, retaining the primitive uniform hexagonal bipyramidal nanostructure during this process. This helped to maintain the initial properties of PBA and further enhances its electrochemical performance. In 1 M KOH electrolyte, this binary oxide, annealed at 500°C, exhibited 148 C g^{-1} at 0.5 A g^{-1} and maintained 74.5% of the original values retained during 5,000 cycles. Furthermore, the constructed ASC (assembled with AC) achieved 22.7 W h kg^{-1} energy density under 640 W kg^{-1}, and the power density could reach 6,400 W kg^{-1} with a remaining energy density of 11.1 W h kg^{-1}. Zhang *et al.* fabricated a flexible hybrid film composed of MXene and PBA-derived Ni–Fe oxides [233]. They utilized MXene layers to wrap the cubic Ni–Fe oxide, forming a macroscopic flexible film. The areal capacitance was calculated to be 1,038 mF cm^{-2} at 0.2 mA cm^{-2}, and the capacity remained at 90.88% of the primitive values over 10,000 charge–discharge cycles. Recently, transition metal phosphides have also been chosen as promising electrode materials. Wei *et al.* first prepared $Co_3[Co(CN)_6]_2$ nanocubes as templates and then annealed and phosphorized them to fabricate CoP nanocubes [234]. This material delivered 600 F g^{-1} at 1 A g^{-1}. They also fabricated FeP_4 *via* a similar access. In an assembled ASC, CoP is positive and FeP_4 is negative; CoP//FeP_4 maintained a capacitance of 89% after 10,000 cycles. It also exhibited 46.38 W h kg^{-1} with a power density of 695 W kg^{-1}. This study demonstrates an effective phosphorization engineering strategy for PB/PBAs to construct functional electrode materials.

Some transition metal compounds such as selenides and phosphides have been recently studied with perfect electrochemical performance, for the application in supercapacitor electrodes. To further enhance the electrochemical performance of supercapacitors, it is desirable to introduce phosphorus and transition metal selenides into transition metal. Accordingly, Zong *et al.* designed P-(Ni, Co)Se_2 selenides with nanotubes anchored on nanoflakes and nanowires grown on activated carbon cloth (Figure 11a) [235]. The SEM image of this derivative revealed uniform and continuous nanocubes with a hierarchical network on the selenide surface (Figure 11b). In the 3 M KOH electrolyte, the CV test possessed different potential windows for different samples at 10 mV s^{-1}, and the P-(Ni, Co) Se_2 NA sample displayed the largest integral area (Figure 11c). From the GCD analysis at 2 mA cm^{-2}, the selenide-based electrode displayed 755 C g^{-1} (Figure 11d). In addition, the selenides could also retain 80.1% of their original values over 3,000 cycles, which was ascribed to the enhancement in conductivity after phosphorus incorporation (Figure 11e). The assembled HSC delivered an energy density of 45 W h kg^{-1} with a power density of 990 W kg^{-1} (Figure 11f). This

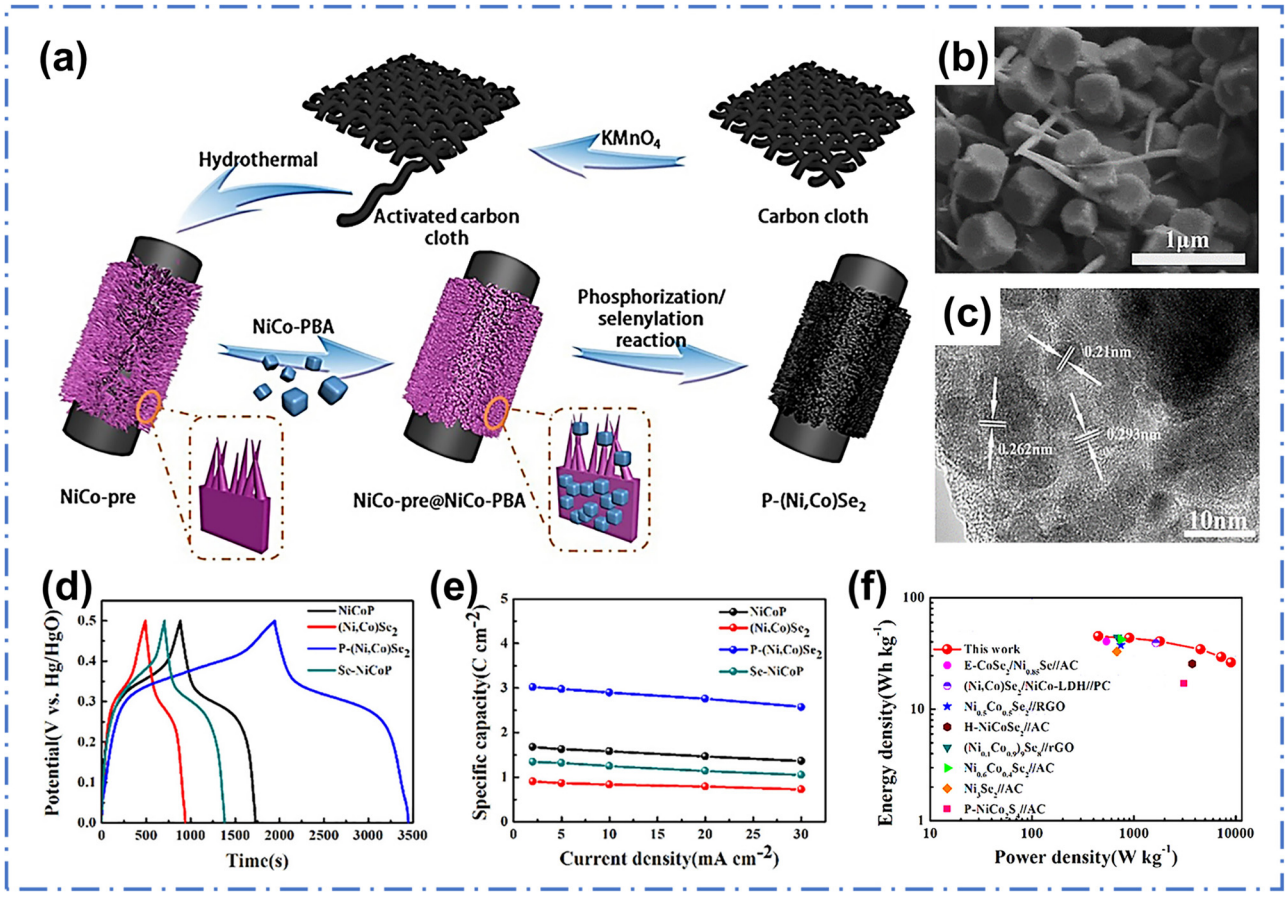

Figure 11: (a) Schematic illustration of the fabrication procedure of P-(Ni, Co) Se_2 NAs on activated carbon cloth. (b) SEM image of P-(Ni, Co) Se_2 NAs. (c) HRTEM image of P-(Ni, Co) Se_2 NAs. (d) GCD curves of P-(Ni, Co) Se_2 electrode at various current densities. (e) Areal capacity of NiCoP, (Ni, Co) Se_2, P-(Ni, Co) Se_2, and Se-NiCoP electrodes at different current densities. (f) Ragone plots of P-(Ni, Co) Se_2//ZIF-8-derived carbon HSC and the previously reported devices. Reproduced with permission from [235]; Copyright 2019, Elsevier.

work provided a new strategy for the composition and the nanostructure design of high-performance supercapacitor electrode materials.

3.3 PB/PBA composites with functional materials

Although PB and its analogs exhibit outstanding properties, such as high stability/redox activity and open frameworks, the relatively poor conductivity of these materials has presented a major obstacle for their applications [236]. Conductive fillers such as carbon materials and other metal compounds must be added to enhance the conductivity of PB and PBA materials. The incorporation of functional materials could also improve their electrochemical performance compared with their pristine forms. For example, MnO_2 nanosheets are an excellent electrode material in supercapacitors but suffer from lower conductivity. CoHCF delivers remarkable cycling stability but a relatively narrow operation voltage window. Hence, Song *et al.* combined the merits of CoHCF and MnO_2 nanosheets to fabricate the nanostructured hybrid composites [237]. This composite exhibits outstanding electrochemical performances.

3.3.1 Graphene

Owing to the excellent performance of graphene and its derivatives, including promising conductivity, high surface area, and chemical stability, they are perfect candidates for combination with PB/PBAs [238]. To enhance their electrochemical activity and conductivity, graphene has been frequently used for fabricating nanocomposites.

A ternary nanocomposite PPy-PB-GO (GO: graphene oxides) was synthesized *via* spontaneous polymerization among pyrrole, PB, and GO [239]. The scheme could be divided into two stages: (i) absorbing pyrrole onto the GO

surface and (ii) using pyrrole to reduce Fe^{3+} to Fe^{2+} and form insoluble PB nanocubes (Figure 12a). The SEM image showed that PB was anchored on the GO matrix (Figure 12b), and the PB nanocubes were protected by PPy. In the electrochemical analysis, the PPy-PB-GO electrodes exhibited 525.4 F g^{-1}, which was considerably better than those of most PBA-based materials and porous carbon materials. The cycling stability tests showed that the PPy-PB-GO electrode could retain 96% of its initial capacitance after 2,000 cycles (Figure 12c), indicating its perfect cycling stability and a high degree of reversibility. Goda *et al.* synthesized Cu-PBA/GO composites *via* depositing Cu-PBA nanocubes on GO surfaces [238]. This nanocomposite delivered 611.6 F g^{-1} at 0.5 A g^{-1} and maintained

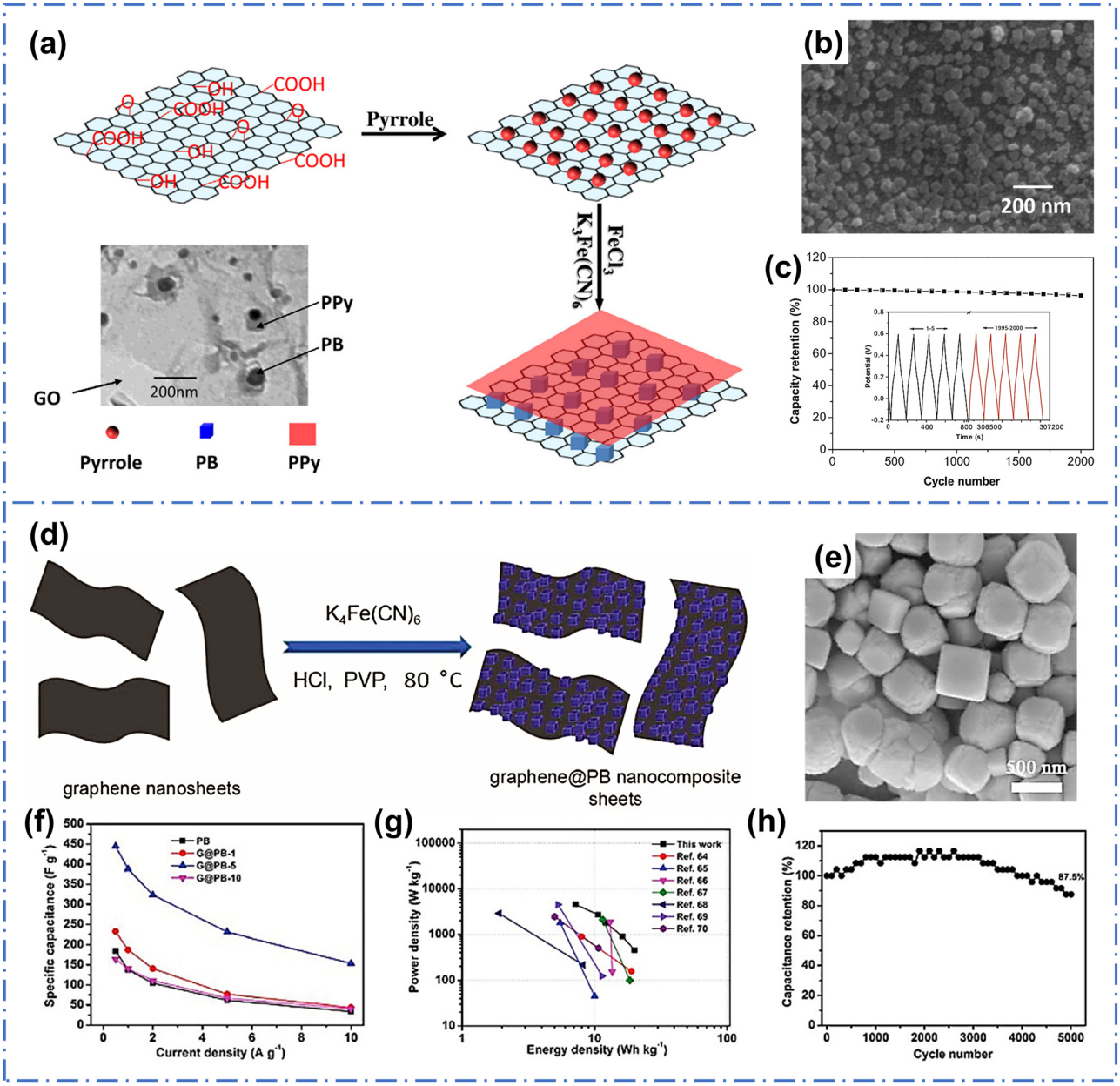

Figure 12: (a) Schematic illustration of the fabrication procedure of PPy–PB–GO composites. (b) SEM image of PPy–PB–GO. (c) The cycling stability of PPy–PB–GO electrode over 2,000 cycles. Reproduced with permission from [239]; Copyright 2015, Elsevier. (d) Schematic illustration of the fabrication of Graphene@PB nanocomposites. (e) SEM image of Graphene@PB-5 nanocomposites. (f) Specific capacitance of samples at 1 A g^{-1} (graphene denoted as G). (g) Ragone plots of Graphene@PB-5//AC ASC compared to the references. (h) Cycling performance of Graphene@PB-5//AC at a current density of 5 A g^{-1}. Reproduced with permission from [240]; Copyright 2018, The Royal Society of Chemistry.

86% primitive values during 2,000 cycles at 4 A g^{-1}. In addition, the assembled supercapacitors could achieve 54.37 W h kg^{-1} at a power density of 200 W kg^{-1}, proving its outstanding electrochemical performance.

Wang *et al.* fabricated interlocked Graphene@PB nanosheets *via* a one-step facile hydrothermal technique [240]. They used $[Fe(CN)_6]^{4-}$ to release Fe^{2+} and oxidize partial Fe^{2+} to Fe^{3+} in acidic media. Subsequently, the graphene nanosheets could constantly absorb Fe^{3+} ions to react with $[Fe(CN)_6]^{4-}$, thus forming PB nanotubes on the graphene nanosheets (Figure 12d). A typical SEM image showed that the PB nanocubes covered both sides of the graphene nanosheet surfaces, forming thicker graphene@PB-5 nanocomposites (Figure 12e). In the electrochemical test, this nanocomposite exhibited 445 F g^{-1} at 0.5 A g^{-1}, displaying better performance than that of other samples at various current densities (Figure 12f). The assembled supercapacitors delivered 74.8 W h kg $^{-1}$ and 5.5 kW kg^{-1} energy density/power density, respectively (Figure 12g). The nanocomposite also maintained a 97.2% initial value over 5,000 cycles (Figure 12h). This can be ascribed to the synergistic effect of the hybrid nanostructure that prevents the aggregation of PB nanoparticles and restacking of graphene nanosheets.

Sookhakian *et al.* prepared PB-nitrogen-doped graphene nanocomposites using the $Fe(NO_3)_3$ solution and $K_4Fe(CN)_6$ *via* a simple process [222]. In a 1 M H_2SO_4 solution, this composite-based electrode delivered 660 C g^{-1} at 1 A g^{-1}. In addition, the stability tests showed that the nanocomposite retained 84.7% of its primitive values during 1,500 cycles, which is also ascribed to the synergetic effects of N-graphene and PB nanoparticles that prevent mechanical deformation. Zhang *et al.* fabricated PB/rGO hydrogels *via* a facile one-pot hydrothermal route (denoted as PB-Co/rGOH) [241]. In their study, the CV tests of this hybrid and other compared samples were analyzed, showing that the capacitance of PB-Co/rGOH was mainly attributable to the EDLC and pseudo-capacitance region. Moreover, this composite-made electrode exhibited the longest discharge time and showed 225.2 F g^{-1} at 1 A g^{-1} with 82.4% original values maintained over 10,000 cycles. Azhar *et al.* fabricated iron oxide/carbon composites with nanoporous structures [236]. The morphology clearly showed that the iron oxide nanoparticles are firmly aggregated to each other on the GO nanosheet surface. The specific capacitance value of the iron oxide/carbon composite was 415.0 F g^{-1} at 2 A g^{-1}, and the capacity retention reached up to 120% over 8,000 cycles. This could be ascribed to the activation of the hybrid that improve the surface wetting of the electrode and led to the fast diffusion of ions in the electrolyte. Xu *et al.* designed cobalt–nickel hexacyanoferrate hybrids with CNT ($K_{2.25}Ni_{0.55}Co_{0.37}Fe(CN)_6$/CNT) *via* a one-step co-precipitation synthesis route [242]. In electrochemical tests, cobalt–nickel hexacyanoferrate hybrids displayed 600 F g^{-1} at 0.2 A g^{-1} and maintained 94% of its original value during 2,000 cycles. When assembling this cobalt–nickel hexacyanoferrate with CNT to test its applications, the hybrid electrode achieved 30 W h kg^{-1} energy density and 60 W kg^{-1} power density at 0.2 A g^{-1}.

3.3.2 Metal compounds

Transition metal compounds (oxides, hydroxides, *etc.*) have also been investigated as perfect functional materials for supercapacitors. The hybridization between PB/PBAs and 2D metal oxides leads to the formation of bidirectional coordinative interactions between them, thus enhancing their electrochemical performance [243]. Previous research has shown that PB/PBAs fabricated with MnO_2 can enhance electrochemical performance [237]. MnO_2-based materials are one of the most promising reversible, environmentally benign, and low-cost electrode materials for supercapacitors. They also deliver higher capacitance performances compared with those carbonaceous counterparts [46]. Zhang *et al.* combined PB with a unique coordination superamolecular network (CSN) with MnO_2 to fabricate CSN-PB/MnO_2 hybrids (Figure 13a) [244]. The SEM image showed that the typical PB was uniformly inserted into MnO_2, and some adhered to the surface of MnO_2, which is favorable for promising electrochemical performance (Figure 13b). In electrochemical tests, this composite electrode exhibited a characteristic pseudocapacitive feature at different scan rates from 10 to 50 mV s^{-1} (Figure 13c). In further studies, the GCD tests of this composite displayed highly symmetrical properties and relatively linear slopes (Figure 13d). Furthermore, in 1 M Na_2SO_4 solution, this composite electrode could deliver 315.3 F g^{-1} at 1 A g^{-1}, which was higher than that of pristine MnO_2 and the CSN-PB electrode. In particular, this composite retained 32.4% of the highest capacitance values at 30 A g^{-1}, indicating good rate capability (Figure 13e). Furthermore, the fabricated ASC, CSN-PB/MnO_2//AC retained 85.5% of the original values over 20,000 cycles at 20 A g^{-1} (Figure 13f). Moreover, this device achieved a maximum energy density of 46.13 W h kg^{-1} and a power density of 1.20 kW kg^{-1}. Its power density could be as high 18.00 kW kg^{-1}, while retaining an energy density of 19.95 W h kg^{-1}. These performances demonstrated their potential applications in supercapacitors.

Das *et al.* [46] fabricated a PB@MnO_2 hybrid electrode material, and this is the first report of a PB composite with metal oxides (Figure 13g). In the morphological

analysis, the FE-SEM image showed that MnO_2 is preferentially deposited on the surface of PB nanocubes, offering a porous surface morphology (Figure 13h). To evaluate its electrochemical properties, GCD experiments were conducted at different current densities (Figure 13i). The specific capacitance of PB@MnO_2 was 608 F g^{-1} at 1 A g^{-1}. Moreover, approximately 68% of the initial values of the PB@MnO_2 hybrid were preserved even at 10 A g^{-1}, indicating promising rate capability compared to pure PB (Figure 13j). Moreover, they assembled a PB@MnO_2 hybrid and polyaniline/graphene nanoplatelet (PG) as ASC. The ASC exhibited great capacitive retention after 4,000 cycles (Figure 13k). Furthermore, it exhibited a 16.5 W h kg^{-1} energy density along with a 550 W kg^{-1} power density

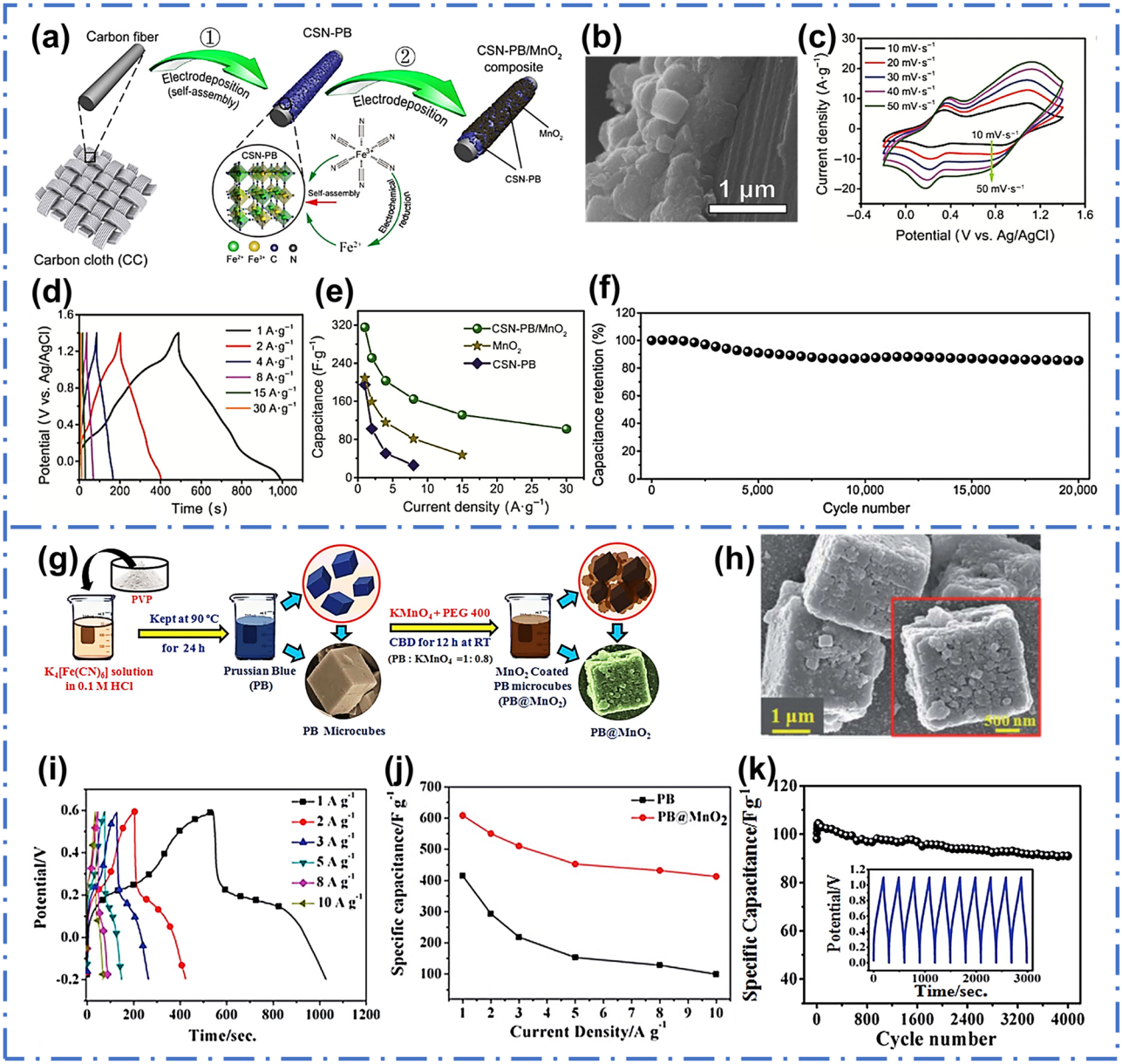

Figure 13: (a) Schematic illustration of the fabrication of CSN-PB/MnO_2 composite. (b) SEM image of CSN-PB/MnO_2 composite. (c) CV curves of CSN-PB/MnO_2 composite at various scan rates. (d) GCD curves of CSN PB/MnO_2 composite electrode at various current densities from 1 to 30 A g^{-1}. (e) The specific capacitance of CSN-PB/MnO_2 composite electrode. (f) Cycling performance of the Fe-PBA/MnO_2//AC device at a current density of 20 A g^{-1} for 20,000 cycles. Reproduced with permission from [244]; Copyright 2019, Springer. (g) Schematic illustration of the synthesis of PB@MnO_2. (h) SEM image of PB@MnO_2 hybrid. (i) GCD curves of PB@MnO_2 at several current densities. (j) The specific capacitance of PB and PB@MnO_2. (k) Cycling performance of the device at the current density of 1 A g^{-1}. Reproduced with permission from [46]; Copyright 2017, The Royal Society of Chemistry.

while retaining 11.3 W h kg^{-1} energy density under 5,497 W kg^{-1} power density. These remarkable behaviors demonstrated that the PB@MnO_2 composite is a potential candidate for electrode materials in supercapacitors. Sun *et al.* designed and synthesized ZnCo-PBA@α-$Co(OH)_2$ composites by loading α-$Co(OH)_2$ nanosheets onto $Zn_3[Co(CN)_6]_2$ nanospheres [245]. In the electrochemical analysis, this composite exhibited 423.92 F g^{-1} at 1 A g^{-1}. In addition, they constructed a ZnCo-PBA@α-$Co(OH)_2$//AC ASC, which displayed a 73.53% original value maintained after 5,000 cycles at 5 A g^{-1}, demonstrating its promising cycling stability. The energy density of the ASC was calculated to be 49.13 W h kg^{-1} with 1734.0 W kg^{-1} power density, indicating that the device is an excellent electrochemical material.

Remarkable works on PB/PBAs as electrode materials for supercapacitors are listed in Table 4.

4 COFs

Covalent organic frameworks (COFs) are novel crystalline nanoporous materials possessing unique design features, perfect channel structures, tunable porosity, and ordered 2D and 3D networks [24,246,247]. In 2005, the first COF was discovered by Liu *et al.* and denoted as COF-1 [47]. Subsequently, more porous COFs were discovered, denoted as COF-5, COF-102, COF-105, and so on. Owing to their

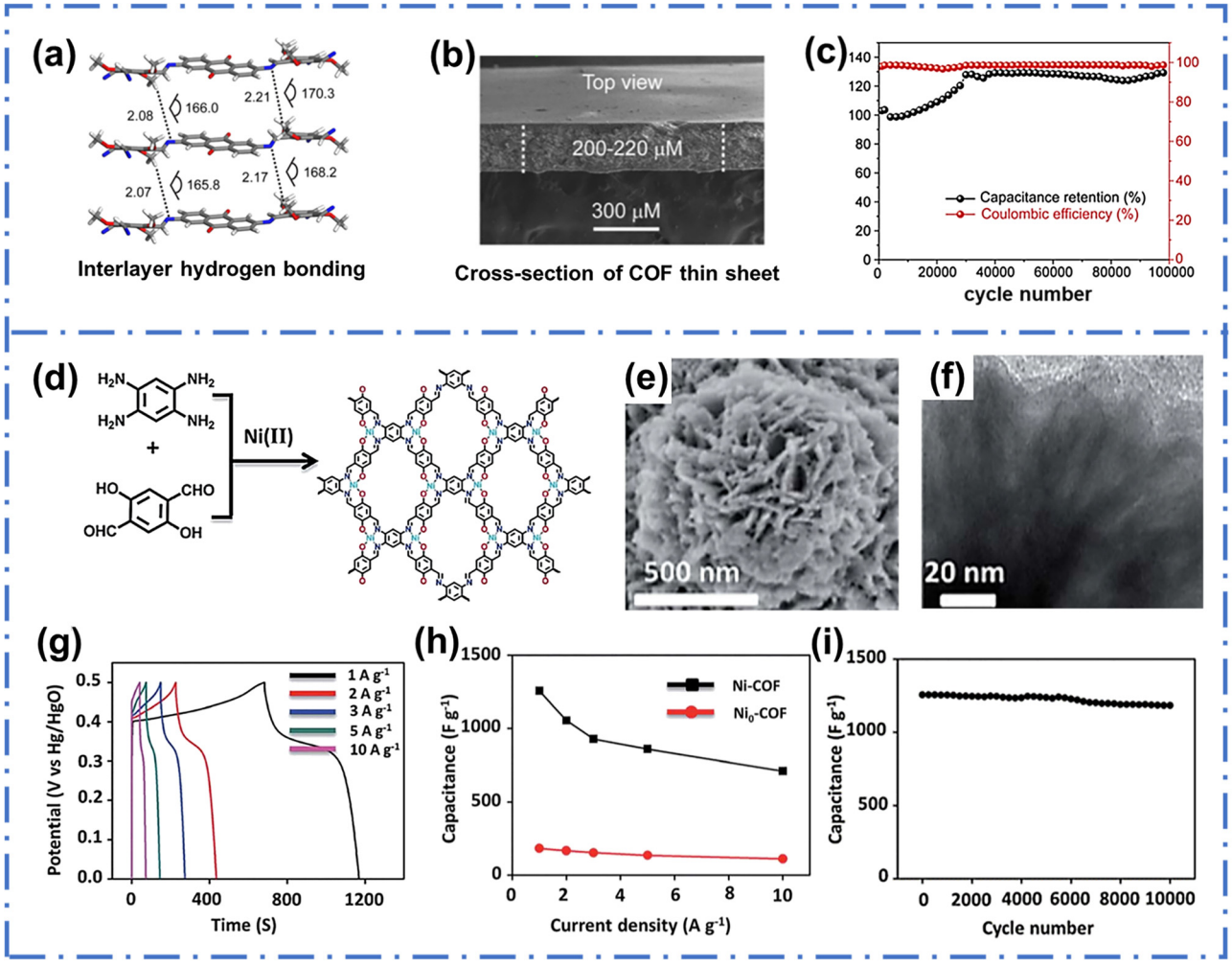

Figure 14: (a): 3D diagrams of interlayer C—H···N H-bonding in TpOMe-DAQ. (b) SEM image of TpOMe-DAQ thin sheet. (c) Cycling stability of TpOMe-DAQ at 10 mA cm^{-2}. Reproduced with permission [52]; Copyright 2018, American Chemical Society. (d) Synthetic scheme of Ni-COF. (e) SEM image of Ni-COF. (f) TEM image of Ni-COF. (g) GCD curves at different current densities (1–10 A g^{-1}). (h) The specific capacitance of Ni-COF and Ni_0-COF. (i) Cycling stability at a current density of 1 A g^{-1}. Reproduced with permission from [53]; Copyright 2019, The Royal Society of Chemistry.

Table 4: Selected PB/PBAs for supercapacitors

PB/PBAs	Samples	Electrolyte	SC	CR (%/cycles)	ED/PD	Ref.
Pristine PBs	CoHCF	0.5 M Na_2SO_4	284 F g^{-1} (1 A g^{-1})	92/5,000 (5 A g^{-1})	47/1,000	[226]
Pristine PBs	CoHCF	0.5 M Na_2SO_4	281.8 F g^{-1} (1 A g^{-1})	93/5,000 (5 A g^{-1})	43.89/27,780	[227]
Pristine PBs	CoHCF	0.5 M Na_2SO_4	288 F g^{-1} (0.5 A g^{-1})	93.1/8,000 (10 A g^{-1})	42.5/990	[228]
Pristine PBs	Co_2HCFe	3 M KOH	2,526 F g^{-1} (0.5 A g^{-1})	90.25/2,000 (5 A g^{-1})	41.4/49,680	[229]
PB derivatives	NiFe-O/Mxene	—	1,038 mF cm^{-2} (0.2 mA cm^{-2})	90.88/10,000 (1 mA cm^{-2})	76.8 mWh cm^{-3}/0.4 W cm^{-3}	[233]
PB derivatives	FeP_4	3 M KOH	345 F g^{-1} (1 A g^{-1})	89/10,000 (10 A g^{-1})	46.38/695	[234]
PBA derivatives	CoP	3 M KOH	600 F g^{-1} (1 A g^{-1})	89/10,000 (10 A g^{-1})	46.38/695	[234]
PBA derivatives	P-(Ni, Co)Se_2	3 M KOH	755 C g^{-1} (2 mA cm^{-2})	80.1/3,000 (20 mA cm^{-2})	45/446.3	[235]
PB composites	PPy-PB-GO	1 M KNO_3	525.4 F g^{-1} (5 A g^{-1})	96/2,000 (5 A g^{-1})	70.2/1,100	[239]
PB composites	G@PB	0.5 M Na_2SO_4	445 F g^{-1} (0.5 A g^{-1})	97.2/5,000 (10 A g^{-1})	10.65/2,700	[240]
PB composites	PB/N/G	1 M H_2SO_4	660 C g^{-1} (1 A g^{-1})	84.7/1,500 (6 A g^{-1})	—	[222]
PB composites	PB-Co/rGOH	1 M KNO_3	225.2 F g^{-1} (1 A g^{-1})	82.4/10,000 (5 A g^{-1})	37.9/10,000	[241]
PBs composites	PB/GO	3 M KOH	415 F g^{-1} (2 A g^{-1})	100/8,000 (200 mV s^{-1})	—	[236]
PB composites	$K_{2.25}Ni_{0.55}Co_{0.37}Fe(CN)_6$/CNTs	4 M KCl	600 F g^{-1} (0.2 A g^{-1})	94/2,000 (1 A g^{-1})	28/1,400	[242]
PB composites	CSN-PB/MnO_2	1 M Na_2SO_4	315.3 F g^{-1} (1 A g^{-1})	85.5/20,000 (20 A g^{-1})	46.13/1,200	[244]
PB composites	PB@MnO_2	1 M KNO_3	608 F g^{-1} (1 A g^{-1})	93/4,000 (1 A g^{-1})	11.3/5,497	[46]
PBAs composites	ZnCo-PBA@αCo(OH)$_2$	6 M KOH	423.92 F g^{-1} (1 A g^{-1})	73.53/5,000 (5 A g^{-1})	49.13/1,734	[245]

intriguing esthetic structures and unique properties such as large surface area, outstanding hydrothermal stability, structural adaptivity, and low density, COFs have become popular candidates for electrode materials in supercapacitors [248]. However, their electrical conductivity and insulating behavior considerably limit their further utilization [249]. To overcome the shortcoming of COFs, designing and fabricating COFs with unique building units, COF derivatives, or constructing COFs with other functional materials are utilized. In the application of supercapacitors, some 2D COFs have been received more research in recent years. Researchers found that their stacked 2D structure with small mesopores greatly impede the mass transfer and the full utilization. Moreover, the conductive COF could also enhance its electrochemical performance and received extensive attention.

4.1 Pristine COFs

COFs have demonstrated remarkable performance as electrode materials for supercapacitors. However, similar to other framework materials (MOFs, PB/PBAs), their pristine forms possess poor electrochemical conductivity and other properties. Introducing functional units such as some redox-active building units into COFs is a simple method of improving their conductivity and stability [250]. Feng *et al.* synthesized a tetragonal 2D porphyrin COF with a high large crystallinity and surface area [251]. The introduction of a porphyrin unit helps form conduction pathways, leading to high-rate charge carrier conduction. Ding *et al.* constructed n-channel 2D COFs [252]. The adoption of benzothiadiazole (BTDA) units forms an electron-conducting framework. Recently, some studies have explored this method *via* condensation reactions and developed a series of special pristine COFs applied in supercapacitors, considerably improving their electrochemical performance.

Halder *et al.* prepared interlayer hydrogen-bonded COF TpOMe-DAQ using TpOMe (2,4,6-trimethoxy-1,3,5-benzenetricarbaldehyde) and DAQ (2,6-diaminoanthraquinone) as reactants, which had both superior chemical stability under drastic conditions and reversible redox response (Figure 14a) [52]. These COFs could be constructed as continuous and uniform thin nanosheets, even at the centimeter scale (Figure 14b). Moreover, quasi-reversible redox peaks were observed at 1 mV s^{-1}, indicating pseudocapacitive properties. Furthermore, GCD analysis was performed, and the areal capacitance was improved from 135 to 169 F g^{-1}. This COF also exhibited a remarkable cycling performance, with almost no initial capacitance

values compromised over 100,000 cycles (Figure 14c). It is postulated that the hydrophobic and steric protection from imine (C═N) bonds, methoxy nearby, and its interlayer hydrogen bonding all result in superior cycling performances.

Some condensation reactions, such as Schiff-base condensation and Knoevenagel condensation, are widely used to introduce functional units to improve their properties. Li *et al.* utilized the Schiff-base condensation reaction to construct an ultrastable triazine-based COF, which is denoted as PDC-MA-COF [253]. In the electrochemical tests, the PDC-MA-COF exhibited 248.0 F g^{-1} along with 74% of the original values retained at higher current densities. The GCD experiments further showed its perfect symmetry and maximum specific capacitance: 335.0 F g^{-1} was achieved at 1.0 A g^{-1}, along with outstanding cyclic stability over 9,000 cycles at 5.0 A g^{-1}. This can be ascribed to the interlayer H-bonding maintaining an ordered nanostructure, enhancing the cycling stability of COF, and providing perfect capacitance retention.

The Knoevenagel condensation reaction is also an important method for fabricating high-molecular-weight organic structures, including COFs. Recently, an increasing number of studies have focused on this condensation reaction to construct high-performance COFs. Zhang *et al.* also synthesized two 2D olefin-linked COFs (g-$C_{48}N_6$-COF and g-$C_{30}N_6$-COF) *via* the Knoevenagel condensation reaction [254]. Their COFs possessed highly crystalline honeycomb-like structures and display well-defined nanofibrillar morphologies. In a micro-supercapacitor, the g-$C_{30}N_6$-COF-MSC exhibited 44.3 mF cm^{-2}, and the g-$C_{48}N_6$-COF-MSC exhibited 41.1 mF cm^{-2}. Moreover, both the COF-MSC delivered perfect cycling stability with almost 95% initial values retained after 5,000 cycles.

Metal elements are also incorporated in unique COFs to enhance their performance. Li *et al.* synthesized a Ni-COF (with Ni^{2+}) for high-performance supercapacitors *via* a facile synthesis route (Figure 14d) [53]. This COF possessed a unique morphology with spherical flower-like shapes and abundant sheets (Figure 14e). It also displayed a unique layered structure and optically translucent features (Figure 14f). The GCD experiments indicated the rapid charge transfer kinetics of Ni-COF (Figure 14g). Owing to its enhanced electrical conductivity, highly dense redox-active centers, and conjugated planar structure, the electrode based on this composite exhibited 1257.0 F g^{-1} at 1.0 A g^{-1}, which was better than Ni_0-COF (without Ni^{2+}) at different current densities (Figure 14h). This electrode delivered approximately 100% of the original values retained over 10,000 cycles (Figure 14i). This research also paved the way for enhancing the electrochemical performance of functional COFs in supercapacitors.

4.2 COFs derivatives

Considering their similarity in structures with MOFs, except for the absence of metal ions, COFs can also serve as a source of microporous carbon particles [256,257]. Zhuang *et al.* used Knoevenagel condensation to synthesize 2D olefin-linked COFs based on olefin (C═C) linkages for the first time (denoted as 2DPPV) [49]. Owing to its highly periodic porous structure and crystalline features, 2DPPV possesses promising electrochemical performance. When fabricated at 800°C, 2DPPV-800 delivered 334.0 F g^{-1} at 0.5 A g^{-1} with almost no noticeable change in the original values over 10,000 cycles. Zhou *et al.* synthesized B–N–C-n materials with MA and 4-FPBA, catalyzed by $Cu(NO_3)_2$ (Figure 15a) [255]. The SEM and TEM image demonstrated capsules with hollow morphology (cavities of 0.02–10 μm) (Figure 15b and c). The CV analysis suggested that the EDLC played a dominant role in the charge–discharge system of B–N–C, which was annealed at 1,000°C, along with 399.4 cm^2 g^{-1} and 230 F g^{-1} at 5 A g^{-1} (Figure 15d). Under various current densities, this value was maintained over 150.0 F g^{-1} (Figure 15e). The cycling text also showed that after 1,400 cycles, B–N–C maintained a capacitance of 192 F g^{-1} (Figure 15f), demonstrating its promising electrochemical properties.

4.3 COF composites with functional materials

To improve the structural stability and electrical conductivity of COF electrodes during cycling, many materials such as metal and nanoporous carbon have been employed to form COF composites. Xu *et al.* fabricated COF composites (denoted as CHCM) for the first time [246]. They combined COF with hydroxyl-terminated hyperbranched polyesters (OHPs) first and then impregnated this hybrid on microporous electrically conducting carbon nanotube films (CNTFs) to construct COF@OHP@CNTF (CHCM). Due to the incorporation of OHP, the capacitance of this hybrid was greatly increased. When the heating time continued over 10 h, the performance of capacitance could also enhance. In 2 M H_2SO_4 solution, this hybrid delivered 425 F g^{-1} at 0.2 mA cm^{-2}. It also retained 80% initial capacitance over 10,000 cycles at 0.8 mA cm^{-2}. Carbon

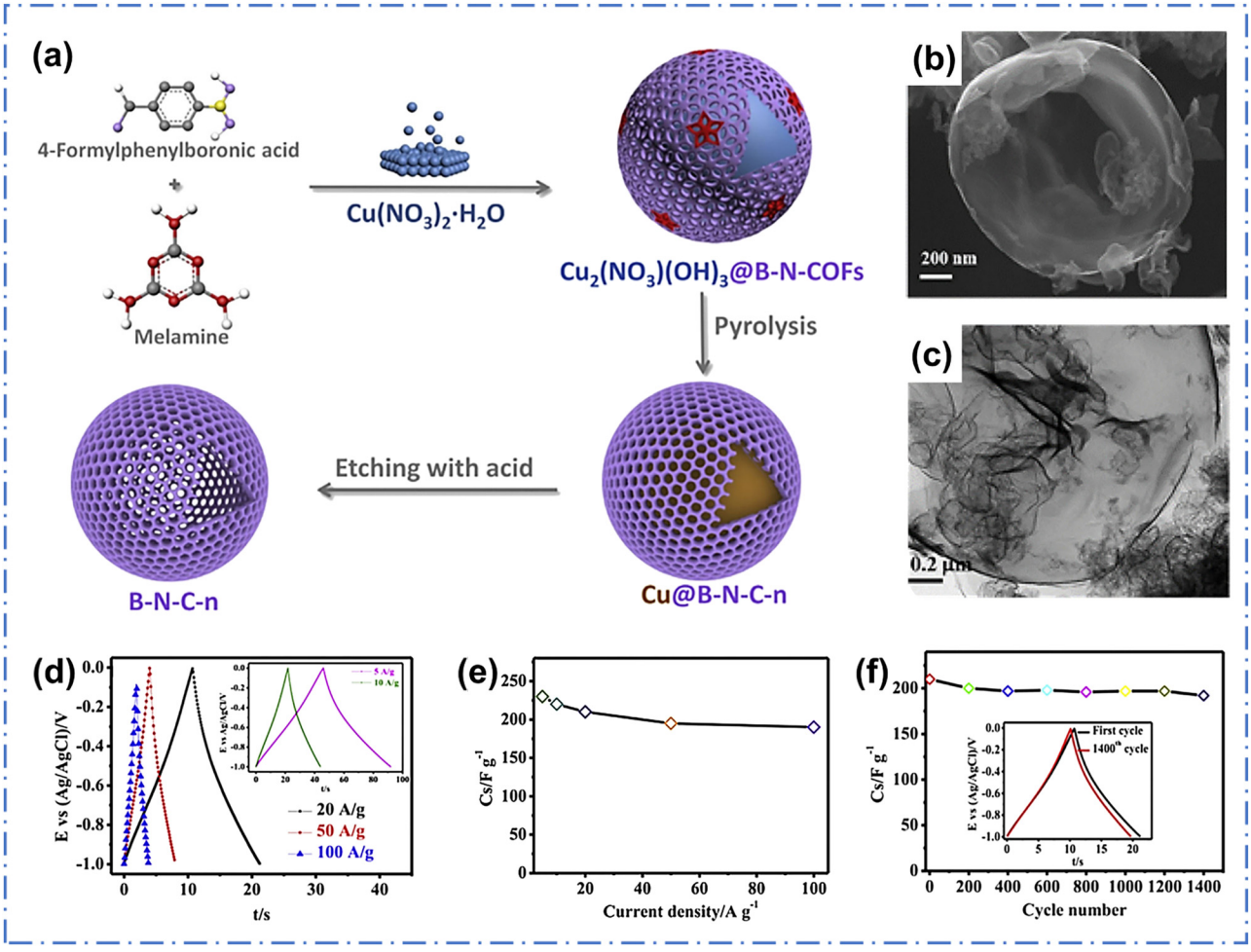

Figure 15: (a) Schematic illustration of the synthesis procedures of the B-N-C capsules. (b) SEM image. (c) TEM image. (d) GCD curves of B-N-C-1,000 at different current densities. (e) The specific capacitance of B-C-N-1,000. (f) Cycling stability of B-C-N-1,000 at a constant current density of 20 A g^{-1}. Reproduced with permission from [255]; Copyright 2018, Elsevier.

materials are promising additives for COFs. Han *et al.* polymerized redox-active TpPa-COFs with single-walled CNT under solvothermal conditions to construct SWCNT-COF nanocomposites [50]. In the GCD experiments, this nanohybrid delivered 153.0 F g^{-1} at 0.5 A g^{-1}, indicating a great potential in the energy storage field.

RGO possesses many merits, including low weight, high flexibility, low volume, and perfect conductivity, thereby making them outstanding carbonaceous additives for electrode materials [259]. Li *et al.* prepared COF/rGO hydrogel composites *via* the *in situ* reaction of their organic linkers in the presence of GO (Figure 16a) [258]. This method included adding GO into the reaction solution under hydrothermal treatment and obtaining the targeted composites. The SEM image of COF/rGO is shown in Figure 16b. This composite possessed a hollow tubular and 3D sponge-like structure, indicating its very thin sheets and good flexibility. In a symmetrical supercapacitor device, COF/rGO electrode could yield 269 F g^{-1} at 0.5 A g^{-1}. It also retained 83% of the highest capacitance (222.0 F g^{-1}) at 10.0 A g^{-1}. Compared with pristine COFs and rGO, this composite delivered excellent performance (Figure 16c). The cycling tests of the COF/rGO materials showed that 96% primitive values retained over 5,000 cycles, proving its promising chemical stability (Figure 16d). An *et al.* fabricated a hierarchical porous anthraquinone-based COFs/graphene aerogel (DAAQ-COFs/GA) composite *via* electrostatic self-assembly and hydrothermal routes (Figure 16e) [54]. The SEM image showed that each nanoflower-shaped DAAQ-COF was closely covered by ultrathin graphene nanosheets and embedded in the 3D graphene networks (Figure 16f), which was ascribed to the powerful electrostatic attraction and π–π interactions. In the electrochemical tests, the electrode exhibited

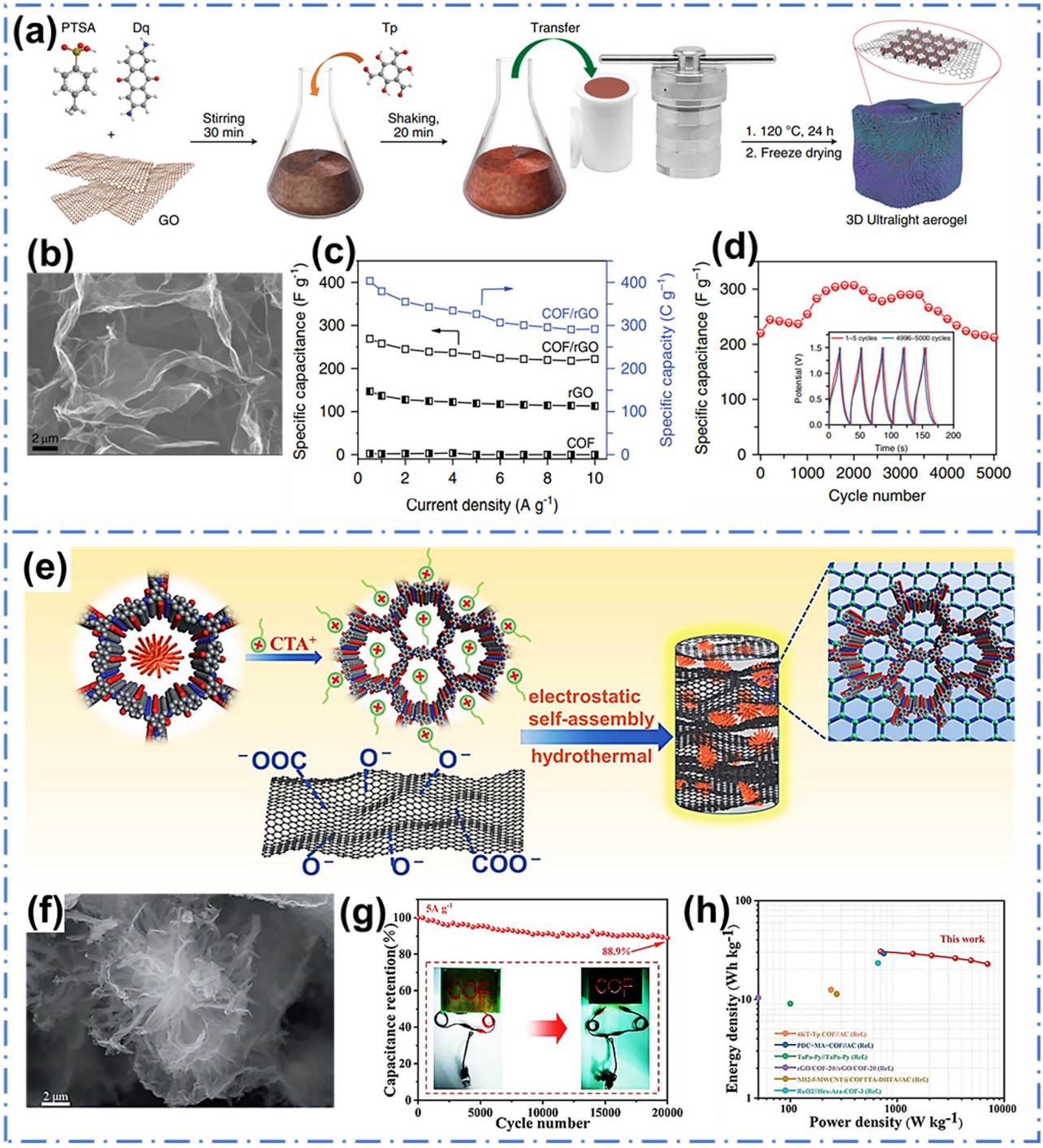

Figure 16: (a) The preparation of COF/rGO aerogel. (b) SEM image. (c) The specific capacitances and capacities under different current density. (d) The cycling stability of COF/rGO at a current density of 8 A g^{-1}. Reproduced with permission from [258]; Copyright 2020, Nature publishing group. (e) The synthesis procedure of DAAQ-COFs/GA composite. (f) SEM image of DAAQ-COFs/GA composites. (g) Cycling stability at 5 A g^{-1} for 20,000 cycles (the inset shows the digital photograph of LEDs powered by DAAQ-COFs/GA//GA ASC). (h) Ragone plot of the assembled ASC. Reproduced with permission from [54]; Copyright 2021, The Royal Society of Chemistry.

a capacitance of 378 F g^{-1} at 1 A g^{-1}. This could contribute to the hierarchical porous properties and rapid Faradaic reactions of the redox sites. Furthermore, in a constructed ASC (DAAQ-COFs/GA//GA), this device presented 88.9% primitive capacitance retained over 20,000 cycles (Figure 16g). This supercapacitor also exhibited 30.5 W h kg^{-1} at a power

Table 5: Selected COFs for supercapacitors

COFs	Samples	Electrolyte	SC	CR (%/cycles)	ED/PD	Ref.
Pristine COFs	TpOMe-DAQ	3 M H_2SO_4	169 F g^{-1} (3.3 mA cm^{-2})	100/100,000 (10 mA cm^{-2})	2.9 μW h cm^{-2}/61.8 μW cm^{-2}	[52]
Pristine COFs	PDC-MA-COF	6 M KOH	335 F g^{-1} (1 A g^{-1})	78/9,000 (5 A g^{-1})	13.5/7,500	[253]
Pristine COFs	g-$C_{30}N_6$-COF	EMIMBF_4/PVDF-HFP	44.3 mF cm^{-2} (0.5 mA cm^{-2})	95/5,000 (1.2 mA cm^{-2})	38.5 mWh cm^{-3}/0.3 W cm^{-3}	[254]
Pristine COFs	g-$C_{48}N_6$-COF	EMIMBF_4/PVDF-HFP	41.1 mF cm^{-2} (0.5 mA cm^{-2})	95/5,000 (1.2 mA cm^{-2})	35.7 mWh cm^{-3}/0.3 W cm^{-3}	[254]
Pristine COFs	Ni-COF	3 M KOH	1,257 F g^{-1} (1 A g^{-1})	94/10,000 (1 A g^{-1})	130/839	[53]
COF derivatives	B–N–C-n	0.1 M KOH	230 F g^{-1} (5 A g^{-1})	83.5/1,400 (20 A g^{-1})	—	[255]
COF derivatives	2DPPV	6 M KOH	334 F g^{-1} (0.5 A g^{-1})	99.99/10,000 (0.5 A g^{-1})	30/6,654	[49]
COF composites	CHCM	2 M H_2SO_4	425 F g^{-1} (0.2 mA cm^{-2})	80/10,000 (0.8 mA cm^{-2})	—	[246]
COF composites	SWCNTs-TpPa-COFs	1 M H_2SO_4	153 F g^{-1} (0.5 A g^{-1})	99.99/2,000 (2 A g^{-1})	—	[50]
COF composites	COF/rGO	0.5 H_2SO_4	269 F g^{-1} (0.5 A g^{-1})	96/5,000 (8 A g^{-1})	—	[258]
COF composites	COF/GO	1 M H_2SO_4	378 F g^{-1} (1 A g^{-1})	88.9/20,000 (15 A g^{-1})	30.5/700	[54]

density of 700 W kg^{-1} (Figure 16h). The research presented insights into the processing and practical application of COF-based materials in supercapacitors.

Remarkable works on all COFs as electrode materials for supercapacitors are listed in Table 5.

5 Summary and outlook

Supercapacitors have a potential for a wide range of practical applications, which may become an excellent replacement for traditional Li-ion batteries and other chargeable batteries. In recent years, research on framework materials, their derivatives, and composites has demonstrated the superior capabilities of these materials and their unique structures. This explains their wide use in supercapacitors, which has attracted considerable attention. We conclude that there are significant advances in the application of supercapacitors. The creative and logical synthesis of excellent nanostructures considerably improves the conductivity, cycling life, capacity, and energy/power density of the assembled supercapacitors. These advances demonstrate the promising performance of framework materials in supercapacitors and provide useful information for the development of higher-performance supercapacitors.

All framework materials (MOFs, PB/PBAs, and COFs) exhibit promising nanostructures, promoting their further application in supercapacitors. The unique design and synthesis facilitate the construction of frameworks with superior structures, enhancing their electrochemical performances. Through special conversions such as derivatization and compositing with some functional materials, they can overcome their shortcomings better than their initial counterparts. It has also attracted considerable attention for the development of new framework materials with outstanding electrochemical properties.

(1) Some pristine MOFs with functional structures, such as promising metal elements, superior ligands, and special morphologies, can deliver excellent electrochemical performance. Especially in ultrathin 2D MOF sheets, the specific capacitances, cycling stabilities, and energy/power densities are all enhanced compared to their counterparts.

(2) With controlled synthesis and special conversions, MOF-derived materials often achieve better properties. Some MOFs were converted into carbonaceous materials, while others were converted into metal compounds with pseudocapacitive properties. Using carbonaceous materials, especially porous carbon

and graphene materials, can significantly improve the cycling stability. Metal compounds, especially metal chalcogenides, exhibit superior capacity performance. Combining derivatives with functional materials, such as carbonaceous materials with metal compounds, can integrate the advantages of two components.

(3) Some pristine MOFs have been combined with other functional materials. This could both remain the initial properties of the MOF and overcome the disadvantages with the help of functional materials. The combination of MOFs with carbonaceous materials can enhance their cycling stability and conductivity. When combined with pseudocapacitive materials (metal compounds and CPs), their capacities are significantly improved compared with their primitive counterparts. Moreover, MOF composites may deliver better electrochemical performance than most MOF derivatives.

(4) Compared with MOFs, PB/PBAs possess hollow core-shell nanostructures that promote the diffusion of the electrolyte and enhance their electrochemical performance. Similar to MOFs, PB/PBAs can also serve as sacrificial precursors or templates for fabricating various derivatives such as transitional metal selenides, oxides, and phosphides.

(5) In contrast to MOFs and PB/PBAs, pristine COFs with superior building units attract more attention than their derivatives and composites. Owing to their special condensation in the synthesis process, COFs with redox-active units, perfect channel structures, and tunable porosities can be successfully constructed. Some COFs with special molecule interactions enhance their charge–discharge cycles.

Numerous framework materials with unique morphologies, nanostructures, and functionalities have been synthesized and widely utilized in supercapacitors. Moreover, framework materials combined with other functional materials have demonstrated potential in enhancing the electrochemical performance, including capacity, cycling stability, and energy/power densities. Over the past several years, rapid developments have been witnessed in the fabrication and application of framework materials, their derivatives, and composites. More efforts are required to realize the practical use of these materials. There are several main challenges to be addressed as follows:

(1) Despite the excellent advances in the study of MOFs for use in supercapacitors, the precise and systematic investigation of the relation between the properties and structures of pristine MOFs is still wanting. Hence, more attention should be focused on innovative synthetic routes for MOFs, especially multimetallic MOFs. Moreover, the relationships between the synthetic routes and MOF morphologies should also be paid more attention. Monometallic MOFs with other transitional metal elements can also investigate their performances in supercapacitors.

(2) MOF derivatives deliver better performance in enhancing capacitance. However, the conversion of pristine MOFs to their derivatives is complex and may not be well controlled. This could lead to the precise synthesis of MOF derivatives with very hard-targeted morphological features. Further research will contribute toward building comprehensive synthesis routes and optimizing the design and fabrication of these functional derivatives. Moreover, the doping in the derivation is a better strategy for obtaining better physicochemical properties compared to their undoped counterparts. However, few studies have been reported on MOFs-based derivatives with metallic heteroatom doped, which will remain a challenge in the future.

(3) With the combination of some carbon materials or pseudocapacitive additives, the electrical conductivity of MOFs and their capacities are enhanced. Coating functional materials onto MOF derivatives, such as adding carbonaceous materials onto metal compounds derived from MOFs, may have a chance to yield the advantages of both materials. Therefore, electrode materials with outstanding capacitance performance and excellent cyclic life can be obtained, making them promising for practical applications. Hence, the preparation and effective synthesis route of functional derivatives and nanocomposites should be further studied. Moreover, the elements doping in composites should also be investigated. Few studies have been reported in MOF composites with heteroatom doped, which will remain the same challenge in the future compared with MOF derivatives.

(4) PB/PBA nanocomposites are still under investigation, and other PB/PBAs with hollow and unique morphologies should also be investigated. Many pristine PB with a hollow structure can deliver promising performance. Hence, more research should focus on the influence of these unique hollow structures on their properties. PB/PBA can also be treated like MOFs to fabricate derivatives and special composites. Some studies have shown that functional pseudocapacitive materials such as metal sulfides, metal hydroxides, and MXene can combine with PB/PBAs to enhance their performance. More research should be conducted on the relations between the transferring charge and these functional materials.

(5) Great progress has been made in the development of pristine COFs with unique building units. Hence, the

development of COF derivatives and COF composites with functional materials should be continuously explored. Similar to MOFs, the relationships between COF morphologies and COF electrochemical performances should pay more attention. This can make research of COFs applied in supercapacitors more effective. For the COF composites, other functional materials with pseudocapacitive properties, like transitional metal compounds and conductive polymers, may become promising additives to enhance their performances.

MOFs, PB/PBA, and COFs all have their characteristics, resulting in different performances. In terms of COFs, some materials delivered an ultrahigh cycling life compared to all other materials, including PB/PBAs and MOFs, although their specific capacitance may not be better than that of pseudocapacitive materials. PB/PBAs also display excellent cycling stability as well as COFs counterparts, but their specific capacitances usually behave better than COFs. MOFs have attracted much more attention than the two previously mentioned, and the pristine MOFs, MOF derivatives, and composites are all the hot research points. Many researchers have reported MOFs with ultrahigh specific capacitance values and outstanding cyclic performances, indicating their application for supercapacitors. Research on framework materials and other promising materials for electrode materials is still active, and a revolution brought about by these frameworks in the field of supercapacitors may be underway.

Funding information: This work was supported by the National Natural Science Foundation of China (U1904215), Natural Science Foundation of Jiangsu Province (BK20200044), Changjiang scholars program of the Ministry of Education (Q2018270), and Jiangsu Students' Innovation and Entrepreneurship Training Program (202111117079Y). The authors also acknowledge the Priority Academic Program Development of Jiangsu Higher Education Institutions.

Author contributions: All authors have accepted responsibility for the entire content of this manuscript and approved its submission.

Conflict of interest: The authors state no conflict of interest.

References

[1] Li Y, Xu Y, Yang W, Shen W, Xue H, Pang H. MOF-derived metal oxide composites for advanced electrochemical energy storage. Small. 2018;14:1704435.

[2] Wang G, Zhang L, Zhang J. A review of electrode materials for electrochemical supercapacitors. Chem Soc Rev. 2012;41:797–828.

[3] Du W, Bai YL, Xu J, Zhao H, Zhang L, Li X, et al. Advanced metal-organic frameworks (MOFs) and their derived electrode materials for supercapacitors. J Power Sources. 2018;402:281–95.

[4] Wu HB, Lou XW. Metal-organic frameworks and their derived materials for electrochemical energy storage and conversion: promises and challenges. Sci Adv. 2017;3:eaap9252.

[5] Zhang W, Zhang F, Ming F, Alshareef HN. Sodium-ion battery anodes: status and future trends. EnergyChem. 2019;1:100012.

[6] Liang Z, Zhao R, Qiu T, Zou R, Xu Q. Metal-organic framework-derived materials for electrochemical energy applications. EnergyChem. 2019;1:100001.

[7] Yan M, Wang WP, Yin YX, Wan LJ, Guo YG. Interfacial design for lithium–sulfur batteries: from liquid to solid. EnergyChem. 2019;1:100002.

[8] Hao J, Li X, Song X, Guo Z. Recent progress and perspectives on dual-ion batteries. EnergyChem. 2019;1:100004.

[9] Zhang L, Hu X, Wang Z, Sun F, Dorrell DG. A review of supercapacitor modeling, estimation, and applications: A control/management perspective. Renew Sustain Energy Rev. 2018;81:1868–78.

[10] Kouchachvili L, Yaïci W, Entchev E. Hybrid battery/supercapacitor energy storage system for the electric vehicles. J Power Sources. 2018;374:237–48.

[11] Snook GA, Kao P, Best AS. Conducting-polymer-based supercapacitor devices and electrodes. J Power Sources. 2011;196:1–12.

[12] Yang Q, Li Z, Zhang R, Zhou L, Shao M, Wei M. Carbon modified transition metal oxides/hydroxides nanoarrays toward high-performance flexible all-solid-state supercapacitors. Nano Energy. 2017;41:408–16.

[13] Zhao Y, Liu J, Horn M, Motta N, Hu M, Li Y. Recent advancements in metal organic framework based electrodes for supercapacitors. Sci China Mater. 2018;61:159–84.

[14] Yao H, Zhang F, Zhang G, Luo H, Liu L, Shen M, et al. A novel two-dimensional coordination polymer-polypyrrole hybrid material as a high-performance electrode for flexible supercapacitor. Chem Eng J. 2018;334:2547–57.

[15] Qu C, Liang Z, Jiao Y, Zhao B, Zhu B, Dang D, et al. "One-for-all" strategy in fast energy storage: production of pillared mof nanorod-templated positive/negative electrodes for the application of high-performance hybrid supercapacitor. Small. 2018;14:1800285.

[16] Gogotsi Y, Simon P. Materials for electrochemical capacitors. Nat Mater. 2008;7:845–54.

[17] Wang DG, Liang Z, Gao S, Qu C, Zou R. Metal-organic framework-based materials for hybrid supercapacitor application. Coord Chem Rev. 2020;404:213093.

[18] Wang Y, Nie S, Liu Y, Yan W, Lin S, Cheng G, et al. Room-temperature fabrication of a nickel- functionalized copper metal-organic framework (Ni@Cu-MOF) as a new pseudocapacitive material for asymmetric supercapacitors. Polymers (Basel). 2019;11:821.

[19] Ramachandran R, Zhao C, Luo D, Wang K, Wang F. Morphology-dependent electrochemical properties of

cobalt-based metal organic frameworks for supercapacitor electrode materials. Electrochim Acta. 2018;267:170–80.
[20] Tian D, Ao Y, Li W, Xu J, Wang C. General fabrication of metal-organic frameworks on electrospun modified carbon nanofibers for high-performance asymmetric supercapacitors. J Colloid Interface Sci. 2021;603:199–209.
[21] Chen C, Wang SC, Xiong D, Gu M, Yi FY. Rationally designed trimetallic Prussian blue analogues on LDH/Ni foam for high performance supercapacitors. Dalt Trans. 2020;49:3706–14.
[22] Qu C, Jiao Y, Zhao B, Chen D, Zou R, Walton KS, et al. Nickel-based pillared MOFs for high-performance supercapacitors: design, synthesis and stability study. Nano Energy. 2016;26:66–73.
[23] Feng X, Ding X, Jiang D. Covalent organic frameworks. Chem Soc Rev. 2012;41:6010–22.
[24] Cao S, Li B, Zhu R, Pang H. Design and synthesis of covalent organic frameworks towards energy and environment fields. Chem Eng J. 2019;355:602–23.
[25] Li J, Yan X, Li X, Zhang X, Chen J. A new electrochemical immunosensor for sensitive detection of prion based on Prussian blue analogue. Talanta. 2018;179:726–33.
[26] Zhang Z, Yoshikawa H, Awaga K. Discovery of a "bipolar charging" mechanism in the solid-state electrochemical process of a flexible metal-organic framework. Chem Mater. 2016;28:1298–303.
[27] Xiong X, Zhou L, Cao W, Liang J, Wang Y, Hu S, et al. Metal-organic frameworks based on halogen-bridged dinuclear-Cu-nodes as promising materials for high performance supercapacitor electrodes. CrystEngComm. 2017;19:7177–84.
[28] Gao S, Sui Y, Wei F, Qi J, Meng Q, Ren Y, et al. Dandelion-like nickel/cobalt metal-organic framework based electrode materials for high performance supercapacitors. J Colloid Interface Sci. 2018;531:83–90.
[29] Worrall SD, Mann H, Rogers A, Bissett MA, Attfield MP, Dryfe RAW. Electrochemical deposition of zeolitic imidazolate framework electrode coatings for supercapacitor electrodes. Electrochim Acta. 2016;197:228–40.
[30] Xu X, Li C, Wang C, Ji L, Kaneti YV, Huang H, et al. Three-dimensional nanoarchitecture of carbon nanotube-interwoven metal-organic frameworks for capacitive deionization of saline water. ACS Sustain Chem Eng. 2019;7:13949–54.
[31] Li D, Xu HQ, Jiao L, Jiang HL. Metal-organic frameworks for catalysis: state of the art, challenges, and opportunities. EnergyChem. 2019;1:100005.
[32] Li H, Li L, Lin R-B, Zhou W, Zhang Z, Xiang S, et al. Porous metal-organic frameworks for gas storage and separation: status and challenges. EnergyChem. 2019;1:100006.
[33] Wang J, Zhong Q, Xiong Y, Cheng D, Zeng Y, Bu Y. Fabrication of 3D co-doped Ni-based MOF hierarchical micro-flowers as a high-performance electrode material for supercapacitors. Appl Surf Sci. 2019;483:1158–65.
[34] Cao X, Tan C, Sindoro M, Zhang H. Hybrid micro-/nano-structures derived from metal-organic frameworks: preparation and applications in energy storage and conversion. Chem Soc Rev. 2017;46:2660–77.
[35] Rajak R, Saraf M, Mohammad A, Mobin SM. Design and construction of a ferrocene based inclined polycatenated Co-MOF for supercapacitor and dye adsorption applications. J Mater Chem A. 2017;5:17998–8011.
[36] Yaghi OM, Li Hailian. Hydrothermal synthesis of a metal-organic framework containing large rectangular channels. J Am Chem Soc. 1995;117:10401–2.
[37] Liu B, Shioyama H, Akita T, Xu Q. Metal-organic framework as a template for porous carbon synthesis. J Am Chem Soc. 2008;130:5390–1.
[38] Qu C, Zhang L, Meng W, Liang Z, Zhu B, Dang D, et al. MOF-derived α-NiS nanorods on graphene as an electrode for high-energy-density supercapacitors. J Mater Chem A. 2018;6:4003–12.
[39] Tao K, Han X, Ma Q, Han L. A metal-organic framework derived hierarchical nickel-cobalt sulfide nanosheet array on Ni foam with enhanced electrochemical performance for supercapacitors. Dalt Trans. 2018;47:3496–502.
[40] Xiao Z, Mei Y, Yuan S, Mei H, Xu B, Bao Y, et al. Controlled hydrolysis of metal-organic frameworks: hierarchical Ni/Co-layered double hydroxide microspheres for high-performance supercapacitors. ACS Nano. 2019;13:7024–30.
[41] Ware M. Prussian blue: artists' pigment and chemists' sponge. J Chem Educ. 2008;85:612–21.
[42] Neff VD. Electrochemical oxidation and reduction of thin films of Prussian blue. J Electrochem Soc. 1978;125:886–7.
[43] Chen J, Huang K, Liu S, Hu X. Electrochemical supercapacitor behavior of ni3(Fe(CN)6)2(H2O) nanoparticles. J Power Sources. 2009;186:565–9.
[44] Luo M, Dou Y, Kang H, Ma Y, Ding X, Liang B, et al. A novel interlocked Prussian blue/reduced graphene oxide nanocomposites as high-performance supercapacitor electrodes. J Solid State Electrochem. 2015;19:1621–31.
[45] Chen Y, Hu L. Novel Co3O4 porous polyhedrons derived from metal-organic framework toward high performance for electrochemical energy devices. J Solid State Chem. 2016;239:23–9.
[46] Das AK, Bera R, Maitra A, Karan SK, Paria S, Halder L, et al. Fabrication of an advanced asymmetric supercapacitor based on a microcubical PB@MnO2 hybrid and PANI/GNP composite with excellent electrochemical behaviour. J Mater Chem A. 2017;5:22242–54.
[47] Ockwig NW, Co AP, Keeffe MO, Matzger AJ, Yaghi OM. Porous, crystalline, covalent organic. Frameworks. 2005;310:1166–71.
[48] Liu B, Zhang X, Shioyama H, Mukai T, Sakai T, Xu Q. Converting cobalt oxide subunits in cobalt metal-organic framework into agglomerated Co3O4 nanoparticles as an electrode material for lithium ion battery. J Power Sources. 2010;195:857–61.
[49] Zhuang X, Zhao W, Zhang F, Cao Y, Liu F, Bi S, et al. A two-dimensional conjugated polymer framework with fully sp2-bonded carbon skeleton. Polym Chem. 2016;7:4176–81.
[50] Han Y, Zhang Q, Hu N, Zhang X, Mai Y, Liu J, et al. Core-shell nanostructure of single-wall carbon nanotubes and covalent organic frameworks for supercapacitors. Chinese Chem Lett. 2017;28:2269–73.
[51] Roy A, Mondal S, Halder A, Banerjee A, Ghoshal D, Paul A, et al. Benzimidazole linked arylimide based covalent organic framework as gas adsorbing and electrode materials for supercapacitor application. Eur Polym J. 2017;93:448–57.
[52] Halder A, Ghosh M, Khayum AM, Bera S, Addicoat M, Sasmal HS, et al. Interlayer hydrogen-bonded covalent

organic frameworks as high-performance supercapacitors. J Am Chem Soc. 2018;140:10941–5.
[53] Li T, Zhang WDa, Liu Y, Li Y, Cheng C, Zhu H, et al. A two-dimensional semiconducting covalent organic framework with nickel(II) coordination for high capacitive performance. J Mater Chem A. 2019;7:19676–81.
[54] An N, Guo Z, Xin J, He Y, Xie K, Sun D, et al. Hierarchical porous covalent organic framework/graphene aerogel electrode for high-performance supercapacitors. J Mater Chem A. 2021;9:16824–33.
[55] Yang J, Zheng C, Xiong P, Li Y, Wei M. Zn-doped Ni-MOF material with a high supercapacitive performance. J Mater Chem A. 2014;2:19005–10.
[56] Kang L, Sun SX, Kong LB, Lang JW, Luo YC. Investigating metal-organic framework as a new pseudo-capacitive material for supercapacitors. Chinese Chem Lett. 2014;25:957–61.
[57] Wen P, Gong P, Sun J, Wang J, Yang S. Design and synthesis of Ni-MOF/CNT composites and rGO/carbon nitride composites for an asymmetric supercapacitor with high energy and power density. J Mater Chem A. 2015;3:13874–83.
[58] Wang L, Feng X, Ren L, Piao Q, Zhong J, Wang Y, et al. Flexible solid-state supercapacitor based on a metal-organic framework interwoven by electrochemically-deposited PANI. J Am Chem Soc. 2015;137:4920–3.
[59] Wang R, Jin D, Zhang Y, Wang S, Lang J, Yan X, et al. Engineering metal organic framework derived 3D nanostructures for high performance hybrid supercapacitors. J Mater Chem A. 2017;5:292–302.
[60] Jiao Y, Pei J, Chen D, Yan C, Hu Y, Zhang Q, et al. Mixed-metallic MOF based electrode materials for high performance hybrid supercapacitors. J Mater Chem A. 2017;5:1094–102.
[61] Sheberla D, Bachman JC, Elias JS, Sun CJ, Shao-Horn Y, Dincă M. Conductive MOF electrodes for stable supercapacitors with high areal capacitance. Nat Mater. 2017;16:220–4.
[62] Xue Y, Zheng S, Xue H, Pang H. Metal-organic framework composites and their electrochemical applications. J Mater Chem A. 2019;7:7301–27.
[63] Zhao W, Peng J, Wang W, Liu S, Zhao Q, Huang W. Ultrathin two-dimensional metal-organic framework nanosheets for functional electronic devices. Coord Chem Rev. 2018;377:44–63.
[64] Zhou H-C, Long JR, Yaghi OM. Introduction to metal–organic frameworks. Chem Rev. 2012;112:673–4.
[65] Kannangara YY, Rathnayake UA, Song JK. Hybrid supercapacitors based on metal organic frameworks using p-phenylenediamine building block. Chem Eng J. 2019;361:1235–44.
[66] Bai Y, Liu C, Shan Y, Chen T, Zhao Y, Yu C, et al. Metal-organic frameworks nanocomposites with different dimensionalities for energy conversion and storage. Adv Energy Mater. 2021;12:2100346.
[67] Yan Y, Gu P, Zheng S, Zheng M, Pang H, Xue H. Facile synthesis of an accordion-like Ni-MOF superstructure for high-performance flexible supercapacitors. J Mater Chem A. 2016;4:19078–85.
[68] Wang Y, Liu Y, Wang H, Liu W, Li Y, Zhang J, et al. Ultrathin NiCo-MOF nanosheets for high-performance supercapacitor electrodes. ACS Appl Energy Mater. 2019;2:2063–71.
[69] Pachfule P, Shinde D, Majumder M, Xu Q. Fabrication of carbon nanorods and graphene nanoribbons from a metal-organic framework. Nat Chem. 2016;8:718–24.
[70] Choi KM, Jeong HM, Park JH, Zhang YB, Kang JK, Yaghi OM. Supercapacitors of nanocrystalline metal-organic frameworks. ACS Nano. 2014;8:7451–7.
[71] Liu C, Bai Y, Wang J, Qiu Z, Pang H. Controllable synthesis of ultrathin layered transition metal hydroxide/zeolitic imidazolate framework-67 hybrid nanosheets for high-performance supercapacitors. J Mater Chem A. 2021;9:11201–9.
[72] Yang F, Li W, Tang B. Facile synthesis of amorphous UiO-66 (Zr-MOF) for supercapacitor application. J Alloys Compd. 2018;733:8–14.
[73] Gao W, Chen D, Quan H, Zou R, Wang W, Luo X, et al. Fabrication of hierarchical porous metal-organic framework electrode for aqueous asymmetric supercapacitor. ACS Sustain Chem Eng. 2017;5:4144–53.
[74] Bi S, Banda H, Chen M, Niu L, Chen M, Wu T, et al. Molecular understanding of charge storage and charging dynamics in supercapacitors with MOF electrodes and ionic liquid electrolytes. Nat Mater. 2020;19:552–8.
[75] Liu S, Kang L, Zhang J, Jung E, Lee S, Jun SC. Structural engineering and surface modification of MOF-derived cobalt-based hybrid nanosheets for flexible solid-state supercapacitors. Energy Storage Mater. 2020;32:167–77.
[76] Xu J, Yang C, Xue Y, Wang C, Cao J, Chen Z. Facile synthesis of novel metal-organic nickel hydroxide nanorods for high performance supercapacitor. Electrochim Acta. 2016;211:595–602.
[77] Jiao Y, Pei J, Yan C, Chen D, Hu Y, Chen G. Layered nickel metal-organic framework for high performance alkaline battery-supercapacitor hybrid devices. J Mater Chem A. 2016;4:13344–51.
[78] Li Y, Xu Y, Liu Y, Pang H. Exposing {001} crystal plane on hexagonal Ni-MOF with surface-grown cross-linked mesh-structures for electrochemical energy storage. Small. 2019;15:1902463.
[79] Abazari R, Sanati S, Morsali A, Slawin AL, Carpenter-Warren C. Dual-purpose 3D pillared metal–organic framework with excellent properties for catalysis of oxidative desulfurization and energy storage in asymmetric supercapacitor. ACS Appl Mater Interfaces. 2019;11:14759–73.
[80] Sanati S, Abazari R, Morsali A, Kirillov AM, Junk PC, Wang J. An asymmetric supercapacitor based on a non-calcined 3D pillared cobalt(II) metal-organic framework with long cyclic stability. Inorg Chem. 2019;58:16100–11.
[81] Liu X, Shi C, Zhai C, Cheng M, Liu Q, Wang G. Cobalt-based layered metal-organic framework as an ultrahigh capacity supercapacitor electrode material. ACS Appl Mater Interfaces. 2016;8:4585–91.
[82] Kannangara YY, Rathnayake UA, Song JK. Redox active multilayered Zn-pPDA MOFs as high-performance supercapacitor electrode material. Electrochim Acta. 2019;297:145–54.
[83] Zheng Y, Zheng S, Xu Y, Xue H, Liu C, Pang H. Ultrathin two-dimensional cobalt-organic frameworks nanosheets for electrochemical energy storage. Chem Eng J. 2019;373:1319–28.
[84] Li B, Gu P, Feng Y, Zhang G, Huang K, Xue H, et al. Ultrathin nickel–cobalt phosphate 2D nanosheets for electrochemical

energy storage under aqueous/Solid-state electrolyte. Adv Funct Mater. 2017;27:1605784.
[85] Li WH, Ding K, Tian HR, Yao MS, Nath B, Deng WH, et al. Conductive metal–organic framework nanowire array electrodes for high-performance solid-state supercapacitors. Adv Funct Mater. 2017;27:1702067.
[86] Liu J, Zhou Y, Xie Z, Li Y, Liu Y, Sun J, et al. Conjugated copper–catecholate framework electrodes for efficient energy storage. Angew Chemie Int Ed. 2020;59:1081–6.
[87] Xia H, Zhang J, Yang Z, Guo S, Guo S, Xu Q. 2D MOF nanoflake-assembled spherical microstructures for enhanced supercapacitor and electrocatalysis performances. Nano-Micro Lett. 2017;9:43.
[88] Dolgopolova EA, Brandt AJ, Ejegbavwo OA, Duke AS, Maddumapatabandi TD, Galhenage RP, et al. Electronic properties of bimetallic metal–organic frameworks (MOFs): tailoring the density of electronic states through MOF modularity. J Am Chem Soc. 2017;139:5201–9.
[89] Chen X, Wu X, Guo H, Fu W. Improvement of capacitance activity for Cu-doped Ni-based metal–organic frameworks by adding potassium hexacyanoferrate into KOH electrolyte. Appl Organomet Chem. 2019;33:e5193.
[90] Rajak R, Saraf M, Mobin SM. Robust heterostructures of a bimetallic sodium-zinc metal-organic framework and reduced graphene oxide for high-performance supercapacitors. J Mater Chem A. 2019;7:1725–36.
[91] Zhang X, Wang J, Ji X, Sui Y, Wei F, Qi J, et al. Nickel/cobalt bimetallic metal-organic frameworks ultrathin nanosheets with enhanced performance for supercapacitors. J Alloys Compd. 2020;825:154069.
[92] Wang J, Zhong Q, Zeng Y, Cheng D, Xiong Y, Bu Y. Rational construction of triangle-like nickel-cobalt bimetallic metal-organic framework nanosheets arrays as battery-type electrodes for hybrid supercapacitors. J Colloid Interface Sci. 2019;555:42–52.
[93] Deng T, Lu Y, Zhang W, Sui M, Shi X, Wang D, et al. Inverted design for high-performance supercapacitor *via* Co(OH)2-derived highly oriented MOF electrodes. Adv Energy Mater. 2018;8:1702294.
[94] Salunkhe RR, Kaneti YV, Kim J, Kim JH, Yamauchi Y. Nanoarchitectures for metal-organic framework-derived nanoporous carbons toward supercapacitor applications. Acc Chem Res. 2016;49:2796–806.
[95] Pan Y, Zhao Y, Mu S, Wang Y, Jiang C, Liu Q, et al. Cation exchanged MOF-derived nitrogen-doped porous carbons for CO2 capture and supercapacitor electrode materials. J Mater Chem A. 2017;5:9544–52.
[96] Yu F, Wang T, Wen Z, Wang H. High performance all-solid-state symmetric supercapacitor based on porous carbon made from a metal-organic framework compound. J Power Sources. 2017;364:9–15.
[97] Liu Y, Li G, Guo Y, Ying Y, Peng X. Flexible and binder-free hierarchical porous carbon film for supercapacitor electrodes derived from MOFs/CNT. ACS Appl Mater Interfaces. 2017;9:14043–50.
[98] Li S, Zhou X, Chen Z, Herbert FC, Jayawickramage R, Panangala SD, et al. Hierarchical porous carbon arising from metal-organic framework-encapsulated bacteria and its energy storage potential. ACS Appl Mater Interfaces. 2020;12:11884–9.
[99] Zhao K, Liu S, Ye G, Gan Q, Zhou Z, He Z. High-yield bottom-up synthesis of 2D metal-organic frameworks and their derived ultrathin carbon nanosheets for energy storage. J Mater Chem A. 2018;6:2166–75.
[100] Zou J, Liu P, Huang L, Zhang Q, Lan T, Zeng S, et al. Ultrahigh-content nitrogen-decorated nanoporous carbon derived from metal organic frameworks and its application in supercapacitors. Electrochim Acta. 2018;271:599–607.
[101] Qian J, Wang X, Chai L, Liang L-F, Li T-T, Hu Y, et al. Robust cage-based zinc–organic frameworks derived dual-doped carbon materials for supercapacitor. Cryst Growth Des. 2018;18:2358–64.
[102] Khan IA, Badshah A, Khan I, Zhao D, Nadeem MA. Soft-template carbonization approach of MOF-5 to mesoporous carbon nanospheres as excellent electrode materials for supercapacitor. Microporous Mesoporous Mater. 2017;253:169–76.
[103] Li ZX, Zou KY, Zhang X, Han T, Yang Y. Hierarchically flower-like N-doped porous carbon materials derived from an explosive 3-fold interpenetrating diamondoid copper metal-organic framework for a supercapacitor. Inorg Chem. 2016;55:6552–62.
[104] Liu W, Wang K, Li C, Zhang X, Sun X, Han J, et al. Boosting solid-state flexible supercapacitors by employing tailored hierarchical carbon electrodes and a high-voltage organic gel electrolyte. J Mater Chem A. 2018;6:24979–87.
[105] Yi M, Zhang C, Cao C, Xu C, Sa B, Cai D, et al. MOF-derived hybrid hollow submicrospheres of nitrogen-doped carbon-encapsulated bimetallic Ni-Co-S nanoparticles for supercapacitors and lithium ion batteries. Inorg Chem. 2019;58:3916–24.
[106] Tang Z, Zhang G, Zhang H, Wang L, Shi H, Wei D, et al. MOF-derived N-doped carbon bubbles on carbon tube arrays for flexible high-rate supercapacitors. Energy Storage Mater. 2018;10:75–84.
[107] Wang L, Wei T, Sheng L, Jiang L, Wu X, Zhou Q, et al. "Brick-and-mortar" sandwiched porous carbon building constructed by metal-organic framework and graphene: ultrafast charge/discharge rate up to 2 V s–1 for supercapacitors. Nano Energy. 2016;30:84–92.
[108] Xu S, Liu R, Shi X, Ma Y, Hong M, Chen X, et al. A dual CoNi MOF nanosheet/nanotube assembled on carbon cloth for high performance hybrid supercapacitors. Electrochim Acta. 2020;342:136124.
[109] Salunkhe RR, Kaneti YV, Yamauchi Y. Metal-organic framework-derived nanoporous metal oxides toward supercapacitor applications: progress and prospects. ACS Nano. 2017;11:5293–308.
[110] Yin X, Li H, Han L, Yuan R, Lu J. NiCo2O4 nanosheets sheathed SiC@CNTs core-shell nanowires for high-performance flexible hybrid supercapacitors. J Colloid Interface Sci. 2020;577:481–93.
[111] Li S, Yang K, Ye P, Ma K, Zhang Z, Huang Q. Three-dimensional porous carbon/Co3O4 composites derived from graphene/Co-MOF for high performance supercapacitor electrodes. Appl Surf Sci. 2020;503:144090.
[112] Xiao Y, Liu S, Li F, Zhang A, Zhao J, Fang S, et al. 3D hierarchical Co3O4 twin-spheres with an urchin-like structure: large-scale synthesis, multistep-splitting growth, and electrochemical pseudocapacitors. Adv Funct Mater. 2012;22:4052–9.

[113] Liu T, Zhang L, You W, Yu J. Core–shell nitrogen-doped carbon hollow spheres/Co3O4 nanosheets as advanced electrode for high-performance supercapacitor. Small. 2018;14:1702407.
[114] Lu Y, Liu Y, Mo J, Deng B, Wang J, Zhu Y, et al. Construction of hierarchical structure of Co 3 O 4 electrode based on electrospinning technique for supercapacitor. J Alloys Compd. 2021;853:157271.
[115] Han D, Wei J, Zhao Y, Shen Y, Pan Y, Wei Y, et al. Metal-organic framework derived petal-like Co3O4@CoNi2S4 hybrid on carbon cloth with enhanced performance for supercapacitors. Inorg Chem Front. 2020;7:1428–36.
[116] Li H, Yue F, Yang C, Qiu P, Xue P, Xu Q, et al. Porous nanotubes derived from a metal-organic framework as high-performance supercapacitor electrodes. Ceram Int. 2016;42:3121–9.
[117] Liu S, Deng T, Hu X, Shi X, Wang H, Qin T, et al. Increasing surface active Co2 + sites of MOF-derived Co3O4 for enhanced supercapacitive performance *via* NaBH4 reduction. Electrochim Acta. 2018;289:319–23.
[118] Dai S, Han F, Tang J, Tang W. MOF-derived Co3O4 nanosheets rich in oxygen vacancies for efficient all-solid-state symmetric supercapacitors. Electrochim Acta. 2019;328:135103.
[119] Vilian ATE, Dinesh B, Rethinasabapathy M, Hwang SK, Jin CS, Huh YS, et al. Hexagonal Co3O4 anchored reduced graphene oxide sheets for high-performance supercapacitors and non-enzymatic glucose sensing. J Mater Chem A. 2018;6:14367–79.
[120] Yin X, Li H, Yuan R, Lu J. NiCoLDH nanosheets grown on MOF-derived Co3O4 triangle nanosheet arrays for high-performance supercapacitor. J Mater Sci Technol. 2021;62:60–9.
[121] Zhou S, Wang S, Zhou S, Xu H, Zhao J, Wang J, et al. An electrochromic supercapacitor based on an MOF derived hierarchical-porous NiO film. Nanoscale. 2020;12:8934–41.
[122] Reddy BP, Mallikarjuna K, Kumar M, Sekhar MC, Suh Y, Park S. Highly porous metal organic framework derived NiO hollow spheres and flowers for oxygen evolution reaction and supercapacitors. Ceram Int. 2021;47:3312–21.
[123] Shin S, Shin MW. Nickel metal–organic framework (Ni-MOF) derived NiO/C@CNF composite for the application of high performance self-standing supercapacitor electrode. Appl Surf Sci. 2021;540:148295.
[124] Wu MK, Chen C, Zhou JJ, Yi FY, Tao K, Han L. MOF–derived hollow double–shelled NiO nanospheres for high–performance supercapacitors. J Alloys Compd. 2018;734:1–8.
[125] Li GC, Liu PF, Liu R, Liu M, Tao K, Zhu SR, et al. MOF-derived hierarchical double-shelled niO/ZnO hollow spheres for high-performance supercapacitors. Dalt Trans. 2016;45:13311–6.
[126] Yuan Y, Zhu J, Wang Y, Li S, Jin P, Chen Y. Facile synthesis of manganese oxide nanostructures with different crystallographic phase and morphology for supercapacitors. J Alloys Compd. 2020;830:154524.
[127] Wang J, Luo X, Young C, Kim J, Kaneti YV, You J, et al. A glucose-assisted hydrothermal reaction for directly transforming metal-organic frameworks into hollow carbonaceous materials. Chem Mater. 2018;30:4401–8.
[128] Chu D, Li F, Song X, Ma H, Tan L, Pang H, et al. A novel dual-tasking hollow cube NiFe2O4-NiCo-LDH@rGO hierarchical material for high preformance supercapacitor and glucose sensor. J Colloid Interface Sci. 2020;568:130–8.
[129] Gong LT, Xu M, Ma RP, Han YP, Xu HB, Shi G. High-performance supercapacitor based on MOF derived porous NiCo2O4 nanoparticle. Sci China Technol Sci. 2020;63:1470–7.
[130] Li S, Duan Y, Teng Y, Fan N, Huo Y. MOF-derived tremelliform Co 3 O 4/NiO/Mn 2 O 3 with excellent capacitive performance. Appl Surf Sci. 2019;478:247–54.
[131] Zhang Y, Ding J, Xu W, Wang M, Shao R, Sun Y, et al. Mesoporous LaFeO3 perovskite derived from MOF gel for all-solid-state symmetric supercapacitors. Chem Eng J. 2020;386:124030.
[132] Xie W, Wang Y, Zhou J, Zhang M, Yu J, Zhu C, et al. MOF-derived CoFe2O4 nanorods anchored in MXene nanosheets for all pseudocapacitive flexible supercapacitors with superior energy storage. Appl Surf Sci. 2020;534:147584.
[133] Yin X, Li H, Yuan R, Lu J. Hierarchical self-supporting sugar gourd-shape MOF-derived NiCo2O4 hollow nanocages@SiC nanowires for high-performance flexible hybrid supercapacitors. J Colloid Interface Sci. 2021;586:219–32.
[134] Yu C, Wang Y, Cui J, Yu D, Zhang X, Shu X, et al. MOF-74 derived porous hybrid metal oxide hollow nanowires for high-performance electrochemical energy storage. J Mater Chem A. 2018;6:8396–404.
[135] Jayakumar A, Antony RP, Wang R, Lee J-M. MOF-derived hollow cage Ni x Co 3– x O 4 and their synergy with graphene for outstanding supercapacitors. Small. 2017;13:1603102.
[136] Mei H, Mei Y, Zhang S, Xiao Z, Xu B, Zhang H, et al. Bimetallic-MOF derived accordion-like ternary composite for high-performance supercapacitors. Inorg Chem. 2018;57:10953–60.
[137] Zhang S, Yang Z, Gong K, Xu B, Mei H, Zhang H, et al. Temperature controlled diffusion of hydroxide ions in 1D channels of Ni-MOF-74 for its complete conformal hydrolysis to hierarchical Ni(OH)2 supercapacitor electrodes. Nanoscale. 2019;11:9598–607.
[138] Lee G, Na W, Kim J, Lee S, Jang J. Improved electrochemical performances of MOF-derived Ni-Co layered double hydroxide complexes using distinctive hollow-in-hollow structures. J Mater Chem A. 2019;7:17637–47.
[139] Wu Y, Chen H, Lu Y, Yang J, Zhu X, Zheng Y, et al. Rational design of cobalt–nickel double hydroxides for flexible asymmetric supercapacitor with improved electrochemical performance. J Colloid Interface Sci. 2021;581:455–64.
[140] Qu C, Zhao B, Jiao Y, Chen D, Dai S, Deglee BM, et al. Functionalized bimetallic hydroxides derived from metal-organic frameworks for high-performance hybrid supercapacitor with exceptional cycling stability. ACS Energy Lett. 2017;2:1263–9.
[141] Xiao Z, Mei Y, Yuan S, Mei H, Xu B, Bao Y, et al. Controlled hydrolysis of metal–organic frameworks: hierarchical ni/Co-layered double hydroxide microspheres for high-performance supercapacitors. ACS Nano. 2019;13:7024–30.
[142] Yang Q, Liu Y, Xiao L, Yan M, Bai H, Zhu F, et al. Self-templated transformation of MOFs into layered double hydroxide nanoarrays with selectively formed Co9S8 for high-performance asymmetric supercapacitors. Chem Eng J. 2018;354:716–26.

[143] Zhao B, Zhang B, Lu C, Cai Z, Li L. Hierarchical hollow nanocages of Ni e Co amorphous double hydroxides for high-performance asymmetric supercapacitors. J Alloys Compd. 2020;833:155130.
[144] Ramachandran R, Lan Y, Xu ZX, Wang F. Construction of NiCo-layered double hydroxide microspheres from Ni-MOFs for high-performance asymmetric supercapacitors. ACS Appl Energy Mater. 2020;3:6633–43.
[145] Wang X, Huang F, Rong F, He P, Que R, Jiang SP. Unique MOF-derived hierarchical MnO2 nanotubes@NiCo-LDH/CoS2 nanocage materials as high performance supercapacitors. J Mater Chem A. 2019;7:12018–28.
[146] Xue X, Zhong J, Liu J, Hou Z, Wu X, Li S, et al. Hydrolysis of metal-organic framework towards three-dimensional nickel cobalt-layered double hydroxide for high performance supercapacitors. J Energy Storage. 2020;31:101649.
[147] Liu P, Bao Y, Bu R, Wang W, Zhang J, Xiao Z, et al. Rational construction of MOF derived hollow leaf-like Ni/Co(VO3)x (OH)2-x for enhanced supercapacitor performance. Appl Surf Sci. 2020;533:147308.
[148] Jia H, Wang Z, Zheng X, Cai Y, Lin J, Liang H, et al. Controlled synthesis of MOF-derived quadruple-shelled CoS2 hollow dodecahedrons as enhanced electrodes for supercapacitors. Electrochim Acta. 2019;312:54–61.
[149] Chen W, Wei T, Mo LE, Wu S, Li Z, Chen S, et al. CoS2 nanosheets on carbon cloth for flexible all-solid-state supercapacitors. Chem Eng J. 2020;400:125856.
[150] Hou S, Lian Y, Bai Y, Zhou Q, Ban C, Wang Z, et al. Hollow dodecahedral Co3S4@NiO derived from ZIF-67 for supercapacitor. Electrochim Acta. 2020;341:136053.
[151] Yang Y, Li ML, Lin JN, Zou MY, Gu ST, Hong XJ, et al. MOF-derived Ni3S4 encapsulated in 3D conductive network for high-performance supercapacitor. Inorg Chem. 2020;59:2406–12.
[152] Liu T, Liu J, Zhang L, Cheng B, Yu J. Construction of nickel cobalt sulfide nanosheet arrays on carbon cloth for performance-enhanced supercapacitor. J Mater Sci Technol. 2020;47:113–21.
[153] Zheng L, Song J, Ye X, Wang Y, Shi X, Zheng H. Construction of self-supported hierarchical NiCo-S nanosheet arrays for supercapacitors with ultrahigh specific capacitance. Nanoscale. 2020;12:13811–21.
[154] Huang Y, Quan L, Liu T, Chen Q, Cai D, Zhan H. Construction of MOF-derived hollow Ni-Zn-Co-S nanosword arrays as binder-free electrodes for asymmetric supercapacitors with high energy density. Nanoscale. 2018;10:14171–81.
[155] Zhao W, Yan G, Zheng Y, Liu B, Jia D, Liu T, et al. Bimetal-organic framework derived Cu(NiCo)2S4/Ni3S4 electrode material with hierarchical hollow heterostructure for high performance energy storage. J Colloid Interface Sci. 2020;565:295–304.
[156] Zhai R, Xiao Y, Ding T, Wu Y, Chen S, Wei W. Construction of NiCo2S4 heterostructure based on electrochemically exfoliated graphene for high-performance hybrid supercapacitor electrode. J Alloys Compd. 2020;845:156164.
[157] Zhao W, Zheng Y, Cui L, Jia D, Wei D, Zheng R, et al. MOF derived Ni-Co-S nanosheets on electrochemically activated carbon cloth *via* an etching/ion exchange method for wearable hybrid supercapacitors. Chem Eng J. 2019;371:461–9.
[158] Mei H, Zhang L, Zhang K, Gao J, Zhang H, Huang Z, et al. Conversion of MOF into carbon-coated NiSe2 yolk-shell microspheres as advanced battery-type electrodes. Electrochim Acta. 2020;357:136866.
[159] Miao C, Xiao X, Gong Y, Zhu K, Cheng K, Ye K, et al. Facile synthesis of metal-organic framework-derived CoSe2 nanoparticles embedded in the N-doped carbon nanosheet array and application for supercapacitors. ACS Appl Mater Interfaces. 2020;12:9365–75.
[160] Chen T, Li S, Wen J, Gui P, Fang G. Metal-organic framework template derived porous CoSe2 nanosheet arrays for energy conversion and storage. ACS Appl Mater Interfaces. 2017;9:35927–35.
[161] Sun P, Zhang J, Huang J, Wang L, Wang P, Cai C, et al. Bimetallic MOF-derived (CuCo)Se nanoparticles embedded in nitrogen-doped carbon framework with boosted electrochemical performance for hybrid supercapacitor. Mater Res Bull. 2021;137:111196.
[162] Lv Z, Zhong Q, Bu Y. In-situ conversion of rGO/Ni 2 P composite from GO/Ni-MOF precursor with enhanced electrochemical property. Appl Surf Sci. 2018;439:413–9.
[163] Wang X, Jing C, Zhang W, Wang X, Liu X, Dong B, et al. One-step phosphorization synthesis of CoP@NiCoP nanowire/nanosheet composites hybrid arrays on Ni foam for high-performance supercapacitors. Appl Surf Sci. 2020;532:147437.
[164] Chu W, Hou Y, Liu J, Bai X, Gao Y, Cao Z. Zn-Co phosphide porous nanosheets derived from metal-organic-frameworks as battery-type positive electrodes for high-performance alkaline supercapacitors. Electrochim Acta. 2020;364:137063.
[165] Kshetri T, Singh TI, Lee YS, Khumujam DD, Kim NH, Lee JH. Metal organic framework-derived cobalt telluride-carbon porous structured composites for high-performance supercapacitor. Compos Part B Eng. 2021;211:108624.
[166] Liu X, Zang W, Guan C, Zhang L, Qian Y, Elshahawy AM, et al. Ni-doped cobalt-cobalt nitride heterostructure arrays for high-power supercapacitors. ACS Energy Lett. 2018;3:2462–9.
[167] Zhu C, He Y, Liu Y, Kazantseva N, Saha P, Cheng Q. ZnO@MOF@PANI core-shell nanoarrays on carbon cloth for high-performance supercapacitor electrodes. J Energy Chem. 2019;35:124–31.
[168] Rawool CR, Karna SP, Srivastava AK. Enhancing the supercapacitive performance of nickel based metal organic framework-carbon nanofibers composite by changing the ligands. Electrochim Acta. 2019;294:345–56.
[169] Rahmanifar MS, Hesari H, Noori A, Masoomi MY, Morsali A, Mousavi MF. A dual Ni/Co-MOF-reduced graphene oxide nanocomposite as a high performance supercapacitor electrode material. Electrochim Acta. 2018;275:76–86.
[170] Feng J, Liu L, Meng Q. Enhanced electrochemical and capacitive deionization performance of metal organic framework/holey graphene composite electrodes. J Colloid Interface Sci. 2021;582:447–58.
[171] Liu Y, Li S, Wang C, Guo L, Wang Y. Accordion-like bimetal-organic framework anchoring on the partially-exfoliated graphite paper for high-performance supercapacitors. Appl Surf Sci. 2020;528:146954.

[172] Van Ngo T, Moussa M, Tung TT, Coghlan C, Losic D. Hybridization of MOFs and graphene: A new strategy for the synthesis of porous 3D carbon composites for high performing supercapacitors. Electrochim Acta. 2020;329:135104.
[173] Cheng J, Chen S, Chen D, Dong L, Wang J, Zhang T, et al. Editable asymmetric all-solid-state supercapacitors based on high-strength, flexible, and programmable 2D-metal-organic framework/reduced graphene oxide self-assembled papers. J Mater Chem A. 2018;6:20254–66.
[174] Azadfalah M, Sedghi A, Hosseini H, Kashani H. Cobalt based metal organic framework/Graphene nanocomposite as high performance battery-type electrode materials for asymmetric supercapacitors. J Energy Storage. 2021;33:101925.
[175] Xiao Y, Wei W, Zhang M, Jiao S, Shi Y, Ding S. Facile surface properties engineering of high-quality graphene: toward advanced Ni-MOF heterostructures for high-performance supercapacitor electrode. ACS Appl Energy Mater. 2019;2:2169–77.
[176] Liu L, Yan Y, Cai Z, Lin S, Hu X. Growth-oriented fe-based MOFs synergized with graphene aerogels for high-performance supercapacitors. Adv Mater Interfaces. 2018;5:1701548.
[177] Cheng C, Xu J, Gao W, Jiang S, Guo R. Preparation of flexible supercapacitor with RGO/Ni-MOF film on Ni-coated polyester fabric. Electrochim Acta. 2019;318:23–31.
[178] Gupta AK, Saraf M, Bharadwaj PK, Mobin SM. Dual functionalized CuMOF-based composite for high-performance supercapacitors. Inorg Chem. 2019;58:9844–54.
[179] Rui K, Wang X, Du M, Zhang Y, Wang Q, Ma Z, et al. Dual-function metal-organic framework-based wearable fibers for gas probing and energy storage. ACS Appl Mater Interfaces. 2018;10:2837–42.
[180] Kim HS, Kang MS, Yoo WC. Boost-up electrochemical performance of MOFs: *via* confined synthesis within nanoporous carbon matrices for supercapacitor and oxygen reduction reaction applications. J Mater Chem A. 2019;7:5561–74.
[181] Zhang F, Ma J, Yao H. Ultrathin Ni-MOF nanosheet coated NiCo2O4 nanowire arrays as a high-performance binder-free electrode for flexible hybrid supercapacitors. Ceram Int. 2019;45:24279–87.
[182] Bai W, Li S, Ma J, Cao W, Zheng J. Ultrathin 2D metal-organic framework (nanosheets and nanofilms)-based: X D-2D hybrid nanostructures as biomimetic enzymes and supercapacitors. J Mater Chem A. 2019;7:9086–98.
[183] Li JH, Chen YC, Wang Y, SenHo, Gu WH, Chuang YJ, CH, et al. Electrochemical evolution of pore-confined metallic molybdenum in a metal-organic framework (MOF) for all-MOF-based pseudocapacitors. ACS Appl Energy Mater. 2020;3:6258–67.
[184] Hong M, Zhou C, Xu S, Ye X, Yang Z, Zhang L, et al. Bi-metal organic framework nanosheets assembled on nickel wire films for volumetric-energy-dense supercapacitors. J Power Sources. 2019;423:80–9.
[185] Xiong S, Jiang S, Wang J, Lin H, Lin M, Weng S, et al. A high-performance hybrid supercapacitor with NiO derived NiO@Ni-MOF composite electrodes. Electrochim Acta. 2020;340:135956.
[186] Zhang J, Li Y, Han M, Xia Q, Chen Q, Chen M. Constructing ultra-thin Ni-MOF@NiS2 nanosheets arrays derived from metal organic frameworks for advanced all-solid-state asymmetric supercapacitor. Mater Res Bull. 2021;137:111186.
[187] Yue L, Wang X, Sun T, Liu H, Li Q, Wu N, et al. Ni-MOF coating MoS2 structures by hydrothermal intercalation as high-performance electrodes for asymmetric supercapacitors. Chem Eng J. 2019;375:121959.
[188] Xu J, Wang Y, Cao S, Zhang J, Zhang G, Xue H, et al. Ultrathin Cu-MOF@ δ-MnO2 nanosheets for aqueous electrolyte-based high-voltage electrochemical capacitors. J Mater Chem A. 2018;6:17329–36.
[189] Li YL, Zhou JJ, Wu MK, Chen C, Tao K, Yi FY, et al. Hierarchical two-dimensional conductive metal-organic framework/layered double hydroxide nanoarray for a high-performance supercapacitor. Inorg Chem. 2018;57:6202–5.
[190] Jiao Y, Hong W, Li P, Wang L, Chen G. Metal-organic framework derived Ni/NiO micro-particles with subtle lattice distortions for high-performance electrocatalyst and supercapacitor. Appl Catal B Environ. 2019;244:732–9.
[191] Zhu G, Wen H, Ma M, Wang W, Yang L, Wang L, et al. A self-supported hierarchical Co-MOF as a supercapacitor electrode with ultrahigh areal capacitance and excellent rate performance. Chem Commun. 2018;54:10499–502.
[192] Li N, Li Y, Li Q, Zhao Y, Liu C, SenPang, et al. NiO nanoparticles decorated hexagonal nickel-based metal-organic framework: self-template synthesis and its application in electrochemical energy storage. J Colloid Interface Sci. 2021;581:709–18.
[193] Qi K, Hou R, Zaman S, Qiu Y, Xia BY, Duan H. Construction of metal-organic framework/conductive polymer hybrid for all-Solid-state fabric supercapacitor. ACS Appl Mater Interfaces. 2018;10:18021–8.
[194] Yue T, Hou R, Liu X, Qi K, Chen Z, Qiu Y, et al. Hybrid architecture of a porous polypyrrole scaffold loaded with metal-organic frameworks for flexible solid-state supercapacitors. ACS Appl Energy Mater. 2020;3:11920–8.
[195] Cheng Q, Tao K, Han X, Yang Y, Yang Z, Ma Q, et al. Ultrathin Ni-MOF nanosheet arrays grown on polyaniline decorated Ni foam as an advanced electrode for asymmetric supercapacitors with high energy density. Dalt Trans. 2019;48:4119–23.
[196] Guo SN, Zhu Y, Yan YY, Min YL, Fan JC, Xu QJ, et al. Metal-organic framework)-polyaniline sandwich structure composites as novel hybrid electrode materials for high-performance supercapacitor. J Power Sources. 2016;316:176–82.
[197] Iqbal MZ, Faisal MM, Ali SR, Farid S, Afzal AM. Co-MOF/polyaniline-based electrode material for high performance supercapattery devices. Electrochim Acta. 2020;346:136039.
[198] Le QB, Nguyen TH, Fei H, Sapurina I, Ngwabebhoh FA, Bubulinca C, et al. Electrochemical performance of composites made of rGO with Zn-MOF and PANI as electrodes for supercapacitors. Electrochim Acta. 2021;367:137563.
[199] Guo SN, Shen HK, Tie ZF, Zhu S, Shi PH, Fan JC, et al. Three-dimensional cross-linked polyaniline fiber/N-doped porous carbon with enhanced electrochemical performance for high-performance supercapacitor. J Power Sources. 2017;359:285–94.
[200] Liu PY, Zhao JJ, Dong ZP, Liu ZL, Wang YQ. Interwoving polyaniline and a metal-organic framework grown in situ for enhanced supercapacitor behavior. J Alloys Compd. 2021;854:157181.

[201] Liu Y, Wang Y, Chen Y, Wang C, Guo L. NiCo-MOF nanosheets wrapping polypyrrole nanotubes for high-performance supercapacitors. Appl Surf Sci. 2020;507:145089.
[202] Wang HN, Zhang M, Zhang AM, Shen FC, Wang XK, Sun SN, et al. Polyoxometalate-based metal-organic frameworks with conductive polypyrrole for supercapacitors. ACS Appl Mater Interfaces. 2018;10:32265–70.
[203] Xu X, Tang J, Qian H, Hou S, Bando Y, Hossain MSA, et al. Three-dimensional networked metal–organic frameworks with conductive polypyrrole tubes for flexible supercapacitors. ACS Appl Mater Interfaces. 2017;9:38737–44.
[204] Zhang C, Tian J, Rao W, Guo B, Fan L, Xu W, et al. Polypyrrole@metal-organic framework (UIO-66)@cotton fabric electrodes for flexible supercapacitors. Cellulose. 2019;26:3387–99.
[205] Jiao Y, Chen G, Chen D, Pei J, Hu Y. Bimetal-organic framework assisted polymerization of pyrrole involving air oxidant to prepare composite electrodes for portable energy storage. J Mater Chem A. 2017;5:23744–52.
[206] Yue L, Guo H, Wang X, Sun T, Liu H, Li Q, et al. Non-metallic element modified metal-organic frameworks as high-performance electrodes for all-solid-state asymmetric supercapacitors. J Colloid Interface Sci. 2019;539:370–8.
[207] Zhang Y, Wang T, Wang Y, Wang Y, Wu L, Sun Y, et al. Metal organic frameworks derived hierarchical hollow Ni 0.85 Se|P composites for high-performance hybrid supercapacitor and efficient hydrogen evolution. Electrochim Acta. 2019;303:94–104.
[208] Song W, Teng X, Liu Y, Wang J, Niu Y, He X, et al. Rational construction of self-supported triangle-like MOF-derived hollow (Ni,Co)Se2 arrays for electrocatalysis and supercapacitors. Nanoscale. 2019;11:6401–9.
[209] Zhou Q, Gong Y, Tao K. Calcination/phosphorization of dual Ni/Co-MOF into NiCoP/C nanohybrid with enhanced electrochemical property for high energy density asymmetric supercapacitor. Electrochim Acta. 2019;320:134582.
[210] Yu F, Xiong X, Zhou LY, Li JL, Liang JY, Hu SQ, et al. Hierarchical nickel/phosphorus/nitrogen/carbon composites templated by one metal-organic framework as highly efficient supercapacitor electrode materials. J Mater Chem A. 2019;7:2875–83.
[211] Li Q, Yue L, Li L, Liu H, Yao W, Wu N, et al. Metal-organic frameworks derived N, S co-doped bimetal nanocomposites as high-performance electrodes materials for supercapacitor. J Alloys Compd. 2019;810:151961.
[212] He S, Guo F, Yang Q, Mi H, Li J, Yang N, et al. Design and fabrication of hierarchical NiCoP–MOF heterostructure with enhanced pseudocapacitive properties. Small. 2021;17:2100353.
[213] Qu Y, Shi C, Cao H, Wang Y. Synthesis of Ni-MOF/Ti3C2Tx hybrid nanosheets *via* ultrasonific method for supercapacitor electrodes. Mater Lett. 2020;280:128526.
[214] Ramachandran R, Rajavel K, Xuan W, Lin D, Wang F. Influence of Ti3C2Tx (MXene) intercalation pseudocapacitance on electrochemical performance of Co-MOF binder-free electrode. Ceram Int. 2018;44:14425–31.
[215] Liu Y, Wang Y, Wang H, Zhao P, Hou H, Guo L. Acetylene black enhancing the electrochemical performance of NiCo-MOF nanosheets for supercapacitor electrodes. Appl Surf Sci. 2019;492:455–63.
[216] Goda ES, Lee S, Sohail M, Yoon KR. Prussian blue and its analogues as advanced supercapacitor electrodes. J Energy Chem. 2020;50:206–29.
[217] Zhu X, Tao H, Li M. Co-precipitation synthesis of nickel cobalt hexacyanoferrate for binder-free high-performance supercapacitor electrodes. Int J Hydrogen Energy. 2020;45:14452–60.
[218] Chen J, Wei L, Mahmood A, Pei Z, Zhou Z, Chen X, et al. Prussian blue, its analogues and their derived materials for electrochemical energy storage and conversion. Energy Storage Mater. 2020;25:585–612.
[219] Kazazi M, Faryabi M. Electrochemically anchored manganese hexacyanoferrate nanocubes on three-dimensional porous graphene scaffold: towards a potential application in high-performance asymmetric supercapacitors. J Power Sources. 2020;449:227510.
[220] Khalid M, Honorato AMB. Bendable tube-shaped supercapacitor based on reduced graphene oxide and Prussian blue coated carbon fiber yarns for energy storage. J Energy Chem. 2018;27:866–73.
[221] Jiang W, Wang T, Chen H, Suo X, Liang J, Zhu W, et al. Room temperature synthesis of high-entropy Prussian blue analogues. Nano Energy. 2021;79:105464.
[222] Sookhakian M, Basirun WJ, Teridi MAM, Mahmoudian MR, Azarang M, Zalnezhad E, et al. Prussian blue-nitrogen-doped graphene nanocomposite as hybrid electrode for energy storage applications. Electrochim Acta. 2017;230:316–23.
[223] Song Z, Liu W, Wei X, Zhou Q, Liu H, Zhang Z. Charge storage mechanism of copper hexacyanoferrate nanocubes for supercapacitors. Chinese Chem Lett. 2020;31:1213–6.
[224] Liang J, Tian B, Li S, Jiang C, Wu W. All-printed MnHCF-MnOx-based high-performance flexible supercapacitors. Adv Energy Mater. 2020;10:2000022.
[225] Zeng X, Yang B, Li X, Yu R. Three-dimensional hollow CoS2 nanoframes fabricated by anion replacement and their enhanced pseudocapacitive performances. Electrochim Acta. 2017;240:341–9.
[226] Yin X, Li H, Wang H, Zhang Z, Yuan R, Lu J, et al. Self-templating synthesis of cobalt hexacyanoferrate hollow structures with superior performance for Na-ion hybrid supercapacitors. ACS Appl Mater Interfaces. 2018;10:29496–504.
[227] Yin X, Li H, Yuan R, Zhang L, Lu J. General formation of Prussian blue analogue microtubes for high-performance Na-ion hybrid supercapacitors. Sci China Mater. 2020;63:739–47.
[228] Wang JG, Zhang Z, Zhang X, Yin X, Li X, Liu X, et al. Cation exchange formation of Prussian blue analogue submicroboxes for high-performance Na-ion hybrid supercapacitors. Nano Energy. 2017;39:647–53.
[229] Zhu P, Li X, Yao H, Pang H. Hollow cobalt-iron Prussian blue analogue nanocubes for high-performance supercapacitors. J Energy Storage. 2020;31:101544.
[230] Ju H, Liu XD, Tao CY, Yang F, Liu XL, Luo X, et al. A novel edge-rich structure of CuO/Co3O4 derived from Prussian blue analogue as a high-rate and ultra-stable electrode for efficient capacitive storage. Electrochim Acta. 2021;366:137410.
[231] Gao JS, Liu Z, Lin Y, Tang Y, Lian T, He Y. NiCo2O4 nanofeathers derived from Prussian blue analogues with enhanced electrochemical performance for supercapacitor. Chem Eng J. 2020;388:124368.
[232] Xie H, Mao L, Mao J. Structural evolution of Ce[Fe(CN)6] and derived porous Fe-CeO2 with high performance for supercapacitor. Chem Eng J. 2021;421:127826.

[233] Zhang M, Zhou J, Yu J, Shi L, Ji M, Liu H, et al. Mixed analogous heterostructure based on MXene and Prussian blue analog derivative for high-performance flexible energy storage. Chem Eng J. 2020;387:123170.
[234] Wei X, Song Y, Song L, Liu XD, Li Y, Yao S, et al. Phosphorization engineering on metal–organic frameworks for quasi-Solid-state asymmetry supercapacitors. Small. 2021;17:2007062.
[235] Zong Q, Zhu Y, Wang Q, Yang H, Zhang Q, Zhan J, et al. Prussian blue analogues anchored P-(Ni,Co)Se2 nanoarrays for high performance all-solid-state supercapacitor. Chem Eng J. 2020;392:123664.
[236] Azhar A, Yamauchi Y, Allah AE, Alothman ZA, Badjah AY, Naushad M, et al. Nanoporous iron oxide/carbon composites through in-situ deposition of Prussian blue nanoparticles on graphene oxide nanosheets and subsequent thermal treatment for supercapacitor applications. Nanomaterials. 2019;9:776.
[237] Song Z, Liu W, Zhou Q, Zhang L, Zhang Z, Liu H, et al. Cobalt hexacyanoferrate/MnO2 nanocomposite for asymmetrical supercapacitors with enhanced electrochemical performance and its charge storage mechanism. J Power Sources. 2020;465:228266.
[238] Goda ES, Hong SE, Yoon KR. Facile synthesis of Cu-PBA nanocubes/graphene oxide composite as binder-free electrodes for supercapacitor. J Alloys Compd. 2021;859:157868.
[239] Zou Y, Wang Q, Xiang C, She Z, Chu H, Qiu S, et al. One-pot synthesis of ternary polypyrrole-Prussian-blue-graphene-oxide hybrid composite as electrode material for high-performance supercapacitors. Electrochim Acta. 2016;188:126–34.
[240] Wang SC, Gu M, Pan L, Xu J, Han L, Yi FY. The interlocked: in situ fabrication of graphene@Prussian blue nanocomposite as high-performance supercapacitor. Dalt Trans. 2018;47:13126–34.
[241] Zhang X, Jiang J, Chen Y, Cheng K, Yang F, Yan J, et al. A flexible and high voltage symmetric supercapacitor based on hybrid configuration of cobalt hexacyanoferrate/reduced graphene oxide hydrogels. Chem Eng J. 2018;335:321–9.
[242] Xu P, Wang G, Wang H, Li Y, Miao C, Qu J, et al. K2.25Ni0.55Co0.37Fe(CN)6 nanoparticle connected by cross-linked carbon nanotubes conductive skeletons for high-performance energy storage. Chem Eng J. 2017;328:834–43.
[243] Jin X, Son SY, Kim MG, Hwang SJ. Unique bi-directional coordinative interaction of 2D inorganic nanosheet with Prussian blue nanocrystal for optimizing its functionality. Nano Energy. 2020;78:105255.
[244] Zhang G, Yao H, Zhang F, Gao Z, Li Q, Yang Y, et al. A high over-potential binder-free electrode constructed of Prussian blue and MnO2 for high performance aqueous supercapacitors. Nano Res. 2019;12:1061–9.
[245] Sun X, Li S, Liu R. A three-dimensional heterogeneous ZnCo-PBA@α-Co(OH)2 nanostructure for high-performance supercapacitors. J Nanopart Res. 2020;22:37.
[246] Xu Z, Liu Y, Wu Z, Wang R, Wang Q, Li T, et al. Construction of extensible and flexible supercapacitors from covalent organic framework composite membrane electrode. Chem Eng J. 2020;387:124071.
[247] Díaz U, Corma A. Ordered covalent organic frameworks, COFs and PAFs. from preparation to application. Coord Chem Rev. 2016;311:85–124.
[248] Peng Y, Huang Y, Zhu Y, Chen B, Wang L, Lai Z, et al. Ultrathin two-dimensional covalent organic framework nanosheets: preparation and application in highly sensitive and selective DNA detection. J Am Chem Soc. 2017;139:8698–704.
[249] Mohammed AK, Vijayakumar V, Halder A, Ghosh M, Addicoat M, Bansode U, et al. Weak intermolecular interactions in covalent organic framework-carbon nanofiber based crystalline yet flexible devices. ACS Appl Mater Interfaces. 2019;11:30828–37.
[250] Khayum MA, Vijayakumar V, Karak S, Kandambeth S, Bhadra M, Suresh K, et al. Convergent covalent organic framework thin sheets as flexible supercapacitor electrodes. ACS Appl Mater Interfaces. 2018;10:28139–46.
[251] Feng X, Liu L, Honsho Y, Saeki A, Seki S, Irle S, et al. High-rate charge-carrier transport in porphyrin covalent organic frameworks: switching from hole to electron to ambipolar conduction. Angew Chemie Int Ed. 2012;51:2618–22.
[252] Ding X, Chen L, Honsho Y, Feng X, Saengsawang O, Guo J, et al. An n-channel two-dimensional covalent organic framework. J Am Chem Soc. 2011;133:14510–3.
[253] Li L, Lu F, Xue R, Ma B, Li Q, Wu N, et al. Ultrastable triazine-based covalent organic framework with an interlayer hydrogen bonding for supercapacitor applications. ACS Appl Mater Interfaces. 2019;11:26355–63.
[254] Zhang F, Wei S, Wei W, Zou J, Gu G, Wu D, et al. Trimethyltriazine-derived olefin-linked covalent organic framework with ultralong nanofibers. Sci Bull. 2020;65:1659–66.
[255] Zhou Z, Zhang X, Xing L, Liu J, Kong A, Shan Y. Copper-assisted thermal conversion of microporous covalent melamine-boroxine frameworks to hollow B, N-codoped carbon capsules as bifunctional metal-free electrode materials. Electrochim Acta. 2019;298:210–8.
[256] Kim DJ, Yoon JW, Lee CS, Bae YS, Kim JH. Covalent organic framework-derived microporous carbon nanoparticles coated with conducting polypyrrole as an electrochemical capacitor. Appl Surf Sci. 2018;439:833–8.
[257] Liu X, Zhou L, Zhao Y, Bian L, Feng X, Pu Q. Hollow, spherical nitrogen-rich porous carbon shells obtained from a porous organic framework for the supercapacitor. ACS Appl Mater Interfaces. 2013;5:10280–7.
[258] Li C, Yang J, Pachfule P, Li S, Ye MY, Schmidt J, et al. Ultralight covalent organic framework/graphene aerogels with hierarchical porosity. Nat Commun. 2020;11:4712.
[259] Wang YF, Yang SY, Yue Y, Bian SW. Conductive copper-based metal-organic framework nanowire arrays grown on graphene fibers for flexible all-solid-state supercapacitors. J Alloys Compd. 2020;835:155238.